1-1-2007

FEA-aided design of a special tensile specimen for steel during quenching.

Chao Zheng
University of Windsor

FEA-AIDED DESIGN OF A SPECIAL TENSILE SPECIMEN FOR STEEL DURING QUENCHING

by

Chao Zheng

A Thesis
Submitted to the Faculty of Graduate Studies
through Engineering Materials
in Partial Fulfillment of the Requirements for
the Degree of Master of Applied Science at the
University of Windsor

Windsor, Ontario, Canada

2007

Your file Votre référence
ISBN: 978-0-494-80238-0
Our file Notre référence
ISBN: 978-0-494-80238-0

ABSTRACT

Quenching is the most effective way to strengthen steel. By cooling steel rapidly enough from an austenitizing temperature to room temperature, a hard and strong phase called martensite is formed from soft austenite. Considerable previous research work has been dedicated to characterize this process, and computer simulation programs have been developed to capture the phase transformation and dimensional change evolution as a function of temperature in the quenching process. Among the successful commercial applications is the prediction of residual stress and distortion brought about by the quenching process, which acts as a guide to optimize the quenching process. But how to measure mechanical properties, which have a nonlinear temperature and microstructure dependence and which are needed to conduct an accurate simulation, remains the most challenging problem to solve. This thesis reveals a special and unique kind of resistance heated specimen which has been designed to measure the nonlinear mechanical properties of tool steels by tensile testing, during each stage of the entire process of quenching.

DEDICATION

To my wife Qi and daughter Gloria

ACKNOWLEDGEMENTS

First of all, I would like to express my gratitude to my academic advisor, Dr. Daniel F. Watt, for his help throughout this research program. From his comprehensive knowledge and deep insight in materials science and engineering derives the idea of launching this challenging research program. His detailed guidance, constructive suggestion and involvement ensured the successful completion of this program.

I would also like to thank BOHLER UDDEHOLM LIMITED for their generous donation of research materials for this program. Help from many of the technicians in Central Technical Research, especially Gangyong Zhang and Andy Jenner for their development of our experimental device and machining of our samples, are also highly appreciated.

Funding for this research program and financial support in the form of research assistantship from Dr. Daniel F. Watt's funding provided by Natural Sciences and Engineering Research Council of Canada (NSERC), and from his personal funds, is especially acknowledged and greatly appreciated.

Further acknowledgement should go to the Province of Ontario, Canada for the financial support through the Ontario Graduate Scholarship (OGS) and also to the University of Windsor for financial support in the form of Graduate Assistantships and partial tuition waiving.

TABLE OF CONTENTS

LIST OF FIGURES

LIST OF TABLES

CHAPTER 1 INTRODUCTION

1.1 Motivation

Heat treatment is an indispensable industrial process to modify properties of steels to suit particular applications. As one kind of heat treatment process, quenching has been known for thousands of years to be the most effective process to harden steels, and it is used extensively throughout the industry to produce high strength steels.

Although the strengthening mechanisms of quenching, and the phase transformation during the heat treatment process, have been the subjects of research over a century, the complicated coupling of thermal, phase transformation and stress/strain changes make the description of heat treatment process more qualitative than quantitative. Thermal and residual stresses develop during heat treatment and quenching, and can result in distortion and even cracking. The latter leads to time consuming and expensive corrective measures of rework and repair welding. Residual stresses can reduce the service performance of steel and result in catastrophic failure during service. Because of the lack of ability to precisely predict the potential level of residual stress, distortion and/or cracking during and after quenching, the design of a heat treatment process generally depends on experience, and may involves a tedious trial and error process. Aggressive quenching is usually avoided so the strengthening ability of quenching cannot be used at its extreme limit, so the depth of effective quench and the improvement in properties are usually compromised.

Over the last three decades, different models have been presented to describe the martensite microstructure evolution and its influence on the mechanical properties and behaviour of steels during the process of quenching. Those developments have led both to atomic level and to finite element simulations to predict the residual stress, deformation and even fracture during quenching process. There are a variety of FEA-based software packages such as SYSWELD ^{TM} [1], DEFORM ^{TM} -HT[2], and DANTE^{TM} [3], which have been developed and commercialized to predict distortions and stresses resulting from heat treatment. These packages have been quite successfully used to conduct heat treatment simulation, to predict the residual stress and distortion brought about by a prescribed heat treatment process[4] and to do process optimization.

Despite these different approaches to the simulation of the quenching process, one thing remains the most difficult and challenging. How to measure the transient mechanical properties of the steel at the elevated temperatures during the quenching process when the microstructure of steel is a mixture of martensite and austenite? These transient temperature and microstructure - dependent mechanical properties of steels at elevated temperatures during quenching process are very difficult to measure experimentally due to the fact that the temperature of steels decreases dramatically from a high austenite temperature to a low temperature, usually room temperature in a very short time. During this time there are microstructure transformations, which include significant volume change and rapid and very large changes in strength and ductility.

Therefore, the mechanical properties of these partially transformed steels are usually not available in literature. But they are crucial for conducting a credible simulation to predict the residual stress, deformation and cracking phenomena during a quenching process. Without those data, it is impossible to predict the onset of quench cracking during and after quenching.

Some of the temperature-dependent mechanical properties that do exist in the literature are achieved by heating the already quenched steel samples to the desired temperature and conducting the tensile test. These data can be seen only as the properties of fully quenched martensite (with minimal tempering for high alloy steels) at only slightly elevated temperature. They do not give the properties of the austenite-martensite mixtures which would exist at these elevated temperatures during quenching. The mechanical properties suitable for use in the simulation of quenching process should be achieved by conducting in-situ tensile test during the quenching process where the microstructure of steel is the mixture of new martensite and the retained austenite which exists at that temperature.

Nowadays, for FEA simulations, the most-practiced method to deal with the data used for austenite-martensite microstructures in the simulation of quenching process is by using the rule of mixtures. Since the microstructure of steel during quenching is a mixture of martensite and austenite, the mechanical properties for the mixed phase is usually derived by applying this rule to the properties of martensite and austenite.

However, the correctness of the derived properties highly depends on the precision of elevated temperature mechanical properties of martensite and austenite, which are also difficult to measure and obtain. And for the complicated microstructure of mixed martensite and austenite, the properties cannot be derived simply by using a linear mixing rule. Since the austenite is a soft phase, it is obvious that it will yield first when subjected to a stress lower than the gross yield stress derived by using the rule of mixtures. Moreover, the ductility of the mixtures cannot be predicted from this rule of mixtures.

In recent years, many sophisticated testing machines like the Gleeble1500/3500 have been developed to conduct dynamic thermal-mechanical tests. These machines rely on resistance heating or induction heating to heat the samples. Because both ends of the sample are gripped and cooled, the middle cross-section of the sample always has the highest temperature. Due to these characteristics, the Gleeble machines are particularly suitable for conducting welding and joining tests. For mechanical property tests, because it is hard to achieve a uniform temperature distribution along the gauge length of samples, few tensile tests have been reported. Much more of the reported results are for compression testing, with the measurement of the strain calculated from the diameter change of the middle cross-section diameter. Because the compression results cannot predict tensile failure, and tensile tests can give out much more useful mechanical data such as fracture strain, data from tensile tests are much more desirable than those from compression tests.

A special kind of tensile specimen is needed, which can utilize the convenience of resistance heating, as in the Gleeble machine, and which can maintain a uniform temperature distribution along its gauge length at elevated temperatures during quenching. The maintenance of a uniform temperature is difficult to obtain, but is necessary to properly measure the mechanical properties at elevated temperatures during the quenching process.

1.2 Research Objectives

The main objective of this research is to develop a tensile test method that will be capable of measuring the transient mechanical properties of the steel at the elevated temperatures experienced throughout the quenching process.

The methods include:

- Design a special kind of tensile specimen to be used in a resistance heating device, which will have a sufficiently uniform temperature distribution along the gauge length of the sample. This uniform temperature will be achieved at any of the different temperatures present when the specimen goes through the entire heating and cooling process encountered during quenching. The temperature of the specimen should be able to be controlled conveniently during quenching, so the tensile test can be successfully conducted at a specified testing temperature .This includes the case when the specimen has been directly quenched to a preset temperature, and is held there for testing. The specimen must be able to change

temperatures rapidly, and quickly establish the uniform temperature without significant overshoot.

- Conduct FEA-based resistance heating and tensile simulations for different dimensions of the specimen to study the influence of dimension changes on the temperature distribution of the specimen, and its suitability for use in tensile tests.
- Validate the feasibility of this design concept through experiments. The temperature distribution along the length of the sample will be measured to determine the optimum dimensions of the sample for the purpose of achieving a uniform temperature distribution.

1.3 Thesis Overview

Chapter 2 first introduces the tool steel H13, which is the material of our research interest, its quenching process and phase transformations. Theories for the kinetics of martensite transformation, plastic strain and residual stress, and different approaches of modeling and simulation of heat treatment are then reviewed.

It is pointed out that the main challenge facing the simulation of heat treatment and quenching process is the lack of the essential mechanical properties at elevated temperatures during quenching process. The ASTM standards have been reviewed, only to find that there is no standardized method suitable for the tensile test at elevated temperatures for steels during quenching process.

Resistance heating is an effective method to heat steels, as it has been implemented in Gleeble machines. Different types of specimens, proposed by other authors, have been reviewed and analyzed through resistance heating simulation. These specimens have either the problem of being hard to achieve a uniform temperature distribution along the gauge length or the problem of being unsuitable for tensile testing. It becomes obvious that another kind of specimen must be designed to overcome the disadvantages of those samples. This new specimen must be able to quickly achieve a uniform temperature distribution along the gauge length at different elevated temperatures, and must also be suitable for in-situ tensile tests during quenching process.

Chapter 3 describes the concept of how to design a special kind of specimen for our specific material, H13, in order to conduct tensile tests successfully in the physical simulation of the quenching process. Resistance heating simulations have been conducted to do parametric studies for the dimensions of the sample in order to find the optimized dimensions for achieving a uniform temperature distribution along the gauge length of the sample. Also the design concept is also pre-verified to be mechanically sound through the stress simulation of the sample under tensile load.

Chapter 4 first describes the design and construction of a steel vacuum chamber used for the resistance heating of the specifically designed sample. The observation of the temperature distributions found for the sample will be compared with the predictions from the FEA simulation. The evolution of the modification of the design of the sample

will be made according to the previous experimental results and the new results will be further verified through experiment.

Chapter 5 will give out the conclusions of this approach to design and validate the feasibility of the specially-designed specimen to conduct the physical simulation of quenching. Its suitability for doing in-situ tensile tests to obtain mechanical properties at elevated temperature for different stages in the quenching process will be discussed.

CHAPTER 2 REVIEW OF LITERATURE

2.1 Tool Steels and Premium H13

Tool steels belong to an extension of alloy steels, specifically designed and manufactured under critical control to meet special quality requirements. In general, because they are used to cut or form other steels, they often are used at very high hardness levels. They usually contain significantly more alloying elements than other alloy steels [5].

The significant increase of alloying elements in tool steels enhances their hardenability greatly, and permits quenching conditions which are less severe to obtain a fully hardened martensite microstructure, especially in thick sections, or sections with a complex geometry. The existence of predominant martensite in fully hardened tool steels is the most significant microstructure feature which differentiates them from general steels.

Among all tool steels, premium H13 is one of the most popular and available hot work tool steels .It is a chromium hot-work tool steel and is used throughout industry for general hot-work applications: 1) light metal die casting dies; 2) metal extrusion dies; 3) hot forging dies; 4) plastic mould cavities. Because it will often be subjected to both high cyclic thermal stresses, and in some cases impact loading, the carbon levels are lower than most tool steels. Lowering the carbon level improves fracture toughness. Increasing the fracture toughness in this case means increasing the resistance to both the initiation

and the propagation of cracks. The typical composition (Wt. %) of H13 is 0.35C 1.5Mo 5.0Cr and 1.0V. The addition of refractory metals such as W, Mo, Cr and V tends to form carbides on tempering that inhibit dislocation motion and reduce the softening effects of heat. Most importantly, they produce secondary hardening, which is an increase in hardness on tempering. The family of chromium hot-work tool steel (H10 to H19) types resist softening at temperatures up to 430°C.

In this research, the Premium H13 grade steel donated by BOHLER UDDEHOLM LIMITED has been chosen as the steel to be studied.

2.2 Quenching Process and Martensite Transformation of Tool Steels

A typical hardening process for hot work tool steel is comprised of two stages: austenitising and quenching. During the austenitising stage, the tool steel work piece is heated in a protective atmosphere to its austenitising temperature, and is held at that temperature for a time long enough to ensure the total dissolution of carbide and alloy elements in the austenite. For large pieces, usually a two-stage heating is scheduled to ensure uniform heating up to over 1000°C. During the quenching stage, the work piece is cooled quickly enough to form martensite, generally using forced convective cooling with nitrogen gas. Rapid cooling from over 1000°C to about 500°C is very important, because this will suppress the precipitation of grain boundary non-ferrous carbides, as well as the formation of soft phases like bainite, ferrite and pearlite. The objective is to obtain martensite as the only predominant phase.

The martensite transformation from austenite is a diffusionless phase transformation. The closely-packed FCC structure of austenite is transformed to a less densely packed body-centered tetragonal (BCT) structure of martensite. Figure 2.1 shows the typical volume change of a transformed steel in the form of a dilatometer plot. The heating curve shows the change of the room temperature ferrite and carbide microstructure to the single phase austenite, which has close-packed atomic structure and therefore shrinkage occurs. On quenching, the austenite cools to a temperature well below the temperature at which it is stable and transforms to a BCT structure of martensite. Accompanying this quenching process, there is a volumetric expansion. This metallurgical transformation expansion contributes to deformation, distortion, and residual stresses, and can even cause cracking.

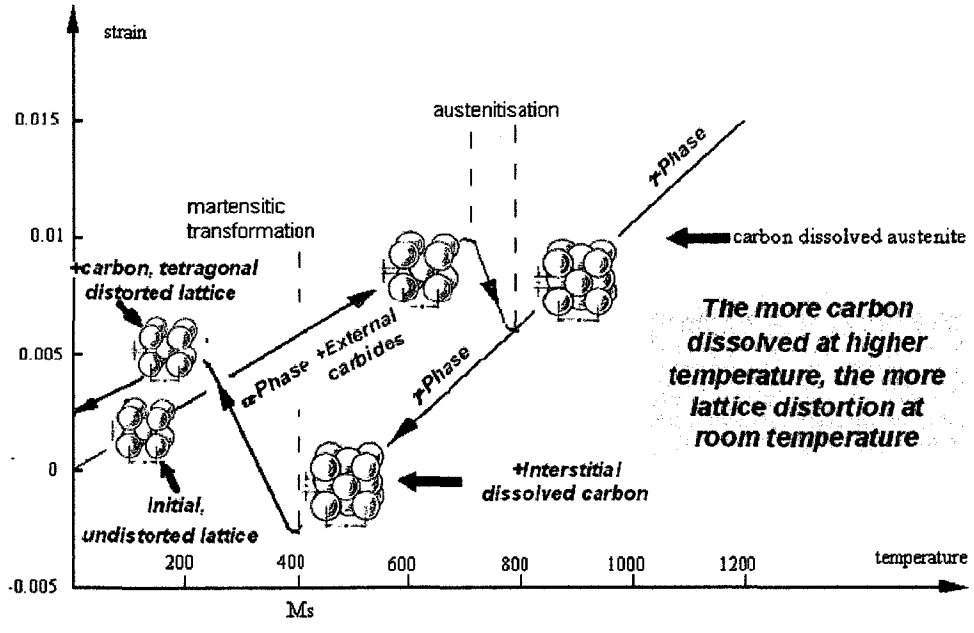

Figure 2.1 Dilatometer curve, typical volume change of a transformed steel[6]

2.3 Kinetics for Martensite Transformation

During the quenching process, the austenite to martensite reaction in steel is considered to be a time independent (athermal) diffusionless shear process. Below the martensite start temperature, *Ms* ,martensite transformation is independent of time and depends only on the temperature at which it occurs. The reaction is essentially instantaneous, and the volume fraction of martensite formed is that which represents the lowest Gibb's Free Energy for the coexistence of austenite and martensite. The volume percentage of martensite transformed from austenite $\xi(T)$ at a given temperature of T can be estimated by the semi-empirical relation developed by Koistinen-Marburger [7]

$$\xi(T) = 1 - \exp[-b(M_s - T)] \tag{1}$$

where b was found to be close to $0.011K^{-1}$.

At the martensite finish temperature, M_f, all the austenite will become martensite. For tool steels, M_f is well below 0°C. Some authors [8,9,10] have used the following equation to calculate the martensite fraction $\xi(T)$ transformed from austenite.

$$\xi(T) = 1 - (\frac{T - M_f}{M_s - M_f})^p \tag{2}$$

where p is assumed to be 2 or 2.5 [8,10].

The effect of stress on the martensite transformation starting temperature, Ms, has also been studied and observed. Tensile stress will increase Ms while compression will lower it. A modified Koistinen-Marburger equation incorporating a stress factor σ_m can be expressed as the following equation.

$$\xi(T) = 1 - \exp[-b(M_s - T) - \psi(\sigma_m)] \tag{3}$$

where $\psi(\sigma_m)$ is a function of stress component.

2.4 Plastic Strain and Residual Stress

Residual stress and deformation result from the non-uniform temperature distribution during the quenching process. As shown in Figure 2.2, H. W. Walton et al [11] have given a good illustration of residual stress development during quenching process.

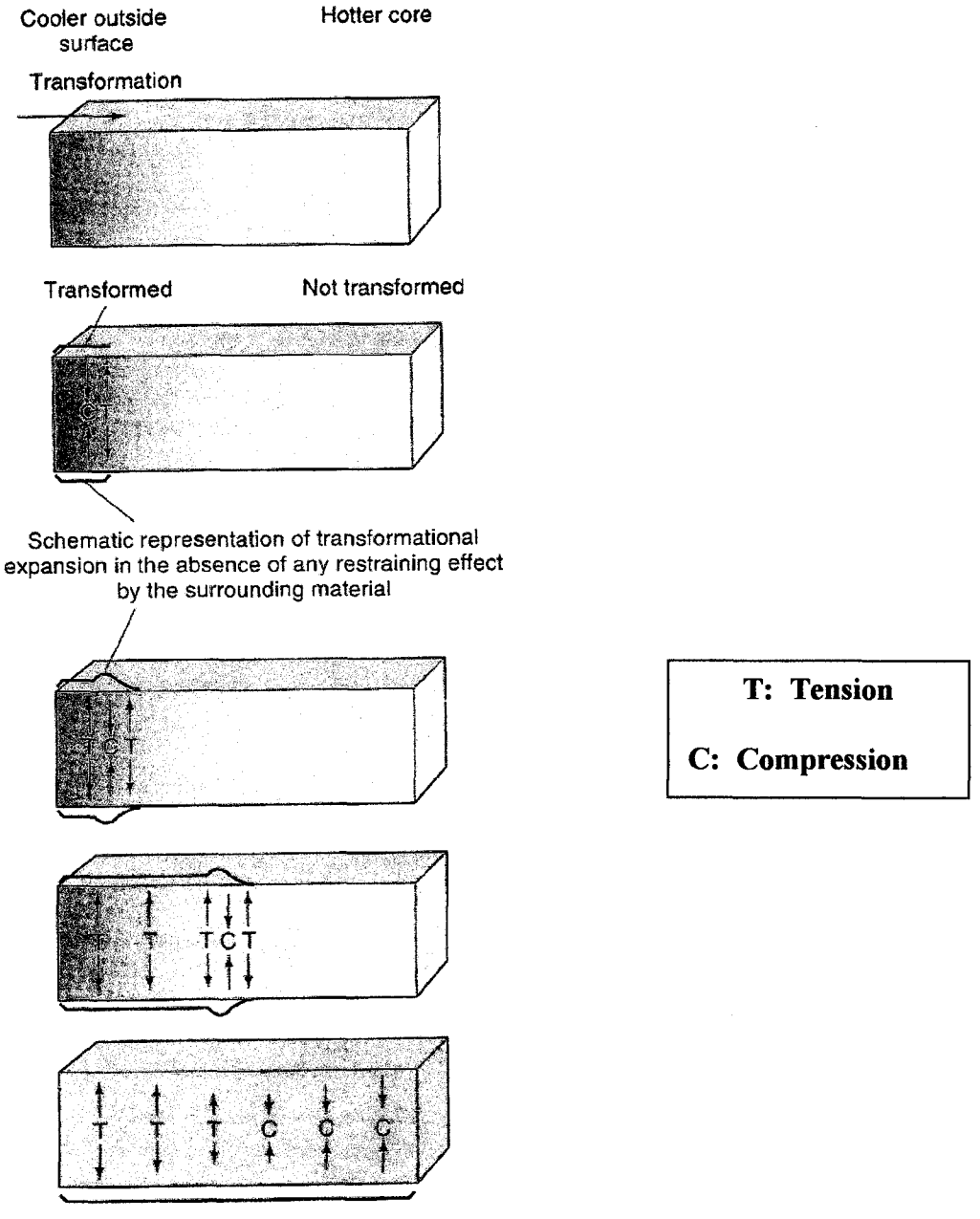

Figure 2.2 Development of residual stress during cooling of steel [11]. The brick shape represents a mathematical element from a block of steel bigger than this page. The left- hand side of the element is at the surface being quenched. The rest of the element extends into the interior. It shows how the residual stresses changes as the transformation interface moves into the bulk of the materials.

Cooling and the martensite transformation happen first on the surface and then extend toward the core of steel block as the interior cools by conduction. Because of the volume expansion when austenite transforms to martensite, the first transformed martensite will be subject to the compressive restraint by the austenite matrix while that matrix will be stretched in tension to maintain continuity, and to obey force equilibrium on a free body section.

While it is still at high temperatures, the austenite matrix will be able to yield easily to accommodate the surface martensite, and so can relax the compression in the first formed martensite. As the transformation goes deeper into the body of the part, the expansion of the newly formed martensite will further put the austenite in front of it in tension, and also act to stretch the previously formed martensite. The result will be that if the surface martensite had any remnant compressive stress, then this will be further relaxed. If it had already reached the relaxed state, then it will develop tensile stresses.

It is important to remember that during quenching, the temperature in the remaining core of austenite will cool from about 1030°C to the Ms temperature, which is about 320°C, and then will form austenite-martensite mixtures down to room temperature. As the temperature of the non-transformed austenite becomes cooler, its yield strength increases, and it becomes less able to relax the stresses caused by the encroaching transformation front.

So in summary, when there is a thin skin of transformation product at the surface, then the still very hot austenite core can yield so as to relax the misfit strains, leaving the martensite skin relatively stress free. As the interior austenite grows cooler and stronger, its ability to allow the newly transformed martensite to relax becomes less effective. When the final core of austenite transforms, it expands and there is minimal ability of the previously transformed product to relax. So the transformation of the final core causes stretching everywhere, and this is most severe in the previously completely relaxed skin.

The details of the final stress distribution are strongly affected by the relative strength of the austenite throughout the process. To model this correctly, it is important to know the mechanical properties of the austenite and the austenite-martenstie mixtures from 1030°C all the way down to room temperature. It is the measurement of these properties that the new tensile specimen described in this thesis has been designed to accomplish.

At room temperature, about twenty percent of the steel at that temperature will be retained untransformed austenite, regardless of whether it is at the surface or deep in the interior of the body.

The relative amount of austenite transformed to martensite at any temperature can be inferred from the overall changes in volume of the bulk materials, or it can be measured directly by neutron or X-ray diffraction. But the mechanical properties of these mixtures have proven to be difficult to measure, except at temperatures close to ambient. The final residual stress will demonstrate a profile of surface in tension and the core in

compression. It is this tensile stress on the surface which causes the cracking of steel during quenching.

2.5 Models and Simulation of Heat Treatment

The phenomenon of the heat treatment process is quite complicated and involves the coupling of thermal, metallurgical and mechanical interactions as shown in Figure 2.3.

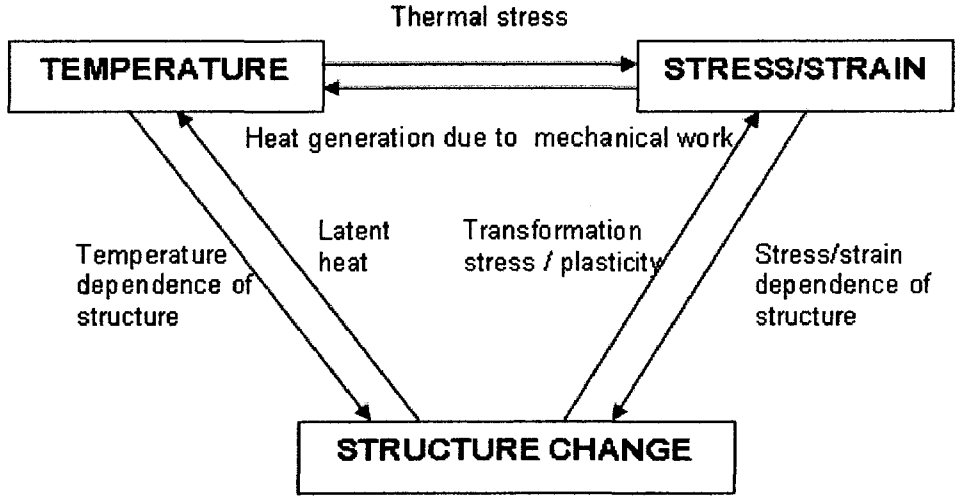

Figure 2.3 Coupling between thermal, metallurgical and mechanical interactions[12]

Temperature distribution changes in steel may cause temperature dependent phase transformations and thereby change its microstructure. For the quenching process, the Koistinen-Marburger equation mentioned above is usually applied to estimate the volume percent of martensite and austenite. Independent of the metallurgical changes, non-uniform temperature changes will cause thermal stress in the steel.

The microstructure change will bring about latent heat related thermal effects and change the temperature distribution. Also the microstructure change will be accompanied by transformation strain and plasticity. Transformation plasticity is associated with two physical phenomena. One is called the Greenwood-Johnson mechanism [13]: the volume variations between the phases generate microscopic internal stresses which are sufficient to induce plastic strain in the weaker phase, e.g. martensite deforming austenite. The second is called the Magee mechanism: anisotropic orientation of the transformed phase due to applied stress, which only exists for the martensite transformation. In the presence of an external stress, martensite needles are formed in a preferential direction.

For different models of transformation-induced plasticity, the transformation-induced plasticity is proposed as follows:

- $\varepsilon^{tp} = \frac{5}{6\sigma_\gamma^y}\frac{\Delta V}{V}\sigma$ Greenwood and Johnson model[13]
- $\varepsilon^{tp} = \frac{1}{4\sigma_\gamma^y}\frac{\Delta V}{V}(3p - 2p^{3/2})\sigma$ Abrassart model[14]
- $\varepsilon^{tp} = \frac{2}{3\sigma_\gamma^y}\frac{\Delta V}{V}(p\log p - p)\sigma$ Leblond model[15]

Where $\frac{\Delta V}{V}$ represents the relative volume variation between the phases during transformation and σ_γ^y the yield stress of austenite.

Stress/strain evolution will induce phase transformations and changes in the microstructure as is shown in the modified Koistinen-Marburger equation, which models the effect of stress on the martensite transformation starting temperature. The mechanical work of deformation will be partially turned into heat and this will further change the temperature distribution.

Many authors have tried to incorporate all the coupled phenomena between thermal, metallurgical and mechanical interactions in heat treatment to create different models to calculate thermal history, phase transformation and stress/strain evolution. They then apply these models to predict residual stress and deformation in heat treatment.

T. Inoue et al [12] created the metallo-thermo-mechanics model which couples stress-strain, thermal and metallurgical behaviour during the heat treatment process. The schematic description of this can be seen in Figure 2.3. This model has been implemented in the heat treatment FEA software "HEARTS" (HEAt tReaTment Simulation program) [16].

S. Denis, P. Archambault and E. Gautier et al [17] presented models for stress-phase transformation couplings in metallic alloys. Their work has been implemented in commercial heat treatment simulation software SYSWELD[18,19] and FORGE.

F. D. Fischer et al[20] has developed another model of elastoplasticity coupled with phase changes to describe materials experiencing phase transformation, in which he

introduced the term of transformation-induced plasticity(TRIP) as an additional strain rate term to the "classic" plastic strain rate term. This model can be properly implemented by using a user-supplied materials subroutine in ABAQUS.

Another important model describing the plastic behaviour of solids during solid-solid transformations for steels is presented by Jean-Baptiste Leblond et al[21]. It simply exploits the usual thermo-mechanical characteristics of materials, and assumes that the transformation plasticity phenomenon arises solely from the microscopic mechanism proposed by Greenwood and Johnson [13].

One of the most important and highly useful models of phase transformation in steel is presented by Lusk and his co-workers. Incorporating the phase transformation model of Lusk et al. [22,23,24,25] and the Bamman-Chiesa-Johnson (BCJ) materials model [11,26,27 ,28], the DANTE heat treatment simulation software has been developed to predict heat treatment distortions and residual stresses during steel heat treatment. Some simulation results are shown in Figure 2.4 and Figure 2.5.

DANTE^{TM} can be provided as a set of user subroutines for ABAQUS finite element solvers. The simulation results from this software are claimed to agree with measurement in a relative sense (within about 15%) regarding microstructure, deformation and residual stress. There are many examples of its application for the prediction of part distortions both during and after heat treatment. It does not claim to be able to predict local cracking probability.

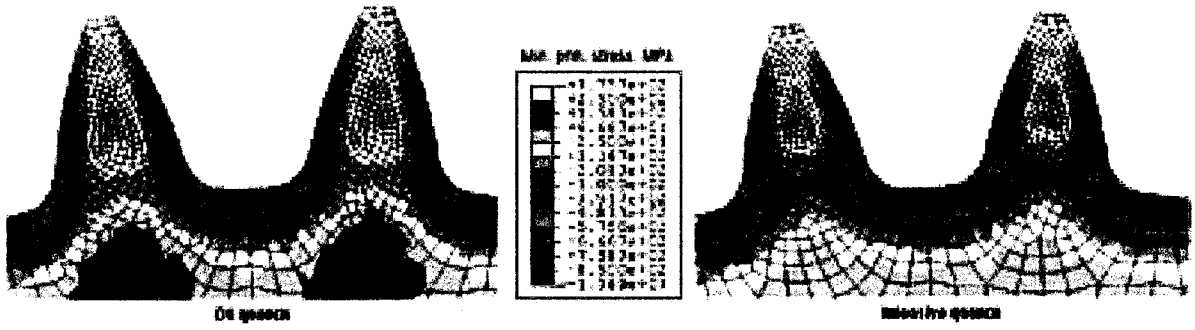

Figure 2.4 Simulation results of residual stress distribution in a gear after quenching [4].

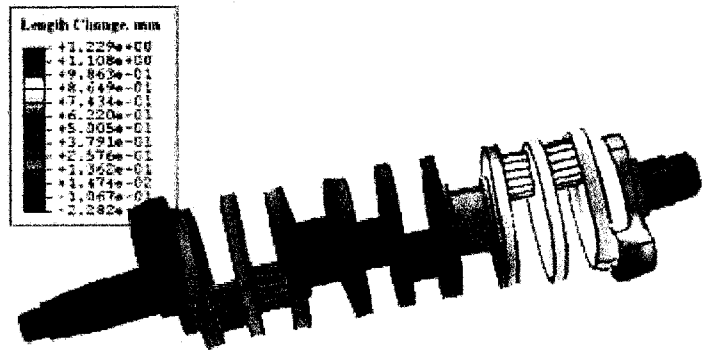

Figure 2.5 Simulation result of deformation of a crankshaft after quenching [4].

Generally, the following equation governing energy conservation takes into consideration of heat transfer, plastic work and latent heat:

$$\rho C_p \frac{\partial T}{\partial t} - div(kgradT) - \sigma_{ij} \dot{\varepsilon}_{ij}^{p} + \sum \rho_J l_J \dot{\xi}_J = 0 \qquad (4)$$

where :

ρ is mass density.

C_p is specific heat

k is heat conductivity

T is temperature

t is time

σ_{ij} is stress tensor

$\dot{\varepsilon}_{ij}^{p}$ is plastic strain rate tensor

ρ_J is the mass density for the J th phase constituent.

l_J is the enthalpy for the J th phase constituent.

$\dot{\xi}_J$ is the change rate of the volume fraction for the J th phase constituent.

$\sigma_{ij}\dot{\varepsilon}_{ij}^{p}$ accounts for the plastic work and $\sum \rho_J l_J \dot{\xi}_J$ accounts for the latent heat resulting from phase transformations.

For the calculation of the stress and strain evolution under complex conditions of heat treatment, the key resultant parameter relies on how to determine the strain rate tensor $\dot{\varepsilon}_{ij}$. The total strain rate tensor is comprised of five components and has been expressed as:

$$\dot{\varepsilon}_{ij} = \dot{\varepsilon}_{ij}^{e} + \dot{\varepsilon}_{ij}^{th} + + \dot{\varepsilon}_{ij}^{tr} + \dot{\varepsilon}_{ij}^{tp} + \dot{\varepsilon}_{ij}^{in} \qquad (5)$$

where:

$\dot{\varepsilon}_{ij}^{e}$ is the elastic strain rate.

$\dot{\varepsilon}_{ij}^{th}$ is the thermal strain rate

$\dot{\varepsilon}_{ij}^{tr}$ is the strain rate due to volume change associated with different phase transformations

$\dot{\varepsilon}_{ij}^{tp}$ is the transformation-induced plastic strain rate .

$\dot{\varepsilon}_{ij}^{in}$ is the inelastic strain rate.

Different models to simulate the heat treatment process mostly concentrate on how to calculate those strain rate elements.

2.6 Major Challenges Facing the Modelling and Simulation of Heat Treatment and Quenching Process

A major limitation of all modeling methods is the scarcity of accurate data, and this was true initially for heat treat simulation. The property data required is similar for any commercially available software package even though the way the data is used is unique and usually proprietary to each.

In order to determine the phase transformation parameters, continuous cooling transformation (CCT) diagrams as shown in Figure 2.6, isothermal transformation (TTT) diagrams, or raw data generated using ASTM standard A-1033 are the ways available to represent the phase transformation kinetics.

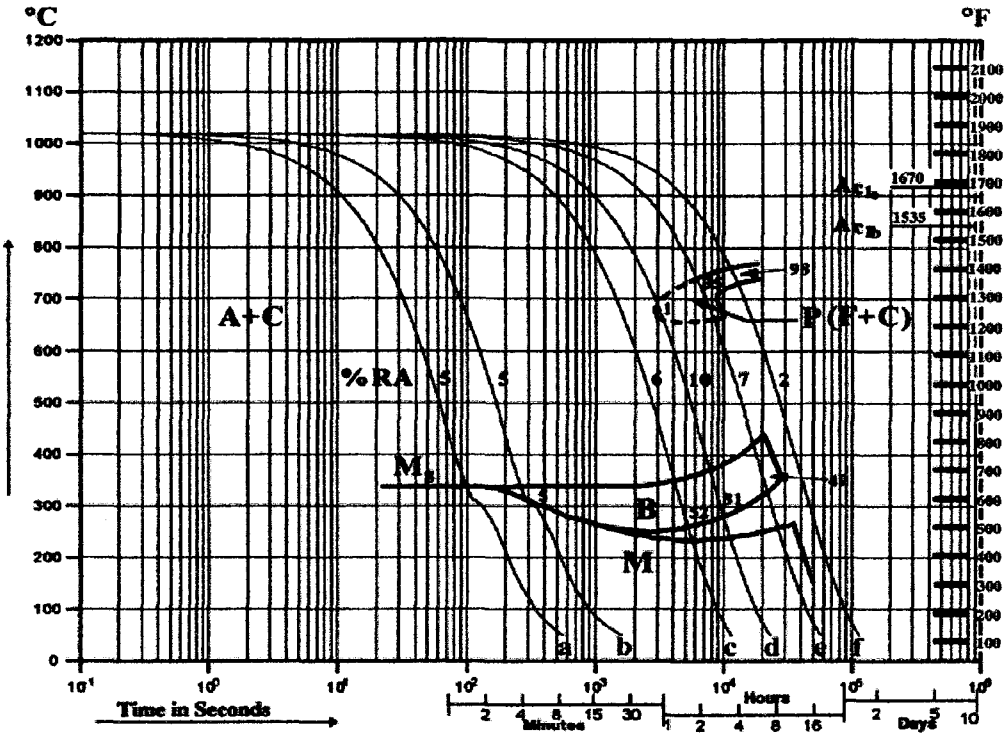

Figure 2.6 CCT Diagram for Premium H13 from Uddelhom[29]

A dilatometer can be used to measure the combined thermal strain and the strain due to volume change associated with phase transformation while steel goes through heat treatment.

But to determine transient mechanical properties of steels at elevated temperatures during heat treatment, especially during the quenching process remains a challenge. Experimental values for the tensile strength and yield stress for martensite, austenite, and their mixture at elevated temperature during quenching is critical to establish yield criteria, determine the transformation induced plasticity and predict the residual stresses, distortion and perhaps even fracture for all the models for heat treatment simulation.

In current practice of heat treatment simulation, the mechanical and physical properties χ of the steel are assumed to be expressed by the rule of mixtures as a linear combination of the properties χ_J of its constituents [30], such as pearlite, austenite, bainite, martensite, as shown in the following equation:

$$\chi = \sum_{J=1}^{N} \chi_J \xi_J \tag{6}$$

where $\sum_{J=1}^{N} \xi_J = 1$ and ξ_J denotes the volume fraction of the J th constituent .

As for quenched steel, its microstructure is a mixture of residual austenite and martensite. Since martensite is the hard phase embedded in the soft matrix of austenite, micro-yielding in austenite will occur when the stress is less than the yield stress derived from the rule of mixtures. To derive the mechanical properties of such a mixed microstructure, a non-linear rule of mixtures is used as given by Leblond[31]. The non-linear rule of mixtures for the yield stress of the mixture of martensite(hard) and austenite(soft) is expressed as the equation:

$$\sigma_y(T) = [1 - f(\xi_\alpha)]\sigma_y^\gamma(T) + f(\xi_\alpha)\sigma_y^\alpha(T) \tag{7}$$

Where:

$f(\xi_\alpha)$ is the non-linear function of the volume fraction of martensite ξ_α;

$\sigma_y^\gamma(T)$ is the temperature-dependent yield stress of austenite;

$\sigma_y^\alpha(T)$ is the temperature-dependent yield stress of martensite.

This approach to calculate mechanical properties is only an approximation of the real world. They are based on the properties of single phases at different temperatures from the austenitizing temperature to room temperature, which are also quite difficult to obtain experimentally.

The precise mechanical data for austenite, martensite and mixtures of them during the quenching process can be obtained only through mechanical tests such as tensile or compression test at the transient temperature and state during the quenching process.

2.7 Current Efforts to Standardize the Measurement of Steel Phase Transformation Kinetics and Dilatation Strains

Currently, there are no open-literature reference sources or databases, providing both the kinetic and thermal strain components associated with steel phase transformations, for heat treatment process modeling and simulation. Data had been collected using non-standardised techniques, resulting in a wide variety of data that has not always proven to be useful for process optimisation in manufacturing operations. Standardized methods of measurement and data interpretation, necessary as a basis for the establishment of a quantitative database for process modeling, need to be developed. Accurate data will enable reliable predictive computer modeling of structures and residual stresses.

In 2001, a collaborative project sponsored by the US Department of Energy under AISI's Technology Roadmap Project on quantitative measurement of steel phase transformation (QMST) by the American Iron and Steel Institute (AISI) in co-operation with over a

dozen companies was launched [32]. The purpose of the QMST collaborative project was to develop a standard practice for obtaining and archiving quantitative steel transformation kinetics and thermal strain data. It has resulted in a new ASTM standard, A1033, "Practice for quantitative measurement and reporting of hypo-eutectoid carbon and low-alloys steel phase transformations"[33]. In this practice, the determination of hypo-eutectoid steel phase transformation behaviour by using high-speed dilatometry techniques for measuring linear dimensional change as a function of time and temperature has been defined.

But how to quantify transformation of austenite while a static elastic stress is applied to the austenite as well as transformation of the austenite while it is undergoing plastic deformation is highly challenging and remains as the future work for the QMST project.

2.8 Tensile Tests at Elevated Temperature

The standard test methods for elevated temperature tension tests of metallic materials has been specified in ASTM designation: E21-05 [34]. The tensile strength, yield strength, elongation and reduction of area of metallic materials at elevated temperatures can be determined from the tensile stress-strain curves. Those properties thereby obtained will be utilized in the estimation of the ability of materials to withstand the application of applied tensile forces under a variety of service conditions.

In the details of ASTM E21-05, Section1.3 says that these test methods do not apply to rapid heating. Section 5.2.2, which lays out the allowable heating methods, says: "Heating shall be by electric resistance or radiation furnace with the specimen in air atmospheric temperature unless other media are specifically agreed upon in advance". Throughout the rest of E21-05, it is clear that the document really assumes that the heating method is to enclose the specimen in a radiant furnace.

Figure 2.7 illustrates the simplest setup of a tensile test. Usually for tensile test at elevated temperatures, an electrical resistance or radiation furnace is built to provide heating and temperature maintenance for the tensile sample.

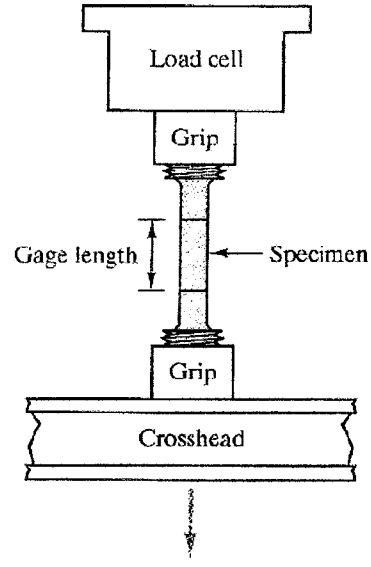

Figure 2.7 A simple tensile test setup [35]

The simplified description of an ordinary tensile specimen is that it typically comprises a long cylinder, the middle third of which length (the gauge section) has a circular cross-section whose diameter is about 0.5 to 0.7 that of the two end sections(the shoulders).

The tensile sample is gripped on the shoulders and pulled to measure its resistance to stretching forces. Reducing the diameter of the middle cross-section makes the stretching load per atom in the shoulders 0.25 to 0.49 times less than the load borne by atoms in the gauge section, so almost all the stretching occurs in the highly stressed gauge section.

For an above-mentioned ordinary tensile sample, the shoulders of the sample will heat up much more slowly than the gauge length and during rapid temperature changes, the middle and the end of the gauge length are at different temperatures. So the methods specified in ASTM E21-05 do not apply to rapid heating.

Also for both heating methods, the grips generally must be cooled, and so the grips cool the specimen shoulders, and the shoulders, unless they are very long, will cool the ends of the gauge length. This creates a significant temperature difference from the middle point of the gauge length to the ends of the gauge length. Experience using the Gleeble machine shows that even when using heated stainless steel grips the best temperature difference along the gauge length is about 60°C [36]. This is unacceptable according to ASTM E21 for elevated temperature tension tests of metallic materials.

In the quenching process, steel experiences cycles of heating and cooling. In order to measure the transient mechanical properties at a certain temperature during the quenching process, the steel sample must be able to change temperature quickly to meet the cooling rate requirement of the quenching process and must also stop and stabilize at the preset tensile testing temperature quickly. Traditional heating in electrical radiation furnace can

not meet these requirements. Also for a standard tensile sample, a non-uniform temperature distribution along the gauge length during quick heating and cooling is unavoidable, and this makes it unsuitable to conduct the tensile test on such a standard sample under the conditions of rapid heating and cooling experienced in the process of quenching of steel.

For the tensile test of steel at elevated temperatures during the process of quenching, different approaches must be taken in order to solve the problems discussed above.

It is very important for the entire gauge length to reach the same temperature in the austenitizing stage. The austenite grain size and the dissolution of non-ferrous carbides are greatly affected by the austenite temperature. The grain size has a huge effect on the hardenability of the steel. The rate of carbide precipitation, especially, above (750°C) has a profound effect on the mechanical properties of H13, especially its fracture toughness and thermal cycling durability. So maintaining a close-to-constant temperature along the entire gauge length in the austenitizing stage and during quenching is important in the present study.

The test system must use a different heating and cooling system other than that specified in ASTM E21-05 to develop an appropriate quenching response. ASTM E21-05 assumes a procedure that heats the specimen slowly to the test temperature, holding it there for 20 minutes, and then pulling it to failure at that temperature. No where in E21-05 is there a mention of cooling the sample to an intermediate temperature, and testing it

there, Because of the shoulders, it would be impossible to quench rapidly and establish a uniform temperature in the gauge length quickly. So the E21 standard specimen for an intermediate temperature quenching will probably produce different austenite decomposition products, at different points along the gauge length.

Therefore, to carry out the present work, it is necessary to invent a new type of specimen, it must be able to both heat and cool rapidly, and it must very quickly establish a constant temperature, both during austenitization, and at any prescribed quench temperature.

2.9 Gleeble Thermal –Mechanical Simulator and Resistance Heating

2.9.1 Gleeble Thermal-Mechanical Simulator

Because of the ease of controlling the electrical current, and therefore resistance heating rate, the family of "Gleeble" dynamic thermal-mechanical simulators, developed by Dynamic Systems Inc. [37], uses resistance heating to develop temperature changes in the samples.

In the Gleeble 1500/3500 thermo-mechanical simulators, a 60Hz low voltage but very high current is passed directly through the specimen, so that the resistance of the specimen itself generates the heat by the Joule effect. Since currents of several thousand amperes can be supplied to enable very fast heating rates in a very short time as

encountered in welding, the machines are well suited to simulate welding. One obvious advantage of using self-resistance heating is that the density of the electrical heating current will be relatively uniform across each cross-section, so isothermal transverse planes can be created along the entire specimen and substantially uniform heat generation over the width of a given cross-section can be ensured. This feature of self-resistance heating makes it much better than exterior radiant heating. Also the self-resistance heating can be controlled precisely and instantly by the control of electrical current input using a loop feedback signal based on the measured temperature.

Shown in Figure 2.8 is a photograph of the vacuum chamber in Gleeble 1500 thermo-mechanical simulator, and Figure 2.9 is a schematic illustration of resistance heating of a sample in the Gleeble Machine.

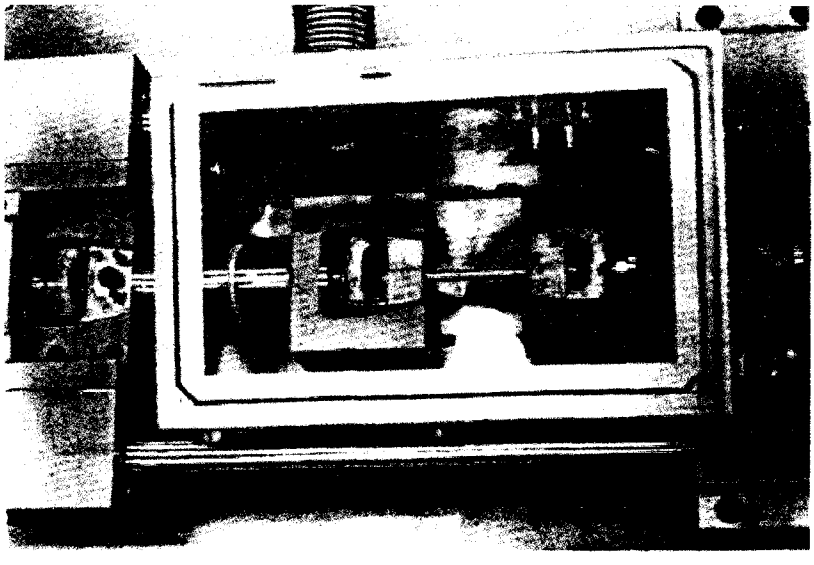

Figure 2.8 Vacuum chamber in Gleeble 1500 simulator.

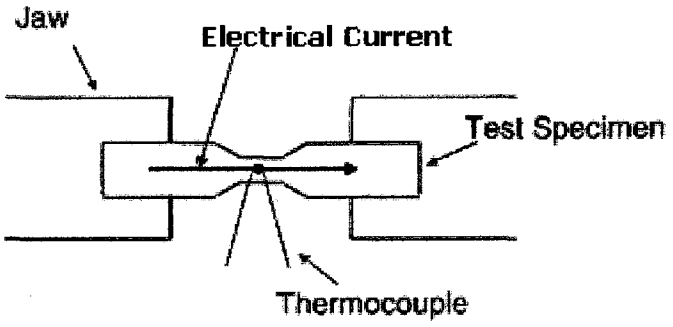

Figure 2.9 Schematic illustration of resistance heating in Gleeble machine

For a resistance heated tensile specimen with varying cross-sections, these cross-sections are connected electrically in series, so they each carry the same total electrical current but at different electrical current densities. Because of this difference in electrical current densities, different heat generation rates will exist for each section. This phenomenon can be quantified through the following calculation on resistance heating.

2.9.2 Resistance heating

Resistance heating is basically the heating of metal when an electrical current flows through it. According to the theory of electricity, the resistant heat generation rate $\dot{Q}$ is proportional to:

$$\dot{Q} = I^2 R \qquad (8)$$

where

I is the electric current

R is the resistance

This is called Joule heating or I-squared-R heating effect.

Considering a section of steel with a length of L and a cross section area of A, and assuming all the heat generated by resistance heating while driving a constant electrical current I through it is used to raise its temperature, then the following equation can be established:

$$\dot{Q}\Delta t = C_p M \Delta T \tag{9}$$

where:

C_p is the specific heat of the steel;

M is the mass of the steel.

So the rate of temperature rise will be

$$\frac{\Delta T}{\Delta t} = \frac{\dot{Q}}{C_p M} = \frac{I^2 R}{C_p M} \tag{10}$$

Since the resistance of the steel:

$$R = \beta \frac{L}{A} \tag{11}$$

where β is the resistivity of the steel

and the mass of the steel :

$$M = \rho V = \rho A L \tag{12}$$

Then the temperature change rate can be expressed as follows:

$$\frac{\Delta T}{\Delta t} = \left(\frac{I}{A}\right)^2 \frac{\beta}{C_p \cdot \rho} = \frac{i^2 \beta}{C_p \cdot \rho} \qquad (13)$$

It is obvious from the above equation that in a specimen with varying cross-sections:

- The temperature rise rate $\frac{\Delta T}{\Delta t}$ will be proportional to i^2, the square of the current density $i = \frac{I}{A}$, because the current density will be higher and the heat will be deposited into a smaller mass.

- Much higher heating rate is expected in the sections of small cross-section area because of high current density i there.

In summary, in an adiabatic system, the temperature increase resulting from resistance heating will be in inversely proportional to the square of the cross section area, when a constant electrical current is driven through a sample with different cross section areas.

2.9.3 Various Samples Used in Gleeble 1500 Thermo-Mechanical Simulator

Shown in Figure 2.10 is a steel cylinder used in Gleeble machine as a standard sample.

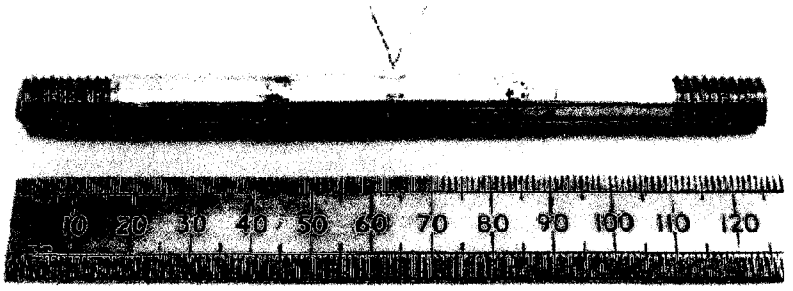

Figure 2.10 Standard sample for Gleeble machine[38]

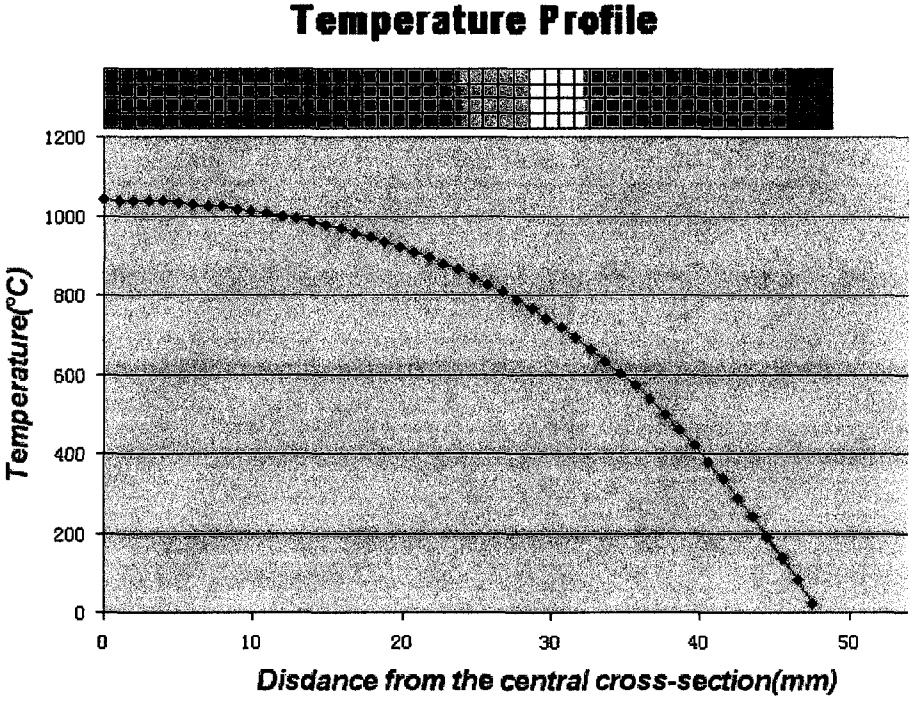

Figure 2.11 The Simulated profile of temperature distribution

When an electrical current is driven through the standard cylinder sample, the resistance heat generation rate will be the same through the whole length of the sample because of the uniform current density through each cross section. But the two ends of the sample

are clamped in grips which are cooled by water. Because of heat loss to the grips through thermal conduction, a non-uniform temperature distribution profile occurs along the gauge length. It is similar to the simulated result by the present author as shown in Figure 2.11. This simulation and all others in this thesis considered heat generation by Joule heating, conduction heat flow and heat loss due to radiation.

For the universally-used standard tensile sample, regardless of the shapes of its cross section, the cross sectional area in the gauge area is designed to be smaller than that of the two ends as shown in Figure 2.12.

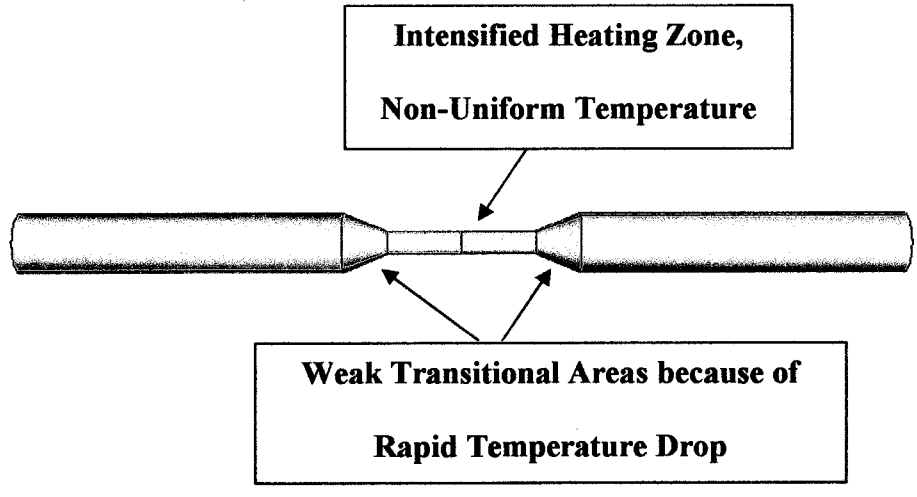

Figure 2.12 Standard tensile sample with varying circular cross section

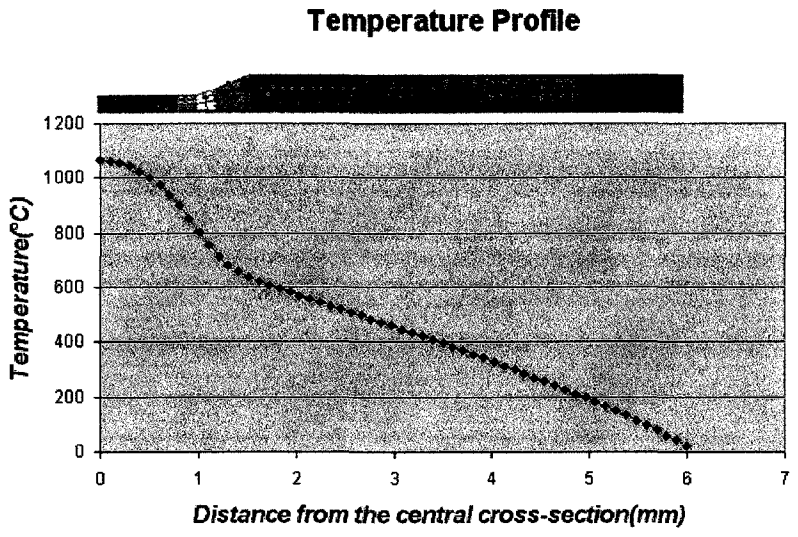

Figure 2.13 Simulation result of the temperature profile along the central line of a standard tensile sample

In fact, for a standard tensile sample shown in Figure 2.12, since its cross section in the gauge area is much smaller than that in the two ends, intensified resistance heating is unavoidable in the gauge area resulting in a non-uniform temperature distribution along the gauge length direction similar to the simulation result(see Figure 2.13 by the present author). In such a situation, the transitional areas from the gauge area to the ends will be much cooler than the central gauge area. This is an undesirable temperature profile not only because of the non-uniform temperature distribution in the gauge area but also the resulted weakness in the transitional areas which will be quenched from a lower temperature.

Norris and Wilson [38] have done 3D resistance heating thermal simulation to optimize the dimensions of standard samples with round, rectangle and square cross sections in order to get a better thermal profile for tensile samples of 6082 aluminium alloy in the

Gleeble thermo-mechanical simulator. In order to achieve a close-to-uniform temperature profile in the gauge area, the gauge length has to be shortened to a dimension comparable to its cross section dimension. For such a tensile sample, the gauge area is no longer subjected to a constant uniaxial tensile stress and neither its stress-strain reactions nor its ductility will be comparable to that of the standard tensile sample.

Liu et al [39] conducted some quantitative research on effects of stress and strain on bainitic transformation kinetics and transformation plasticity by experimenting on a special specimen shown in Figure 2.14 using a Gleeble 1500 testing machine with resistance heating .

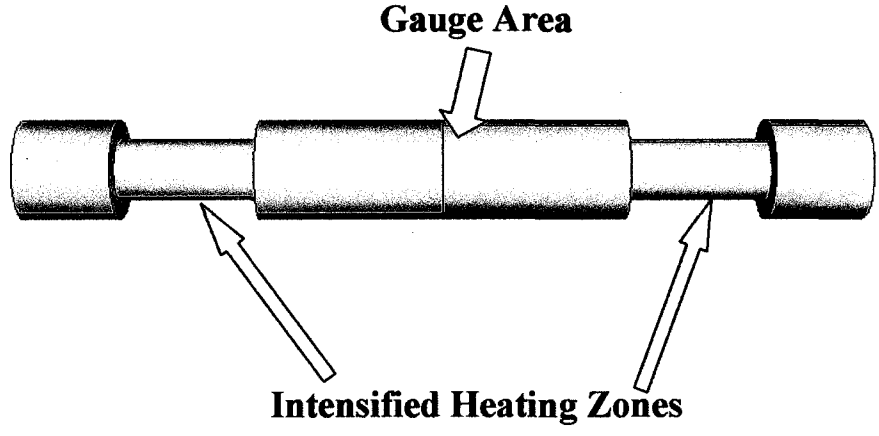

Figure 2.14 Analysis of another specifically designed sample [39]

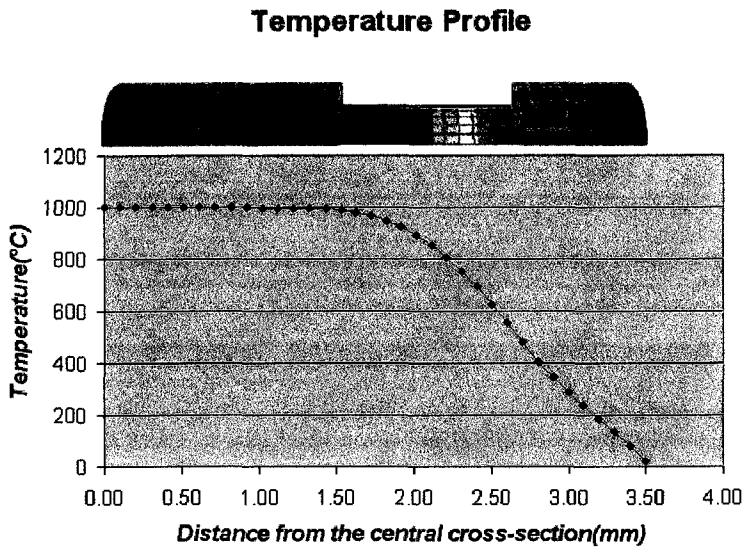

Figure 2.15 Simulation result of temperature profile along the central line of the special specimen

Figure 2.15 shows that the simulation results of resistance heating for Liu's specifically designed sample in Figure 2.14, using the material properties of the Premium H13 steel. The simulation result shows that even with a close-to-uniform temperature distribution in the central gauge area, there is continuous temperature drop in the intensified heat generation area as it comes closer to the end. The temperature drop in those narrow cross-section areas will result in a weak zone after quenching. If a tensile test is performed on such a sample, the weak narrow cross section area will be the area to yield and break first. It is of some use at low loads and it can be useful for studying transformation kinetics, but it is not a good tensile sample design for measuring mechanical properties (strength or ductility).

To achieve uniform temperature distribution along the gauge length of resistance heated samples in dynamic materials testing system like the Gleeble1500, a lot of effort has been made. Ferguson [40] has a patented apparatus which has the function of eliminating the longitudinal temperature gradient of samples for compression deformation testing , by serially connecting a specially designed resistance heating anvil to each end of the sample.

Also on the Dynamic System Inc.'s official web page[41], it is shown that a uniform temperature distribution in torsion test samples can be achieved by surrounding the sample with a end-heating element as shown in Figure 2.16. The heating element will establish a second circuit parallel to the sample and be heated when a parallel current is driven through it. This will provide extra heating for the ends of the sample, which will then generate a uniform temperature distribution along the gauge length of the sample. For this kind of exterior heating through the use of parallel resistance heating of an end-heating element, some disadvantages exist. First, the material chosen for the end-heating element has to be studied and selected in order to match the requirement for the heating of the sample. And also the heating of the sample will not respond to the exterior heating as fast as to the direct resistance heating. Therefore, with this kind of design, it is hard to meet the critical condition of rapid temperature changes required during the quenching process. So this method of heating is not good for the physical simulation of quenching process, or for doing in-situ tensile tests.

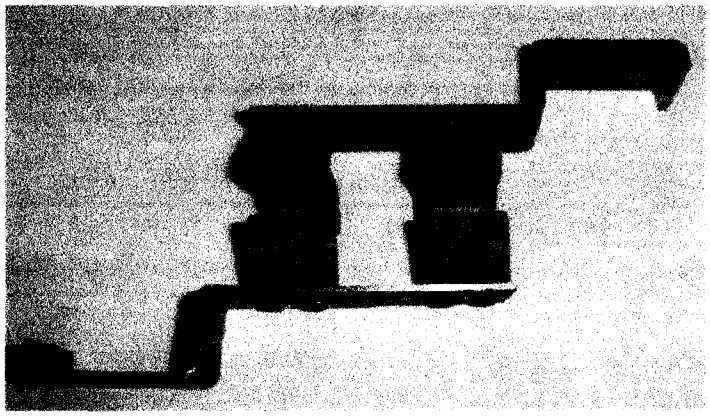

Figure 2.16 The End-heating element for torsion testing [41]

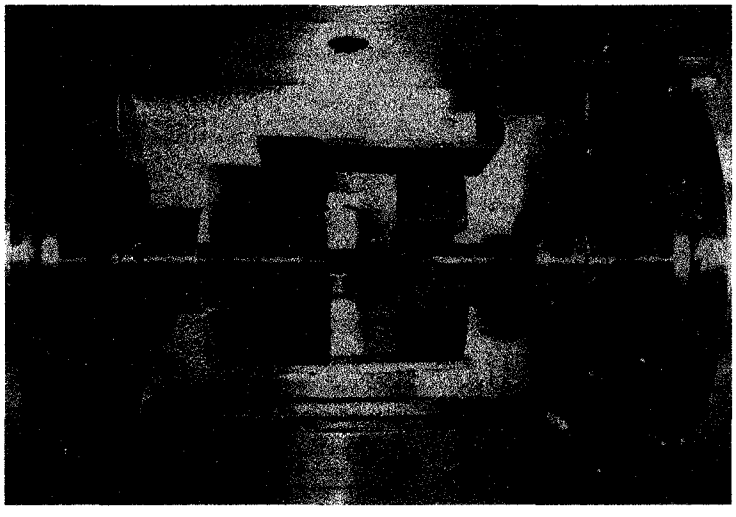

Figure 2.17 The installation of the end-heating element with the torsion specimen in the working chamber[41]

2.10 Other Methods of Heating

Induction heating is another way to heat steels quickly. Due to the characteristics of induction heating, heating is concentrated on the surface layer of the sample, the thickness of which depends on the frequency of the electrical current through the

inductor. Nagayama et al [42] have used hollow cylindrical samples which were heated by induction methods.

For the induction heating, there are some disadvantages. Any conductive materials under the influence of the magnetic field of the induction current will be heated as well and should be cooled or insulated electrically. Also for tensile samples , the shoulders of the sample still need to be held in grips which should be cooled. The grips themselves will also be heated by the electromagnetic field as well as the thermocouples. So at elevated temperatures, there is still the problem of a non-uniform temperature distribution along the gauge length for tensile samples. The spacing of the induction coils can be adjusted through a tedious process of trial-and-error to balance the heat loss to the grips through the shoulders. To our knowledge, none of the authors has published data on the uniformity of the temperatures achieved.

Some other experimental methods have been built to analyze the high-temperature mechanical properties of steels. Pierer et al[43] have used an in-situ tensile test method, the SSCT test, which have been developed over more than ten years to analyze the high-temperature mechanical properties of steel under continuous casting conditions. The details of the SSCT test or Submerged Split Chill Tensile test have been described in the article [44] and it is specifically designed to conduct process-near tensile test on solidifying steel to estimate the strength and crack susceptibility of the strand shell. It seems that using this SSCT test, the materials properties are evaluated under a temperature gradient field [45].

Compared to the characteristics of exterior heating such as resistance radiation heating or induction heating, direct resistance heating has the obvious advantage of changing the temperature of steel samples quickly by simply adjusting the electrical current.

2.11 Summary

The literature review reveals that:

- Numerical modelling and simulation of heat treatment process have been well established and can be used to improve the design of quenching process
- What is lacking are the mechanical data at elevated temperatures when the steel is austenite or in the transient states of mixtures of martensite and austenite. Those data are essential to conduct a better simulation for quenching process.
- There is no standard method to measure mechanical data at elevated temperatures when the steel is in the transient states of mixtures of martensite and austenite.
- Direct resistance heating can be used to heat steel much more quickly and give the convenience of controlling the temperature of steel sample by adjusting the current. Therefore, it is a potential method to be used in the physical simulation of quenching processes of steels.
- One major problem exists when the standard tensile sample is used in resistance heating: there is a non-uniform distribution of temperature along the gauge length.
- The design of a tensile sample using resistance heating, capable of giving useful tensile data, has not been fully developed. There are some non-standard sample

designs existing in the literature. But those designs have either the problem of not being able to achieve a uniform temperature distribution in the gauge area, or the other problem of being not suitable for tensile test.

This research is justified by focusing on the design of a special specimen, which will take advantage of resistance heating to balance the local heat generation, heat conduction and heat loss through radiation. It will allow the heating and cooling to be easily controlled to mimic the quenching process of steel, and at the same time, avoid the disadvantage of the non-uniform temperature distribution along the gauge length, so that the in-situ tensile tests can be conducted. The mechanical properties measured through these in-situ tensile tests during the quenching process will be a critical addition for numerical simulation of the quenching process. This will allow much better optimization of quenching processes, especially with the prediction of the potential for quench cracking especially.

CHAPTER 3 FEA-AIDED DESIGN OF SPECIMEN

3.1 Experimental Materials

The experimental materials, Premium H13, is a hot work tool steel donated by BOHLER UDDEHOLM LIMITED. The chemical composition of this batch of the material is shown in the Table 3.1:

Table 3.1 Chemical composition of Bohler Premium H13

C	Si	Mn	P	S	Cr	Mo	V	Cu
0.4	1.03	0.48	0.011	0.0002	5.15	1.4	0.94	0.08

The material was supplied in annealed state with a hardness of 185HB/53.9HC and grain size of ASTM:9.0

Its austenitizing temperature (under protective atmosphere) is 1020-1050°C, and Ms is about 320°C.

The other physical properties of Uddeholm Premium H13 are given in Appendix A.

3.2 Design of the Specimen

In the design of a resistance heated tensile that will simulate the different stages of a quenching heat treatment, the following three conditions must be satisfied:

1. The temperature of the sample should be able to be controlled precisely by the electrical current, occasionally with assistance of the cooling gas. It must also be able to change temperature rapidly and predictably.

2. The temperature along the gauge length of sample should be close to be uniform in order to ensure a uniform microstructure before and after quenching. It must also be uniform in order to perform the tensile test at the desired test temperature.

3. All of the transitional sections of samples connected to the gauge area of the sample must be stronger than the gauge area so the majority of the tensile strain is confined to the gauge length. Otherwise, a transitional section might break before the full cycle of the tensile test is finished along the gauge area.

In order to satisfy the first condition, the specimen can be designed to be flat and thin. This allows the heating of sample to be easily controlled by varying the electrical current

to control heating, to balance the radiation losses that assist rapid cooling. When the sample is flat, gas cooling will be even more effective because of a larger exposed surface to the cooling gas. With a thin specimen, the temperature differences through the cross section of the bulk sample will be minimized.

It was difficult to satisfy the second and third conditions due to the special characteristics of resistance heating, combined with the required stress distribution, because both of these are dependent on the specimen cross-section in different ways. The strength change of steel, before and after experiencing quenching, also had to be accounted for in each part of the specimen geometry.

As mentioned before in the literature review, when a constant current flows through a cylindrical sample with constant cross-section area, the generation of heat will be uniform along the gauge length but a lot of this heat will be conducted out though the end clamps. The gripping system must be water-cooled. This will result in an non-uniform temperature along the length of the sample with the highest temperature in the mid-section. This problem of non-uniform temperature distribution will be especially severe for a traditional tensile sample, whose cross-section area in the gauge area is much smaller than that in the end section, resulting in an even more intensified heat generation in the gauge area, and a greater conduction of heat by the specimen shoulder to the clamps.

Because of this non-uniform temperature along the length of traditional tensile sample, the temperature of transitional area of the gauge area adjacent to the shoulders will be much lower than that of the mid-section in the gauge area. In fact, somewhere in the shoulders or in the transitional gauge length area, the temperature will remain lower than austenite formation temperature, while the mid section of gauge length is high in austenite temperature range, to ensure dissolution of non-ferrous carbides. The higher the austenitizing temperature, the larger is the austenite grain size and the higher the hardenability. But in the transitional part of the sample just below the austenite formation temperature, the annealed microstructure is much softer than the quenched microstructure of martensite. The result could be a much lower strength in the transitional area or even in the shoulders after the quenching of the sample. Therefore, the tensile test cannot be conducted successfully on such a traditional tensile sample geometry when used in this in-situ dynamic quenching tensile test.

In order to satisfy the aforementioned three conditions, a unique design for a tensile specimen for quenching simulation in a resistance heating chamber has been developed as shown in Figure 3.1 (a) and (b).

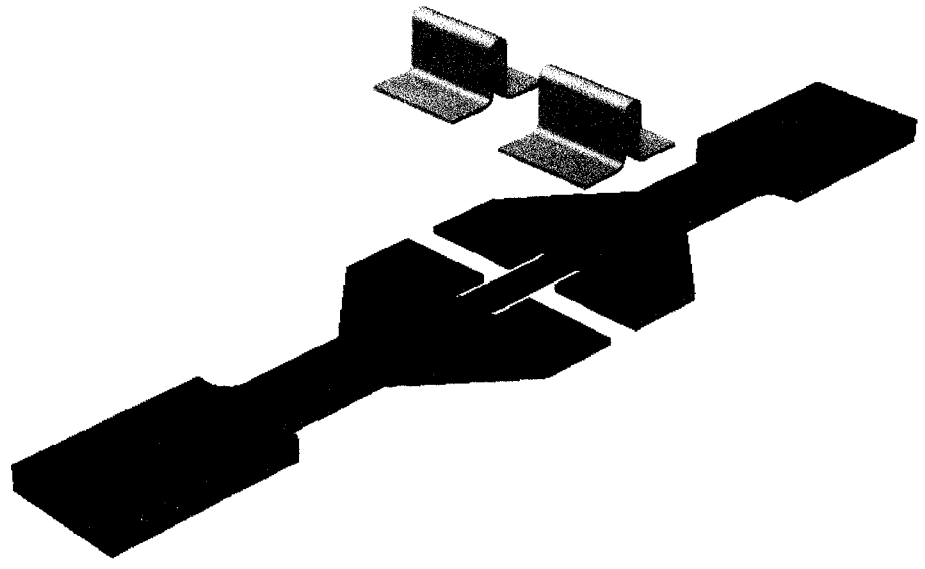

(a)

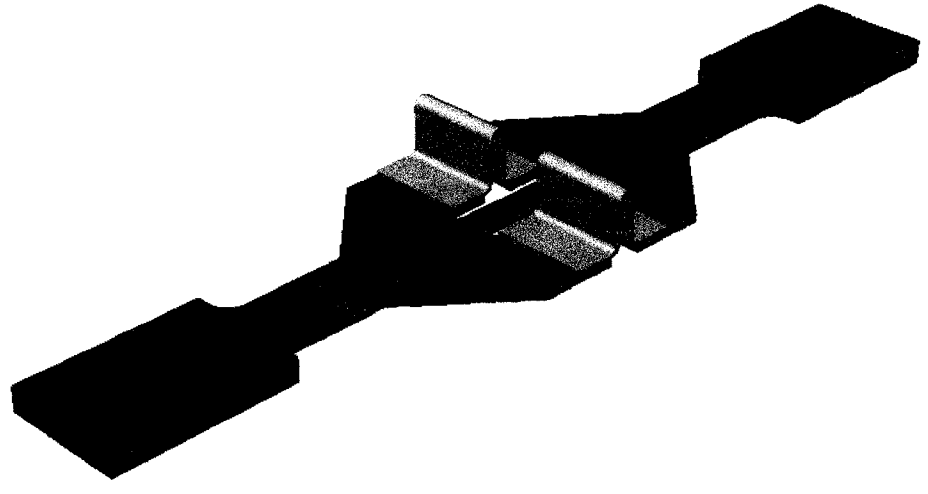

(b)

Figure 3.1 Specimen for quenching simulation and tensile testing

a) The sample and connecting bridges b) The assembly of sample and connectors

In this design, the sample can be divided to seven sections as shown in Figure 3.2:

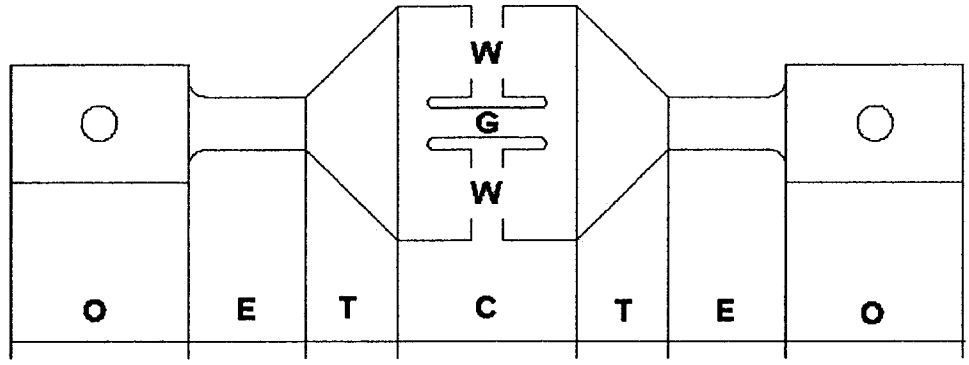

Figure 3.2 Seven sections of the sample

- Two O sections for clamping purposes;
- Two E sections are extensions that connect O sections to T sections;
- Two T sections are transition sections for connecting the E section to the central C section .
- The single C section between the two T sections is the central area of the sample which is composed of two W wing sections and one G gauge area .

The two W wings of the central section of the sample are designed with the purpose of branching out the electrical current at the ends of the gauge length, and therefore avoiding concentrated heating in the gauge area. Each of the outer wings is cut through in the middle and this leaves a gap in the steel wing. This gap is then bridged by welding onto it a specially designed non-steel connecting bridge as shown in Figure 3.1(b). The connecting bridges are made of materials of high melting temperature and conductivity to allow high currents to pass through them. They become quite soft.

Their special shape has very little resistance to a tensile load, which allows almost all tensile load to be concentrated in the central tensile sample. This special kind of design makes the wings of the central section connected in the sense of current flow but essentially disconnected in the sense of mechanical force. Current flow in the sample can also be schematically illustrated in Figure 3.3.

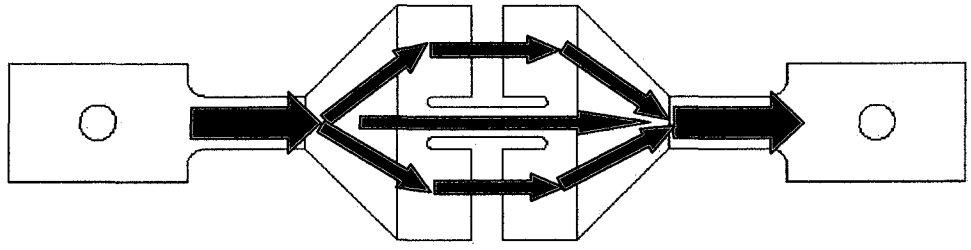

Figure 3.3 Schematic illustration of current flow in the sample during resistance heating

The cross-section area for the E sections is 9*4 or 36mm^2 while the cross-section area for the central C sections, (G+2W) is (40-2*2)*1.2 or 43.2 mm^2. Because heat generation rate per unit volume is in inverse proportion to the square of the cross-sectional area and radiation losses are proportional to surface area, the E sections will have a higher heat generation rate than T, C (G + 2W) sections and lower radiation loss. Despite the intense heat loss by conduction through the clamps, the E sections reach the highest temperature found within the entire sample. This is important because it allows them to provide conductive heat flow to both the grips, and the C sections, and thereby they add heat to the ends of the gauge length making the temperature more uniform along the length direction of the sample.

The E sections are designed to be thicker than the C (G + 2W) sections, so the C (G + 2W) sections have a much higher surface-to-volume ratio. The heat dissipation through radiation and gas convection will be much stronger in the central C (C +2W) section than in the E and T sections. These radiation losses help create a heat sink in the C section somewhat like the heat sink in the clamping O sections where heat is sucked out through conduction by water cooling. The hotter areas radiate more heat than cooler ones. This will alleviate temperature non-uniformity along the gauge length of the sample. Also cooling and temperature control will be easier in the central C (G+2W) section by the introduction of cooling gas.

One other consideration that must be addressed is the fact that the strength of quenched steel can be many times higher than that of annealed steel. For this particular material H13, the central gauge area is designed to be 5*1.2*9 mm^3, so it has a cross section area of 6mm^2 or one sixth of the cross section area of the E extension section (6/36). This makes the E extension sections strong enough, even in the annealed conditions so they will not be seriously deformed or break before tensile test is conducted successfully on the hardened central gauge area of the tensile sample.

3.3 Resistance Heating Simulation and Optimization for the Design of the Tensile Specimen

3.3.1 Modelling for Resistance Heating Simulation

The geometries of the sample and the bridge connectors are generated in CATIA V5R14 and imported into ABAQUS V6.5 CAE to assemble, mesh and analyze. ABAQUS provides a fully coupled thermal-electrical procedure to analyze a Joule heating problem.

Because of the symmetry in the specimen, only half of the specimen is modeled as shown in Figure 3.4 to save CPU time. To simplify the modelling, two O end sections which are in contact with water-cooled clamps have been excluded and the outer boundary ends of E extension sections are assumed to be held at 20°C.

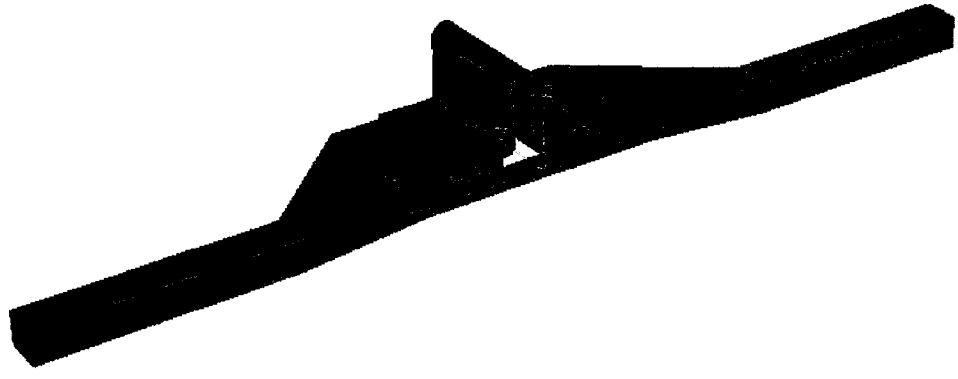

Figure 3.4 The half of the specimen to be modelled

The element type specified in coupled thermal-electrical heating simulation is *ELEMENT, TYPE=DC3D6E, which is 8-node linear coupled thermal-electrial brick.

The closely welded contacts between the B connecting bridges and the W wing sections are set to be "tied-up" in the model so that the heat and electrical conduction through the contact surfaces can be realized.

The temperature distribution along the length of the sample in steady state will be studied through the simulation. A steady state analysis can be obtained by specifying the STEADY STATE parameter on the keyword of *COUPLED THERMAL-ELECTRICAL procedure. For this particular problem, all electrically generated heat has been used to heat the sample so the *JOULE HEATING FRACTION is set to be 1.0.

3.3.2 Governing Equations and Boundary Conditions for Resistance Heating Simulation

For resistance heating, the governing equations are listed as follows:

$$\frac{\partial^2 V}{\partial x^2}+\frac{\partial^2 V}{\partial y^2}+\frac{\partial^2 V}{\partial z^2}=0 \tag{14}$$

$$i=-\frac{1}{\beta}\sqrt{\left(\frac{\partial V}{\partial x}\right)^2+\left(\frac{\partial V}{\partial y}\right)^2+\left(\frac{\partial V}{\partial z}\right)^2} \tag{15}$$

$$\rho C_p \frac{\partial T}{\partial t}-div(k\cdot gradT)-i^2\beta=0 \tag{16}$$

where:

V is electrical potential

i is electrical current density

β is electric resistivity

ρ is mass density

C_p is heat capacity

k is heat conductivity

3.3.3 Boundary Conditions

Boundary conditions are set as follows:

- The outer boundary ends of E extension sections are set to be fixed at 20°C;
- Distributed surface electrical currents are applied onto the two ends of the sample: one in and one out as shown in the following piece of code:

```
*Dsecurrent
_PickedSurf48,CS,-<DSEC>
** Name: SURFCURR-2   Type: Surface current
*Dsecurrent
_PICKEDSURF54,CS,<DSEC>
```

- Radiation occurs from all the surfaces to the ambient chamber at 20° C ; Surface radiation to ambient chamber satisfies the following equation:

$$H = -e\sigma A\left(T^4 - T_0^4\right) \tag{17}$$

where:

H - radiation heat flow rate

e -emissivity

σ -Stefan-Boltzmann constant: 5.670e-8 $W / m^2 * K^4$

A -surface area

T -surface temperature

T_0 -ambient temperature

- No surface heat loss through air convection is considered because the sample is in vacuum.

3.3.4 Properties of the Materials Used

The temperature –dependant material properties used for the simulation of resistance heating are shown as follows:

a) Bohler Premium H13 :

Thermal conductivity and electrical conductivity for premium H13 are shown in Figure 3.5 and Figure 3.6 respectively:

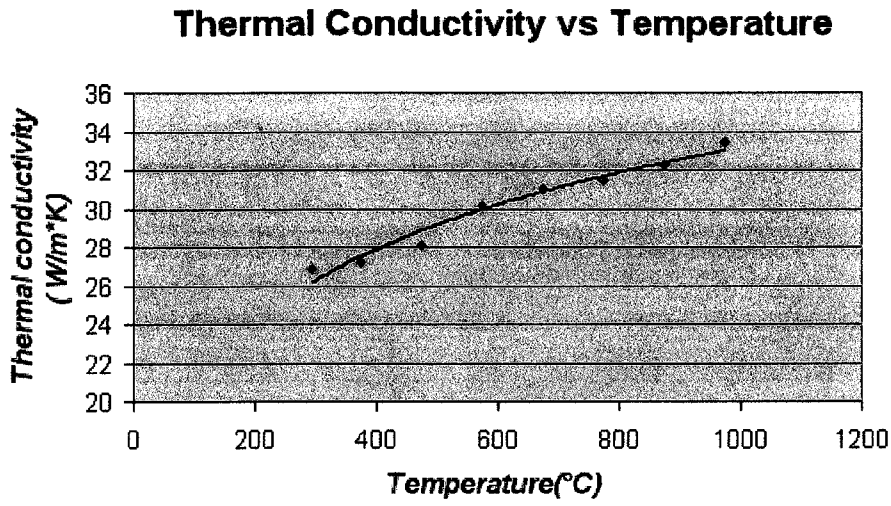

Figure 3.5 Thermal conductivity variation with temperature for Bohler W302 Superior /Premium H13[see APPENDIX A]

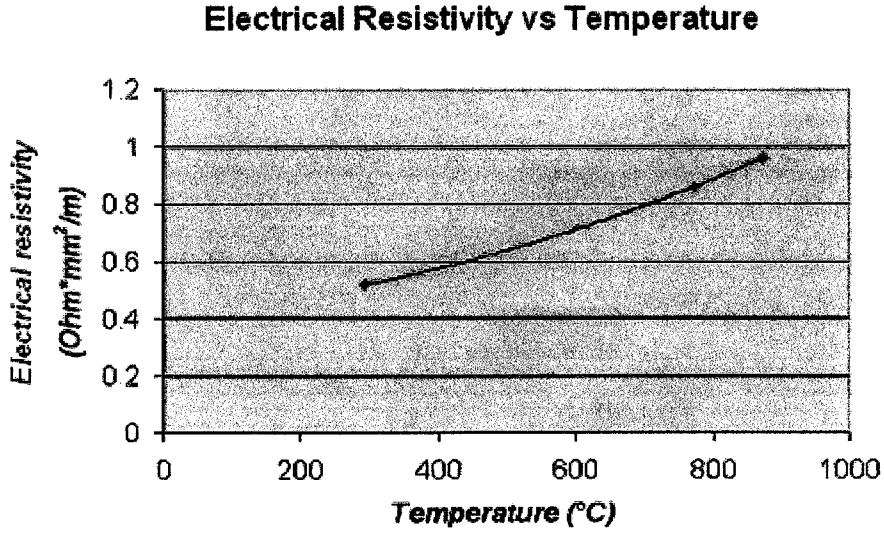

Figure 3.6 Electrical resistivity vs temperature for Bohler W302 Superior /Premium H13[See APPENDIX A]

The total normal radiation emittance for steel [46] is shown in Table 3.2.

Table 3.2 Radiation emittance for steel[46]

Metal	Temperature(°C)		
	100	500	1000
Steel(Polished)	0.13-0.21	0.18-0.26	0.55-0.88
Steel(Cleaned)	0.21-0.38	0.25-0.42	0.50-0.77

For the steel sample, the middle of the central gauge section will be heated to reach a temperature of 1020°C -1050°C .And since surface radiation is more dominant in the high temperature range, the emissivity for steel sample will be set to be 0.635 or (0.55+0.77)/2.

b) The Connecting Bridge material (CuNi alloy)

Material used for the two connecting bridges must satisfy the conditions of high electrical conductivity and with a melting point much higher than 1050°C, as well as having low strength and high ductility after quenching from high temperature. They must be soft annealed before the tensile test is attempted.

Table 3.3 Properties of copper and copper-nickel alloys [47]

Composition And Designation	Resistivity at 20°C (nΩ·m)	Melting Point Liquidus/Solidus (°C)	Tension/Shear Elastic Modulus(GPa)	Yield Strength (MPa)
Copper C10100,C10200	17.1	1083	115/44	420
90Copper10Nickel C70600	190	1150 /1100	140/52	90-110
80Copper20Nickel C71000	265	1200/1150	140/52	90-110
70Copper30Nickel C71500	375	1240/1170	150/57	125

Shown in Table 3.3 are the properties of copper and copper-nickel alloys. Based on above-mentioned conditions, those materials have been compared as follows:

Pure copper has the highest conductivity but the lowest melting point of 1083°C. Copper nickel alloy's liquidus/solidus temperatures will increase with the content of nickel. For 70 copper 30 nickel, liquidus/solidus temperatures are 1240/1170°C, which can meet the requirement for temperature, while both the electrical resistivity and the mechanical strength are low enough. So 70copper30 nickel was selected to be the material for the B connecting bridges.

The detailed mechanical, thermal and physical properties for 1mm thick flat strip of 70copper30nickel (annealed at 705°C) at 20°C [47] are shown below:

Mechanical properties:

- Elastic modulus: tensile 150GPa and shear 75GPa,
- Tensile strength: 380MPa
- Yield Strength: 125MPa
- Elongation : 36%
- Hardness: 86HRB
- Mass density : 8.94g/cm^3

Thermal and physical properties:

- Liquidus temperature: 1240°C
- Solidus temperature: 1170°C
- Coefficient of linear thermal expansion: 16.3 μ m/m·K at 20°C to 3000°C
- Specific heat: 380 J/kg·K at 20°C
- Thermal conductivity: 29W/m·K at 20°C.

Electrical properties:

- Electrical resistivity: 375n Ω·m at 20°C with a temperature coefficient of 4.8e-5/K in the range from 20 to 200 °C.

Total normal radiation emittance for nickel and copper [46] are shown in Table 3.4:

Table 3.4 Radiation emittance for nickel and copper

Metal	Temperature(°C)		
	100	500	1000
Nickel		0.09-0.15	0.14-0.22
Copper		0.02	

Since 70Copper30Nickel alloy has the color of silver-like nickel, its emissivity is assumed to be closer to that of nickel. Also the connector is located at the middle section of the sample, its temperature should be close to 1000°C. So in the simulation, an emittance of 0.18 or (0.14+0.22)/2 is used for the 70Copper30Nickel alloy surface.

3.4 Optimizing the Specimen Geometry

Two parameters have been adjusted through simulation: the length of the extension sections and the thickness of the connecting bridges.

a) The length of the E extension section.

Since E extension sections experience the highest flow of electrical current and the lowest surface heat loss when being resistance heated, it is expected that at a certain

length along the extension the intensified heating in the E extension will generate enough heat to compensate for the end conduction heat loss through the clamps. Therefore, beyond this point, these extensions will create a more uniform temperature distribution along the central part of the sample.

b)The thickness of CuNi connecting bridges.

Increasing the thickness of the connecting bridges will lower their electrical resistance. So a relatively stronger electrical current will flow through the connecting bridges, and a relatively lower electrical current will pass through the gauge area. Balancing these alternative current paths is important to create a uniform temperature distribution along the gauge length.

It is expected that the temperature in the T transitional sections will be equal to or a little higher than the temperature in the gauge area, so they will be fully austenitized and hardened during the quenching simulation. Therefore, they will be strong enough to stand the tensile test later.

The length of the E extension section is set to be 10, 20, 30, 40, 50mm and the thickness of CuNi connecting bridges is set to be 0.30, 0.45, 0.60, 0.75mm.

For any different combination of the length of the E extension section and the thickness of CuNi connecting bridges, the simulation is run by changing the electrical current

density applied to the outer ends of the extensions until the mid point in the gauge area reaches the expected austenitizing temperature of 1020°C, and then the temperature distribution along the length direction of the sample is recorded.

A parameter study program [see Appendix B] is developed to investigate the steady-state temperature distribution when different electrical current density is applied to the outer ends of the extensions. Also a post data processing program in PYTHON [see Appendix C] to analyze the temperature distributions along the length of the sample is developed to access the output database and derive the results.

- For connecting bridges of 0.6mm in thickness:

For connecting bridges of 0.6mm in thickness, the relationship between the boundary surface current density and the temperature of the middle node of the sample is shown in Table 3.5.

Table 3.5 Simulation results of the temperature of the middle node of the sample with the boundary surface current density.

Temperature (°C) in the middle of the gauge length					
Boundary Surface Current Density (A/m^2)	**Length of E extension section**				
	10mm	**20mm**	**30mm**	**40mm**	**50mm**
8.00E+06	577.113	645.561	685.398	708.74	721.775
8.50E+06	618.139	684.565	722.782	744.348	755.939
9.00E+06	657.81	722.21	758.533	778.456	788.835
9.50E+06	696.261	758.687	793.028	811.432	820.709
1.00E+07	733.397	793.664	826.387	843.259	851.433
1.05E+07	769.489	827.651	858.577	873.971	881.235
1.10E+07	804.452	860.686	889.654	903.792	910.258
1.15E+07	838.385	892.459	919.934	932.83	938.339
1.20E+07	871.494	923.455	949.286	960.982	965.229
1.25E+07	903.558	953.654	977.778	988	991.348
1.30E+07	934.727	982.896	1005.54	1014.14	1016.91
1.35E+07	965.267	1011.42	1032.61	1039.54	1041.84
1.40E+07	995.018	1039.35	1058.42	1064.27	1066.2
1.45E+07	1023.96	1066.49	1083.42	1088.45	1090.08
1.50E+07	1052.33	1092.94	1107.84	1112.21	1113.6

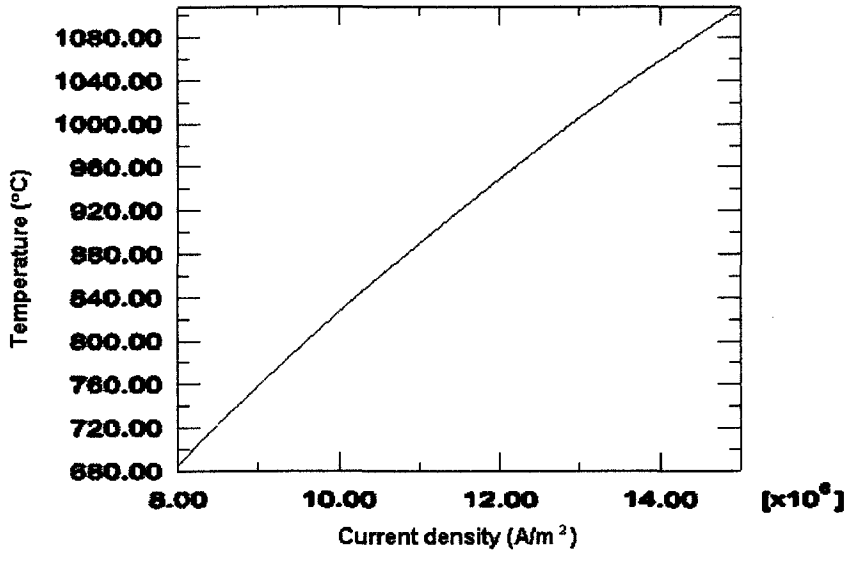

Figure 3.7 The temperature of the middle node in the gauge area changes with the end boundary electrical current density for a sample with the extension zones of 30mm in length and connecting bridges of 0.6mm in thickness.

- For connecting bridges with a thickness of 0.45mm,

For connecting bridges with a thickness of 0.45mm, the relation between the applied electrical current and the temperature of the middle node of the sample is shown in Table 3.6.

Table 3.6 Temperatures of the middle node of the samples for different surface electrical current density when using connecting bridges of 0.45mm in thickness

Temperature (°C) in the middle of the gauge length					
Boundary Surface Electrical Current Density (A/m2)	**Length of E extension section**				
	10mm	**20mm**	**30mm**	**40mm**	**50mm**
8.00E+06	627.325	689.385	725.557	746.913	758.769
8.50E+06	670.214	730.099	764.778	784.322	794.904
9.00E+06	711.628	769.589	802.255	820.324	829.817
9.50E+06	751.677	807.583	838.552	855.246	863.619
1.00E+07	790.515	844.245	873.668	888.835	896.223
1.05E+07	828.008	879.976	907.509	921.371	927.971
1.10E+07	864.55	914.417	940.362	953.119	958.912
1.15E+07	900.054	947.815	972.371	983.855	988.772
1.20E+07	934.486	980.499	1003.3	1013.73	1017.51
1.25E+07	967.951	1012.06	1033.47	1042.62	1045.62
1.30E+07	1000.62	1042.82	1062.99	1070.55	1072.99
1.35E+07	1032.43	1073	1091.57	1097.66	1099.69
1.40E+07	1063.48	1102.3	1118.97	1124.14	1125.86
1.45E+07	1093.84	1130.83	1145.74	1150.2	1151.65
1.50E+07	1123.48	1158.83	1171.86	1175.69	1176.9

It is obvious that the temperature at the central node of the sample will increase with the increase of the length of the E extension sections and with the surface current density applied at the two end boundaries. The increase of the length of the extension section will have a similar impact on the temperature profile as that of raising the temperature of the end boundary.

For a given surface current density applied at the two end boundaries and the length of the extension section, the temperature of the central node of the sample will increase with the decrease of the thickness of the connectors. This can be explained as follows. When the thickness of the bridge connectors decreases, their resistance will increase, which will drive more current though the central gauge area. As a result, the central gauge area will be heated to a higher temperature.

The magnitude of applied electrical current density at the two end boundaries which can be used to heat the sample's middle node to 1020°C can be derived from Table 3.5 and Table 3.6 and is shown in Table 3.7.

Table 3.7 The Magnitude of surface electrical current density applied at the two ends required to heat the sample's middle node to 1200°C

The thickness of the connectors in mm	Length of E extension section				
	10mm	20mm	30mm	40mm	50mm
0.60	1.44316	1.36536	1.32671	1.31154	1.30640
0.45			1.22768	1.21085	
0.30		1.11308	1.08430	1.06828	

3.4.1 The Effect of the Length of the Extension Sections on the Temperature Profile of the Samples:

For samples with different lengths for the extension sections but the same thickness of 0.6mm for the connecting bridges, the temperature profiles when the central middle nodes of samples are heated to 1020°C are compared as follows:

a) The length of E extension sections is 10mm:

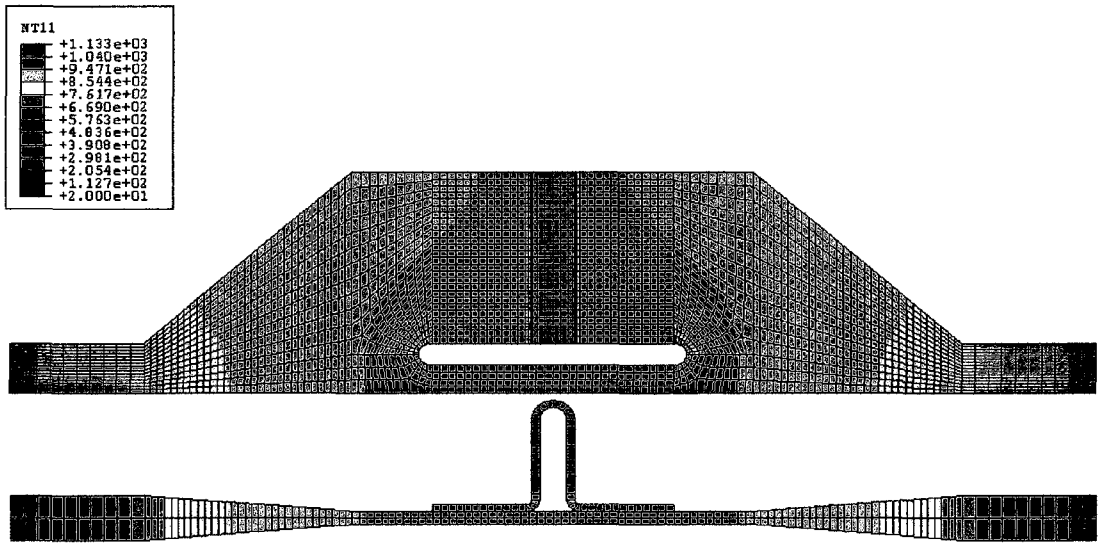

Figure 3.8 Simulation result of the temperature profile for a sample with the extension sections of 10mm in length.

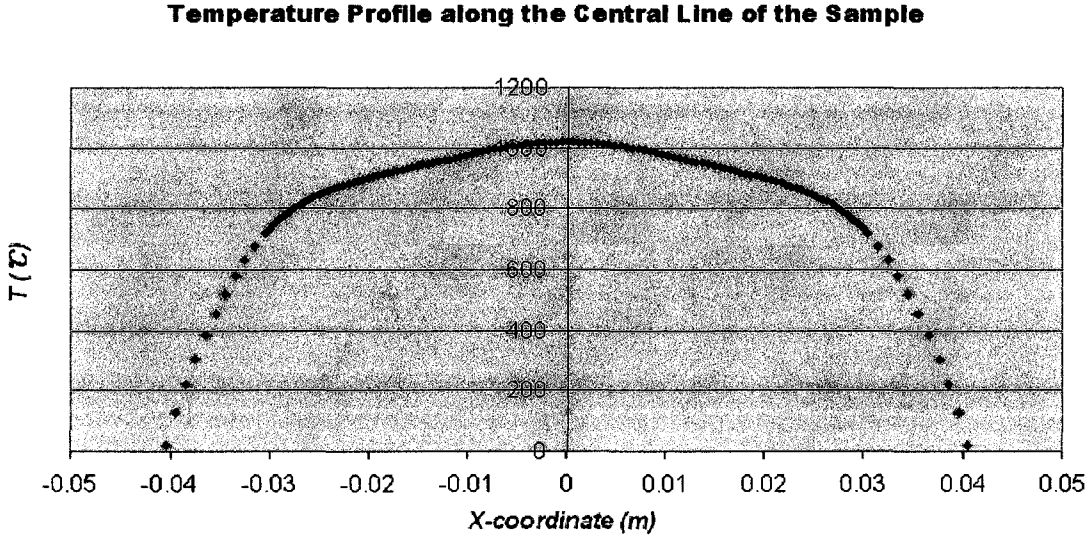

Figure 3.9 Simulation result of the temperature profile along the central line for a sample with the extension sections of 10mm in length.

b) The length of E extension sections is 20mm:

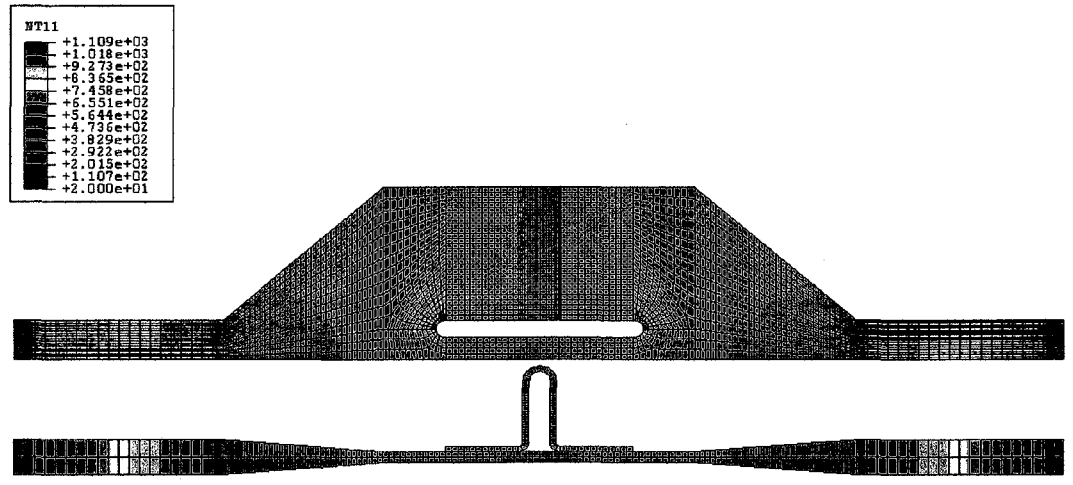

Figure 3.10 Simulation result of the temperature profile for a sample with the extension sections of 20mm in length.

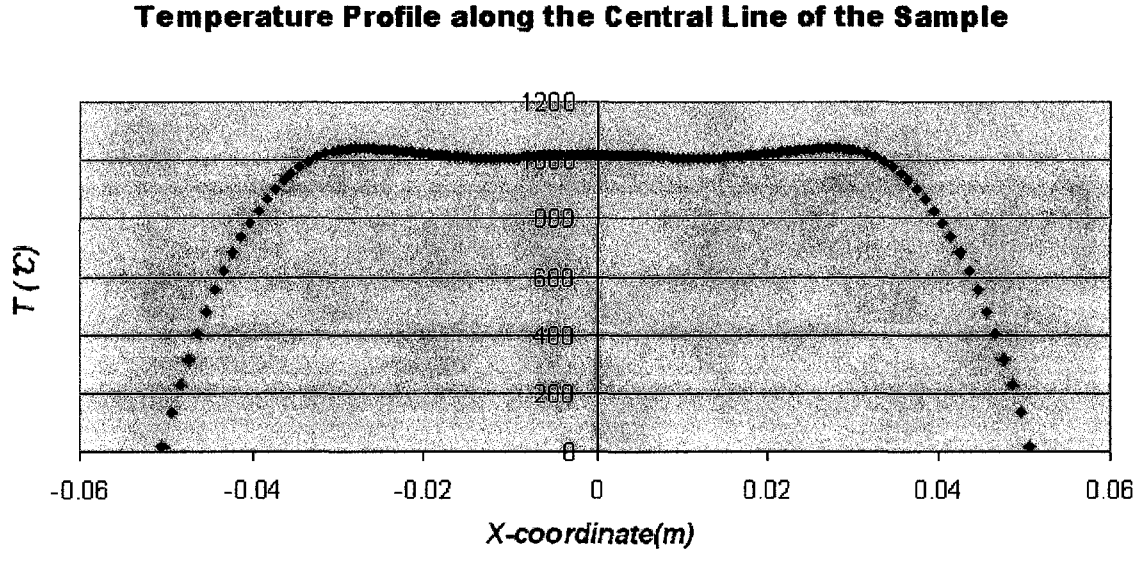

Figure 3.11 Simulation result of the temperature profile along the central line for a sample with the extension sections of 20mm in length.

c) The length of E extension sections is 30mm:

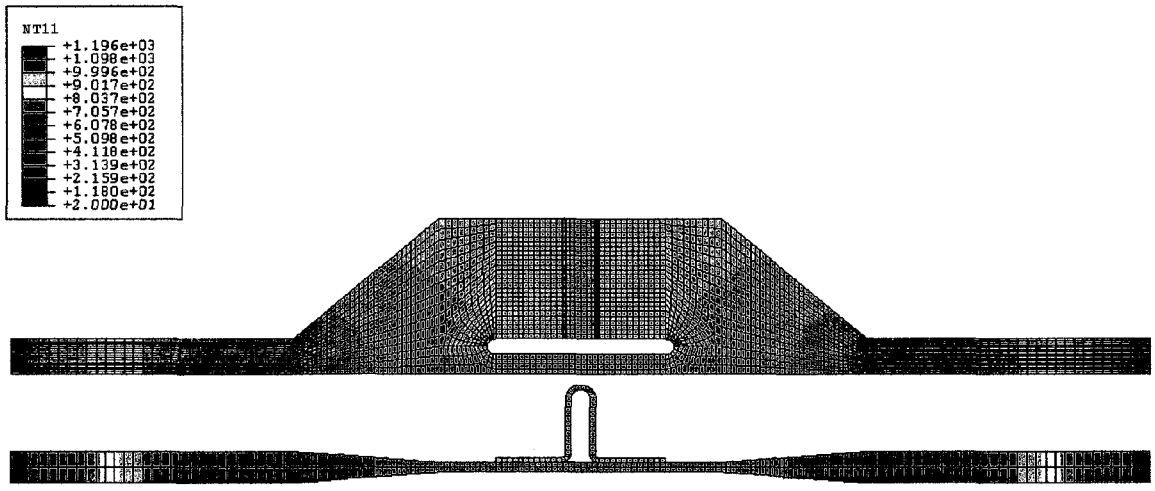

Figure 3.12 Simulation result of the temperature profile for a sample with the extension sections of 30mm in length.

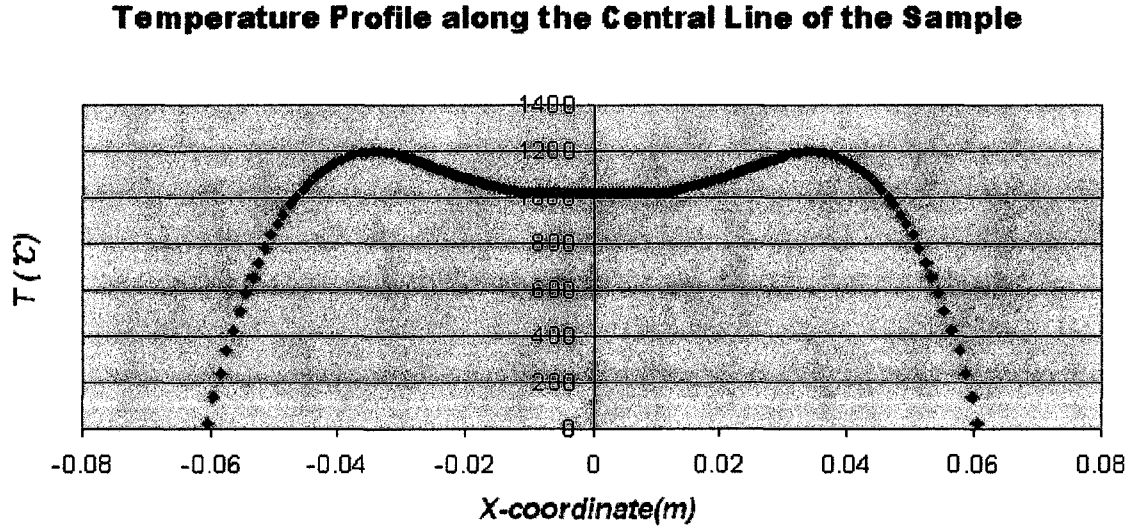

Figure 3.13 Simulation result of the temperature profile along the central line for a sample with the extension sections of 30mm in length.

d) The length of E extension sections is 40mm:

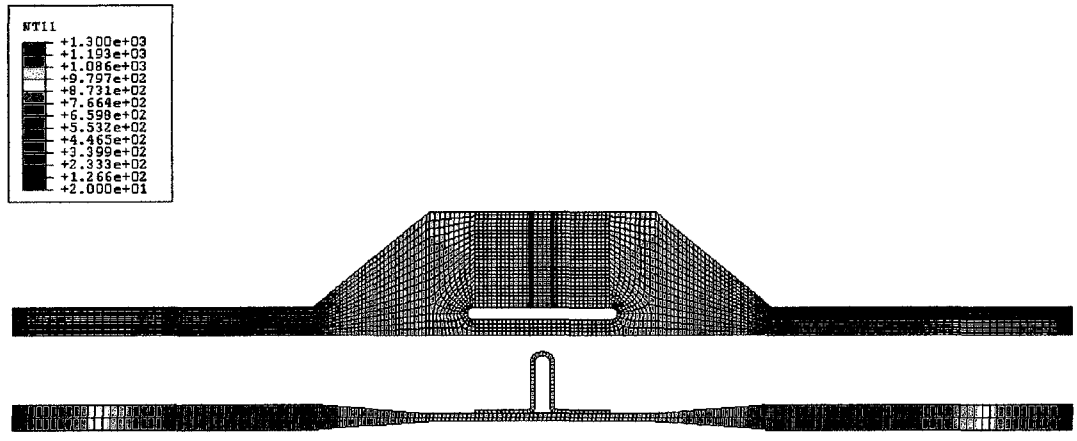

Figure 3.14 Simulation result of the temperature profile for a sample with the extension sections of 40mm in length.

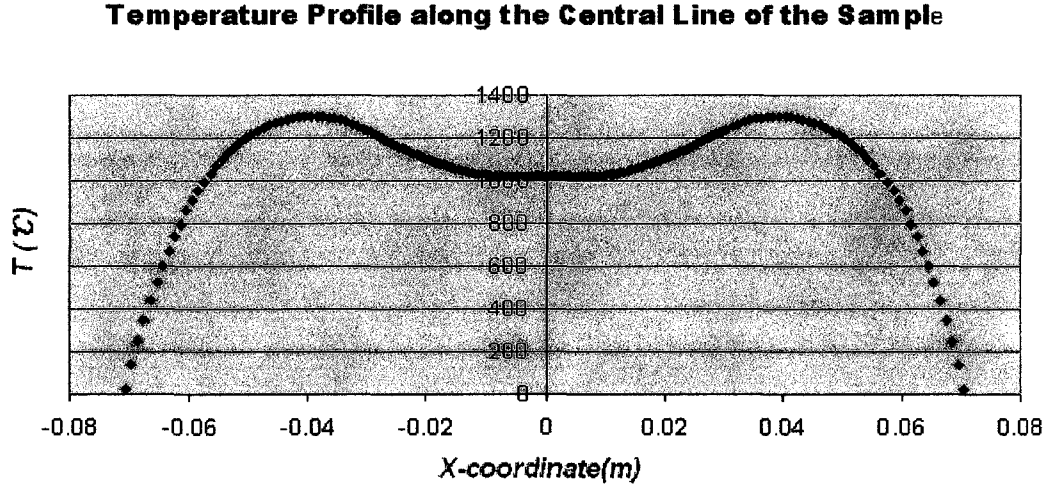

Figure 3.15 Simulation result of the temperature profile along the central line for a sample with the extension sections of 40mm in length.

e) The length of E extension sections is 50mm:

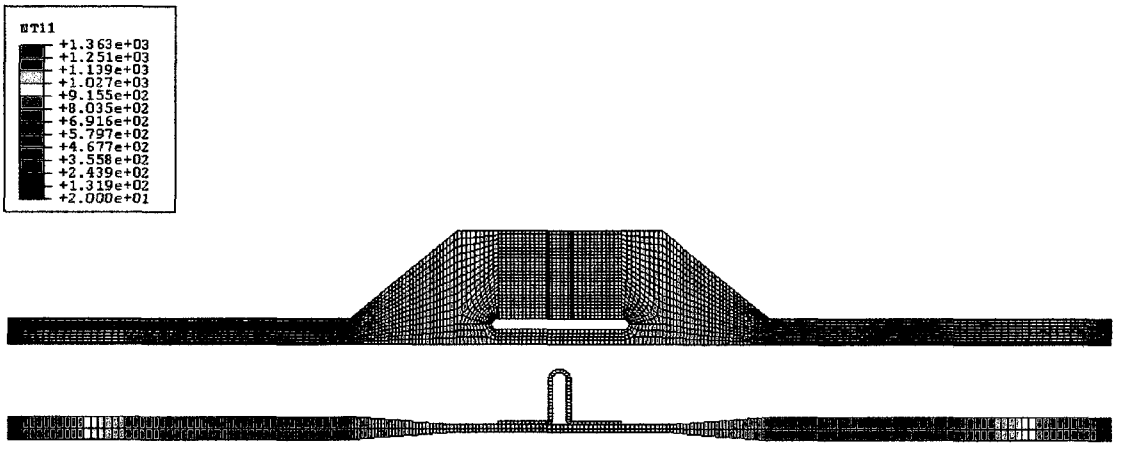

Figure 3.16 Simulation result of the temperature profile for a sample with the extension sections of 50mm in length.

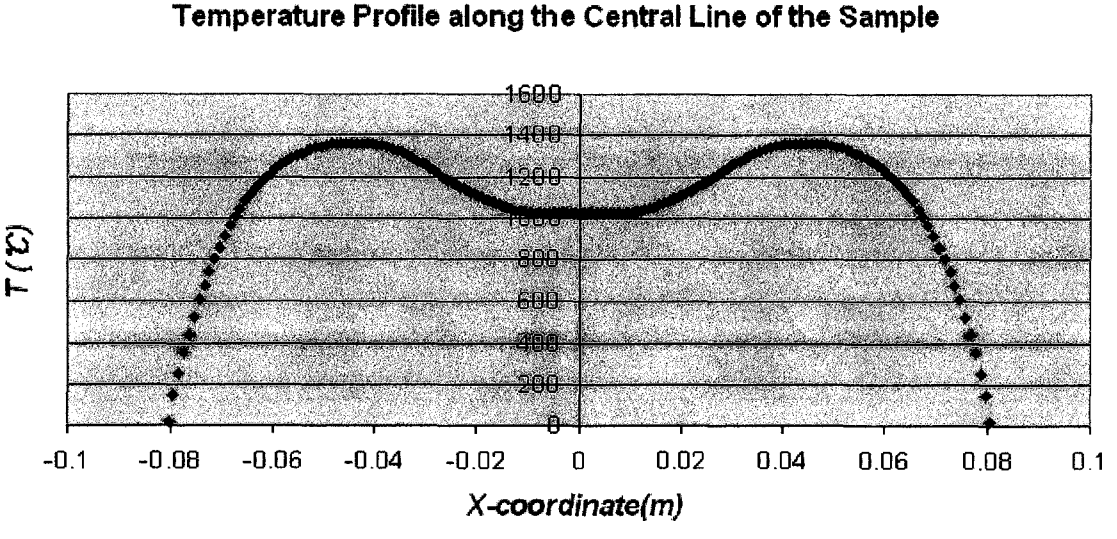

Figure 3.17 Simulation result of the temperature profile along the central line for a sample with the extension sections of 50mm in length.

The effect of the length of the extension section can be summarized in the following Table 3.8:

Table 3.8 The Influence of the length of extension zone

Length of Extension Zone (mm)	Boundary Surface Current Density (A/m2) to reach 1020°C	Mid Node Temperature (°C)	Temperature At the ends of the gauge length (°C)	Temperature Difference (°C) in Gauge Area |x|<=9mm	Maximum Temperature (°C) Along the central line In Extension Zone
10	1.44316e+7	1020.04	983.35	36.69	1020.04 **
20	1.36536e+7	1020.08	1009.23	10.85	1040.04
30	1.32671e+7	1020.15	1020.90	-0.75	1195.54
40	1.31154e+7	1020.07	1023.73	-3.66	1299.62
50	1.30640e+7	1020.13	1025.32	-5.19	1363.20

** The highest temperature is in the middle of the gauge area and out of the extension zones

Based on the comparison in the above table, the sample with an extension zone length of 30mm has the most uniform temperature distribution in the gauge area with a

temperature difference of only 0.75°C when its central node position is heated to 1020°C. The highest temperature of 1195.54°C happens in the extension zones (E).

Note that 1 $A/m^2 = 10^{-6} A/mm^2$, the electrical current driven through the sample should be larger than 1.3 x 107 A/m^2 * $36mm^2$ or 470Amps to heat the sample to a temperature of 1020°C in the middle of the gauge length. The current has been amplified through two stage transformers by a factor of 500 from the current of less than 1 Amps (and 110V) at the wall outlet.

3.4.2 The Influence of the Thickness of the Connecting Bridges on the Temperature Profile of the Samples:

The change of the thickness of the connecting bridges will bring change to their resistance, and therefore the ratio of the bridge currents to the central gauge area current. This will produce different temperature profiles in the samples.

For samples with extension zones of 30mm in length, but connecting bridges of different thicknesses, resistance heating simulations have been conducted. The resulting temperature profiles for samples with connecting bridges of different thickness are given as follows:

a) The thickness of connecting bridges is 0.45mm:

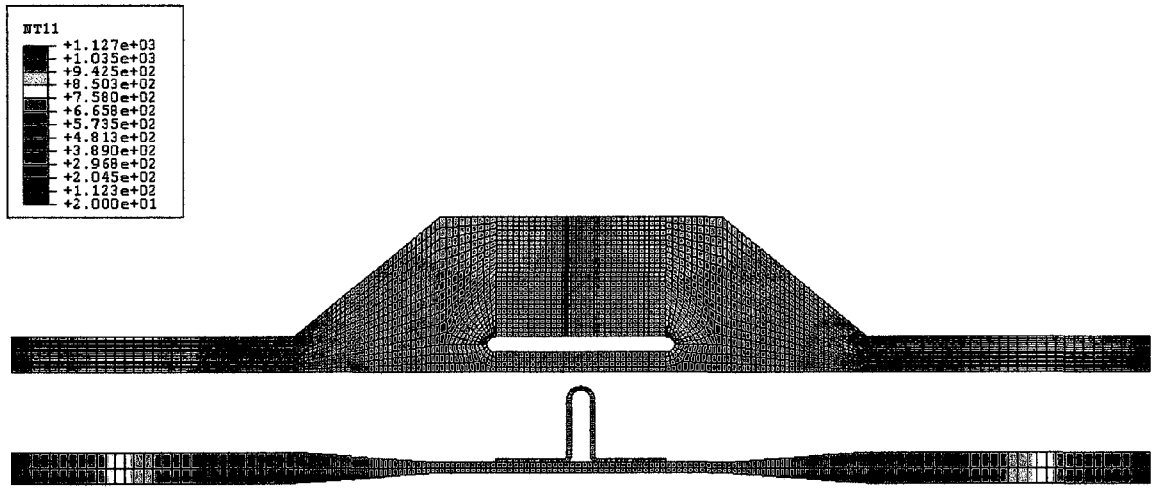

Figure 3.18 Simulation result of the temperature profile for a sample with connecting bridges of 0.45mm in thickness

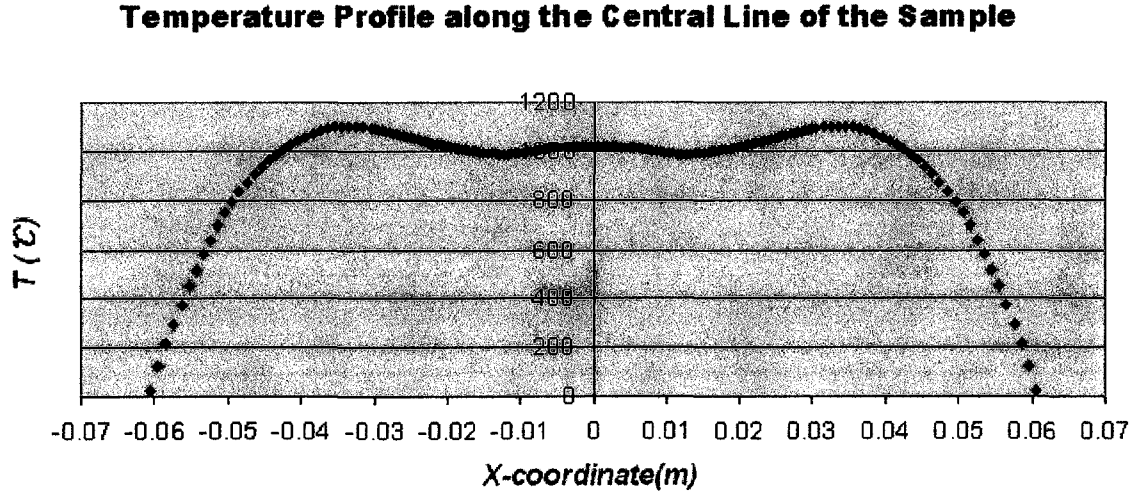

Figure 3.19 Simulation result of the temperature profile along the central line for a sample with connecting bridges of 0.45mm in thickness

b) The thickness of connecting bridges is 0.3mm:

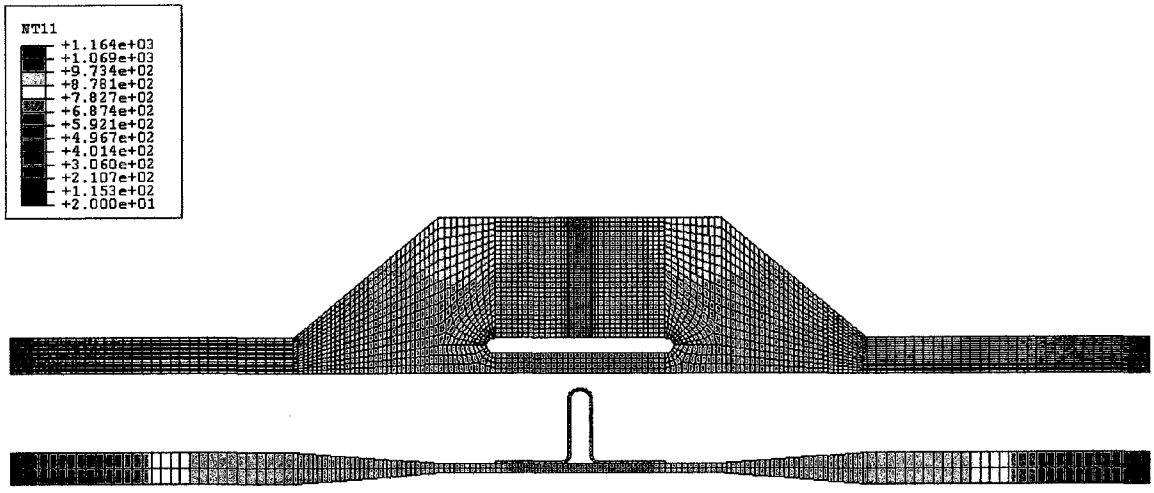

Figure 3.20 Simulation result of the temperature profile for a sample with connecting bridges of 0.30mm in thickness

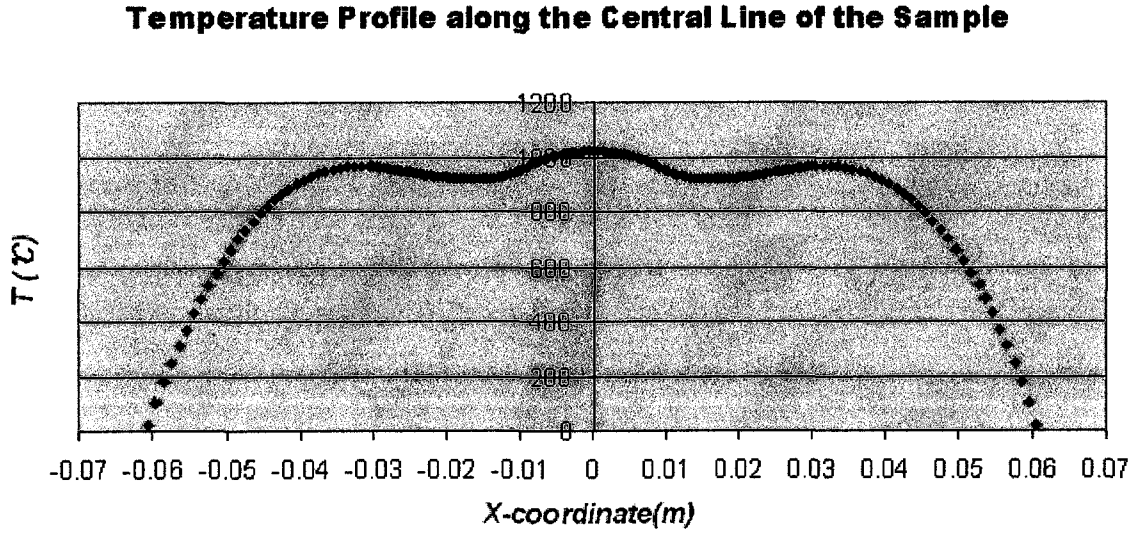

Figure 3.21 Simulation result of the temperature profile along the central line for a sample with connecting bridges of 0.30mm in thickness

It is obvious that with the decrease of the thickness of connectors, an arch-shape distribution of temperature in the central gauge will be produced and temperature uniformity in the gauge length will deteriorate. This is the direct consequence of a more intensive heating in the central gauge area, because the increase in the electrical resistance of connectors will cause a relatively stronger current to flow through the central gauge area.

c) The thickness of connecting bridges is 0.75mm:

How about the effect of increasing the thickness of the connectors on the temperature distribution and profile of the sample? For this purpose, the temperature distribution and profile for a sample with an extension zone length of 30mm and connecting bridges thickness of 0.75mm has been simulated. The results are shown in :

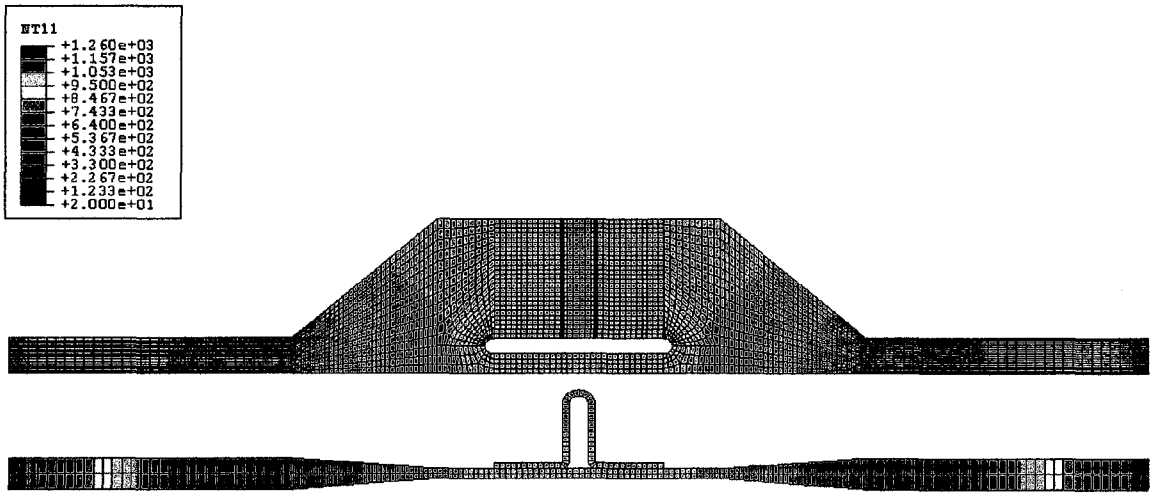

Figure 3.22 Simulation result of the temperature profile for a sample with connecting bridges of 0.75mm in thickness

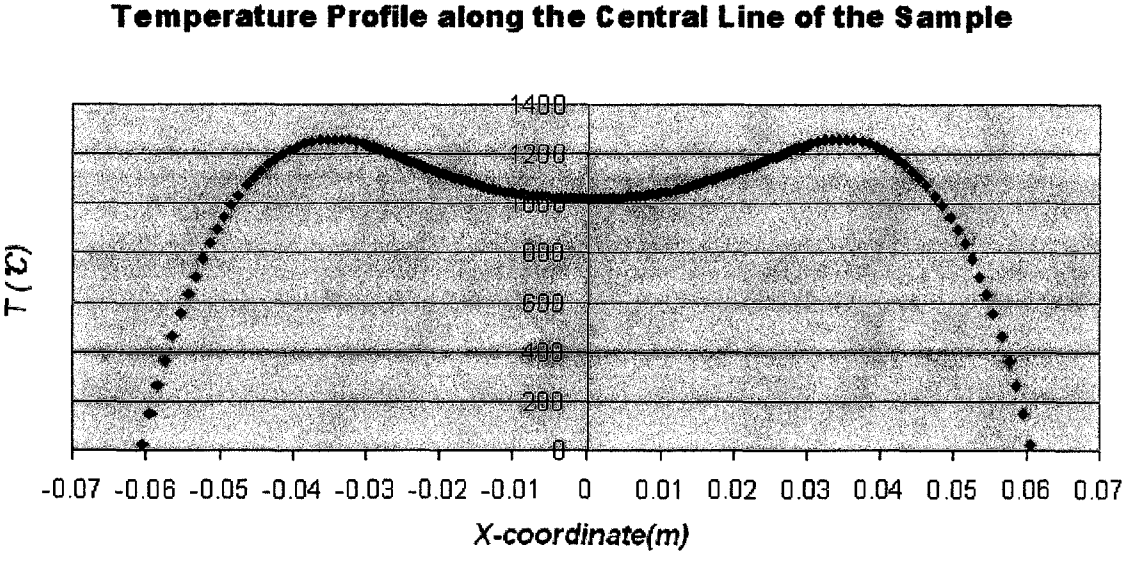

Figure 3.23 Simulation result of the temperature profile along the central line for a sample with connecting bridges of 0.75mm in thickness

The temperature at the ends of gauge area is 1035.19°C while the temperature at the central node position is 1020°C. There is a difference of 15.19°C. But it is important to notice that this difference is a reversal of the normal temperature gradient where the midpoint of the gauge length is at the highest temperature. The highest temperature in the intensified heating zones in the extension sections is 1260.00°C.

The impact of the thickness of connecting bridges can be summarized in the following Table 3.9:

Table 3.9 The Influence of the thickness of connecting bridges

Thickness of Connecting Bridges(mm)	Boundary Surface Current Density (A/m2) to reach 1020°C	Mid Node Temperature (°C)	Temperature At the ends of the gauge length (°C)	Temperature Difference (°C) in Gauge Area When |x|<=9mm	Maximum Temperature (°C) Along the central line
0.30	1.08430e+7	1020.80	963.06	51.74	1020.80 **
0.45	1.22768+7	1020.07	996.32	23.75	1100.00
0.60	1.32671e+7	1020.15	1020.90	0.75	1195.54
0.75	1.40077e+7	1020.07	1035.25	-15.18	1260.00

** The highest temperature is in the middle of the gauge area rather than in the extension zones

It is expected that the temperature at the ends of the gauge area would be a little higher than that in the middle of the gauge area. So after quenching the strength at the ends will be a little stronger than that of the central area, the much higher temperature in the intensified heating zone means that they may be overheated and be detrimental to the successful conduction of the tensile test.

3.5 Tensile Simulation

In order to find the optimal thickness for the connecting bridges so that the connectors will be much weaker than the gauge length during the tensile tests, and therefore not present any significant resistance to the tensile test on the material, tensile test simulations have been conducted on samples with connecting bridges of different thickness.

The same half model used for resistance heating as shown in Figure 3.4 is used for tensile test so the result of temperature distribution from resistance heating simulation can be incorporated into the model for tensile simulation.

The boundary condition is set as:

- The nodes at the left end of the sample are completely fixed
- The nodes at the right end of the sample are given a displacement of 2 mm along the central direction or X direction to mimic the tensile test.

Material properties used in the simulation are derived from a nonlinear mixture of the single phase properties of martensite and austenite.

Tensile simulations are conducted for samples with connecting bridges of 0.6mm and 0.75mm in thickness respectively when the middle of the gauge area is at the temperature of around 300°C (which is lower than the martensite transformation temperature Ms). So the steel is a mixture of martensite and austenite. The reason for choosing 300°C in the middle of gauge area as the temperature to perform tensile simulation is that at this temperature only a small amount of austenite has changed to martensite, and the gauge area is not as strong as at a lower temperature when more austenite transforms to martensite. Since the copper-nickel alloy will not experience phase transformation, the relative strength of the central gauge area to the connecting bridges will be low. If at this stage, a tensile test can be justified for such a design of this type of specimen, then there will be no problem present for tensile tests at other temperatures.

a) For connecting bridges of 0.6mm in thickness:

For the sample with connecting bridges of 0.6mm in thickness, the temperature distribution when the middle temperature of the gauge area is 300°C is shown in Figure 3.24 and the stress distribution of S11 is shown in the Figure 3.25:

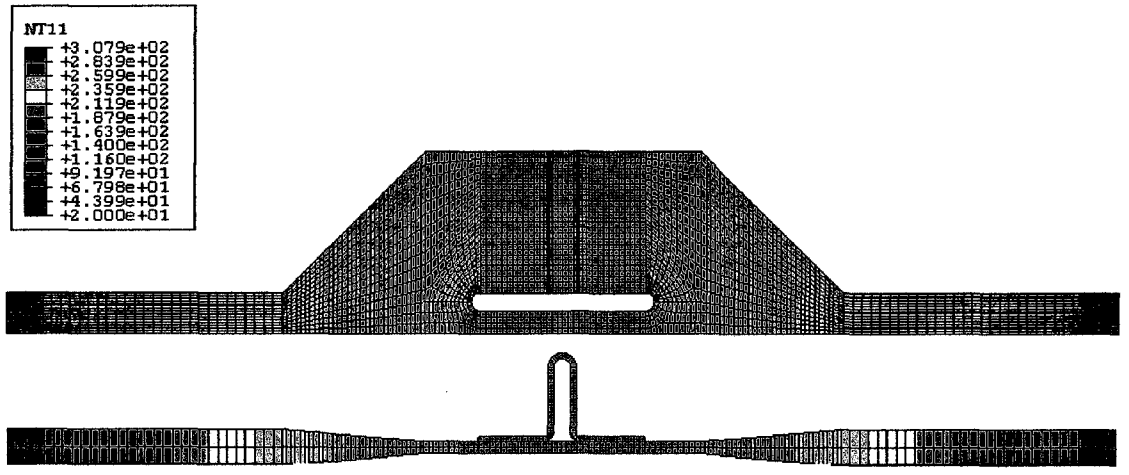

Figure 3.24 The simulation result of the temperature profile for a sample with extension zone length of 30mm, bridge thickness of 0.6mm when the middle of the gauge length is cooled to 300°C.

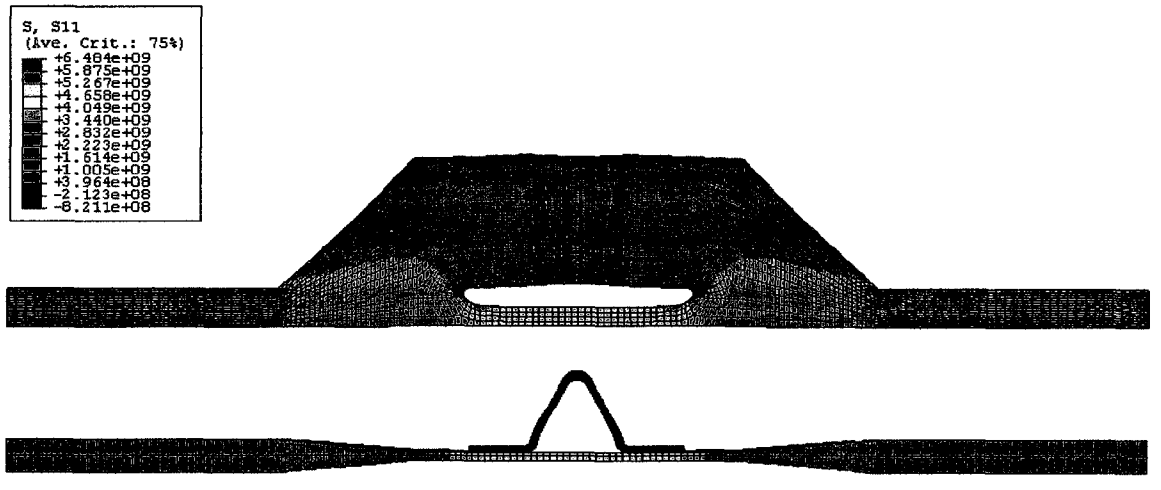

Figure 3.25 The simulation result of the profile of stress s11 for a sample with extension zone length of 30mm, bridge thickness of 0.6mm when the middle of the gauge length is cooled to 300°C.

The s11 for the central gauge area is 4.946 e+9 N/m^2 compared with 8.245e+8 N/m^2 for the extension section. This simulation shows that the load applied on the central gauge area accounts for (1.2*5*4.946 e+9)/(4*9*8.245 e+8) or 99.98% of the total load applied for the tensile test.

b) For connecting bridges of 0.75mm in thickness:

For the sample with connecting bridges of 0.75mm in thickness, the temperature distribution for the sample when the middle temperature of the gauge area is 300°C is shown in Figure 3.26 and the stress distribution of S11 is shown in the Figure 3.27:

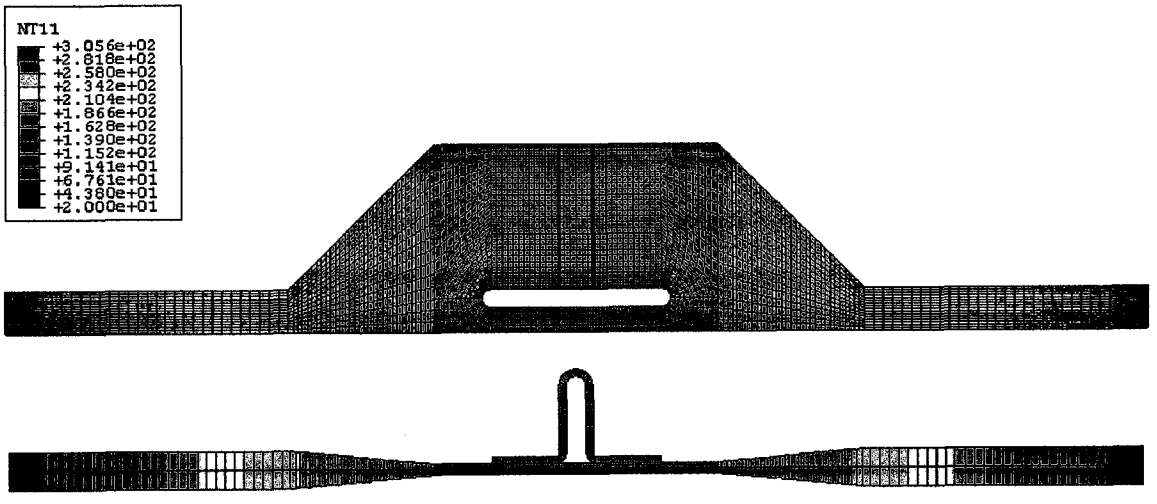

Figure 3.26 The simulation result of the temperature profile for a sample with extension zone length of 30mm, bridge thickness of 0.75mm when the middle of the gauge length is cooled to 300°C.

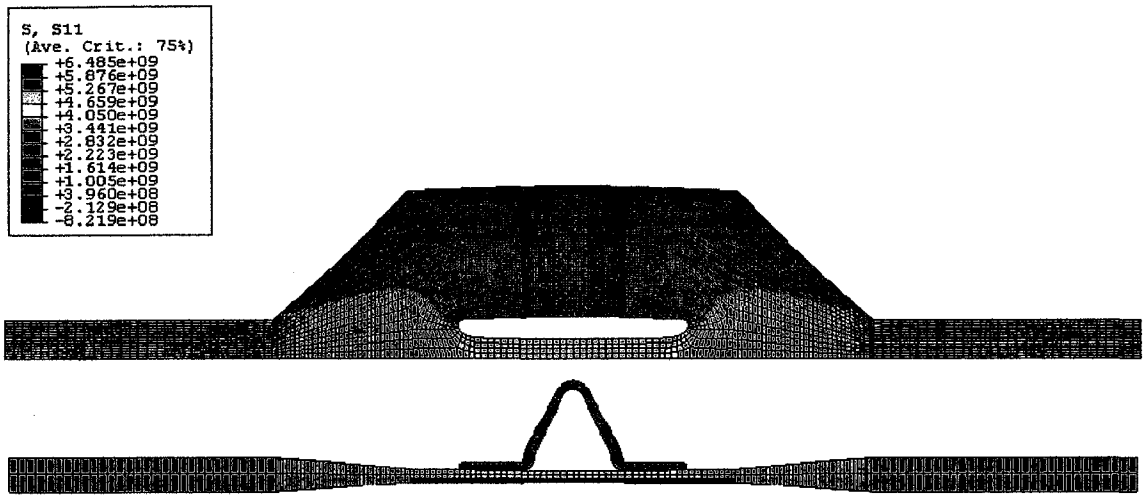

Figure 3.27 The simulation result of the profile of stress s11 for a sample with extension zone length of 30mm, bridge thickness of 0.75mm when the middle of the gauge length is cooled to 300°C.

The s11 for the central gauge area is 4.946 e+9 N/m^2 compared with 8.245 e+8 N/m^2 for the extension section. It can be estimated that the load applied on the central gauge area accounts for (1.2*5*4.94621 e+9)/(4*9*8.24580 e+8) or 99.98% of the total load applied for the tensile test.

Summarizing the results from the above tensile simulation, it can be concluded that the connecting bridges are much weaker than the central gauge area. The pliability of the connecting bridges is attributed to its weak mechanical properties as well as the special design of their shape. It will not present much resistance to the tensile test as over 99 percent of the total load will be carried by the central gauge in a tensile test.

CHAPTER 4 EXPERIMENTAL VERIFICATION OF DESIGN CONCEPT

4.1 Description of Tensile Test Chamber

In order to verify the design concept of the tensile specimen for the physical simulation of heat treatment, a vacuum chamber device with electrical heating, water-cooled clamping and conduction system and gas quenching has been designed and constructed as shown in the figure below.

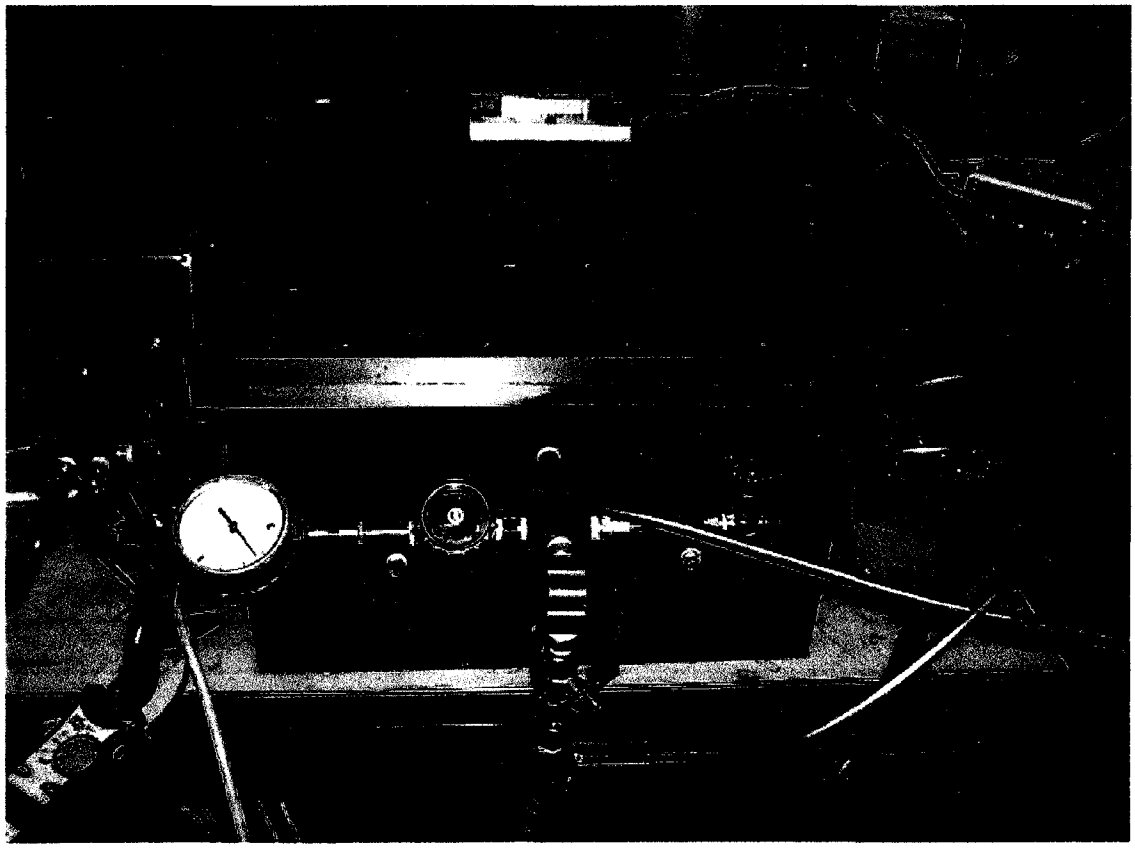

Figure 4.1 Vacuum electric resistance heating system with water cooling and gas quenching

Some features of this device are listed as follows:

- The chamber can be evacuated by a mechanical pump to a vacuum of 660mmHg.
- The sample is clamped at its two ends in solid copper cylinders which are cooled by circulating water.
- The electrical current is driven through the copper cylinders and the sample.
- The electrical current can be increased through two transformers up to at least 450 amperes. Current higher than 450A will exceed the limit of the electrical breaker and cause it to cut out automatically and open the circuit.*

---

* *A current of 450A through the sample draws less than 1A through the wall outlet. This implies a defective breaker and this will be observed by the university electricians the next time the unit is used.*

- The copper cylinders go through the chamber wall and between each cylinder and wall there exist double O-Ring rubber sealing to prevent air leaks to provide vacuum tightness. The complete electrode-wall construction also electrically insulates the cylinders from the chamber wall.
- The copper cylinders can move freely along their axis, so tensile tests can be, in principle, conducted by applying tensile force at the outer ends of the copper cylinder. Completion of this aspect of the testing is not part of the present thesis research.
- There is an observation window through which the heating and cooling of the sample can be observed and monitored through an optical or infra-red camera and the dimension change of the sample through the process can, in principle, also be recorded by some optical device.
- The electric power source of a 110volt, 15 ampere from the wall plug is fed to a 60 ampere variable auto- transformer which in turn feeds a second 5 kVA, 10:1 single phase step-down transformer. The high current from the second transformer is then driven through the sample via the copper clamping cylinders. All the transformers, the copper clamping cylinders and the sample are connected in series to form a circuit. The temperature on the high current output side of the second transformer has been monitored and it does not exceed a 10°C rise during a 30 minute test run.
- The electrical current between the variac and the second transformer is measured with a panel meter and the current between the second transformer and the electrode clamps is measured using a clip-on ammeter.

4.2 Experiments on the Heating and Cooling Behaviour of Samples with Different Dimensions

1) Sample A

This specimen has an extension zone length of 30mm and a central area width of 40mm as listed in Table 4.1. This is the sample for which the FEA simulation predicted the most uniform temperature distribution along the gauge length of the sample.

Table 4.1 Dimensions of Sample A

Length of extension (E section)	30mm
Total width of central zone (C section)	40mm
Thickness of the connecting bridges	0.6mm
Width of the connecting bridges	15.5mm

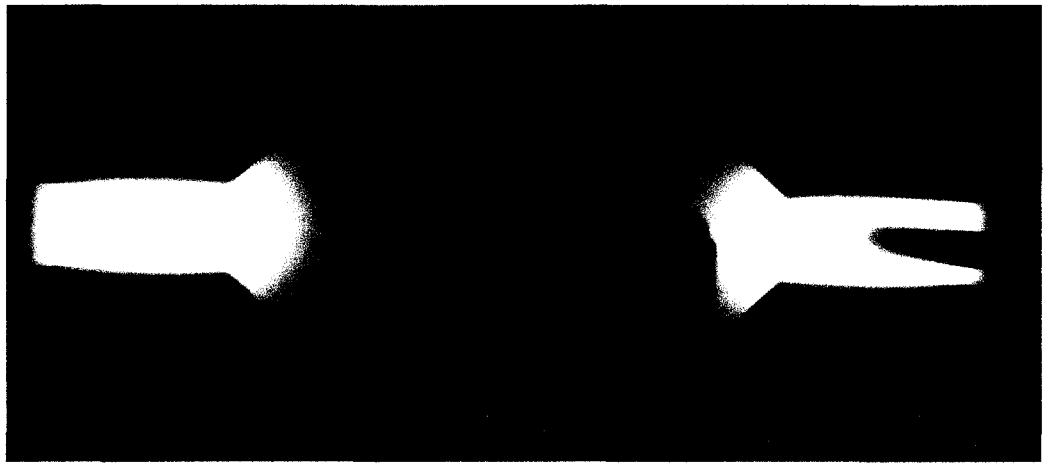

Figure 4.2 Temperature profile for a sample with extension length of 30mm and central zone width of 40mm.

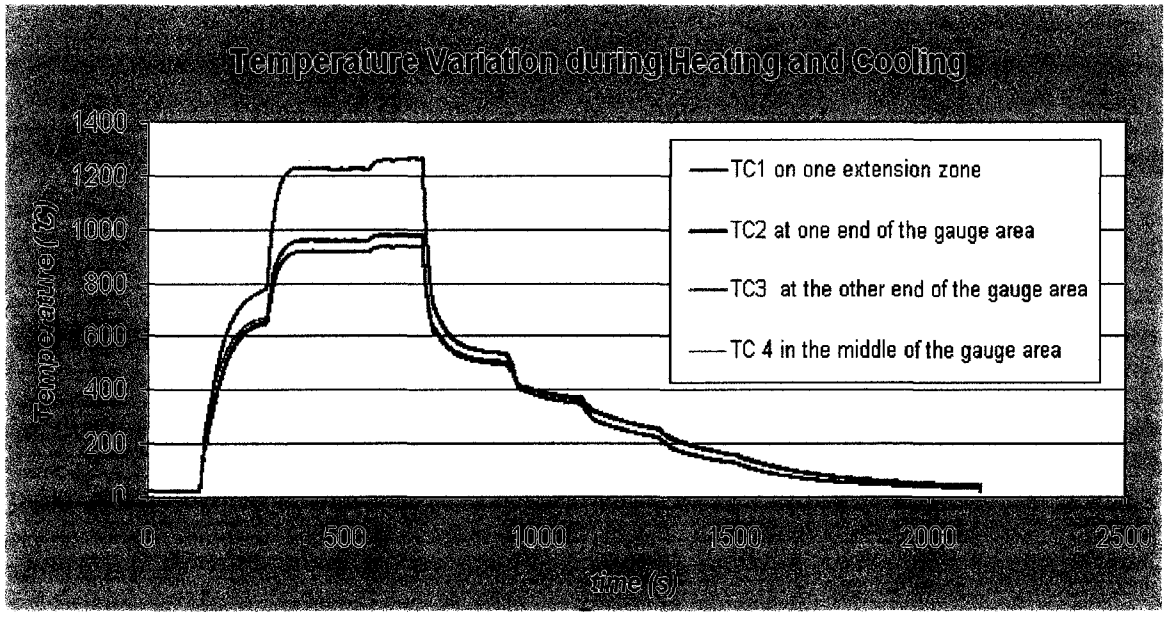

Figure 4.3 Heating and cooling curves of sample A.

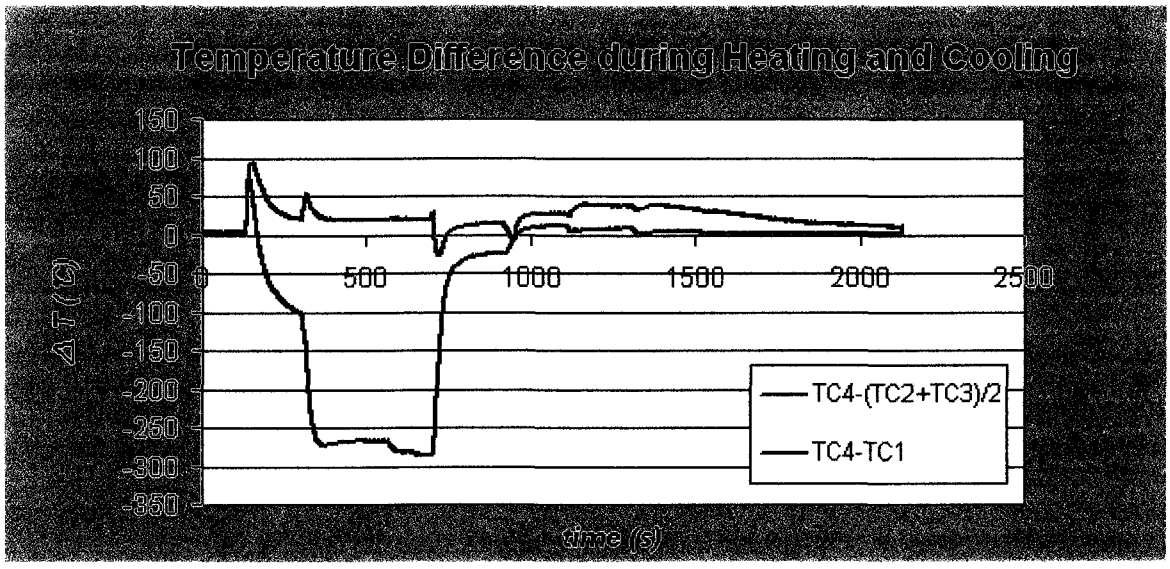

Figure 4.4 Temperature differences reached during the heating and cooling process for sample A.

Figure 4.3 shows the temperatures on the extension zone, in the middle and at the two ends of the gauge length. Figure 4.4 shows the temperature differences between the middle of the gauge length (TC4) and the ends of the gauge length ((TC2+TC3)/2) and also between the middle of the gauge length (TC4) and the extension area (TC1).

The heating of the sample is composed of two stages:

1. The starting current driven through the sample was set to 346A. At first, the temperature in the middle of the sample rose faster than those at the ends of the gauge length. The temperature in the extension section was about 100°C higher than that in the middle of gauge area.
2. During the second stage of heating, the current driven through the sample was increased to 460 A. At the end of the second heating stage, the temperature in the middle of the gauge area reached 980°C and was still about 20°C higher than

those at the ends of the gauge length. The temperature on the extension zone was about 260°C higher than that in the middle of gauge area.

The analysis of the above experiment result discloses that the temperature at the ends of the gauge length is lower than the temperature in the middle of the gauge length as well as that on the extension section. And the temperature of the bridge connectors can be much lower than those of other areas. Heat generated in a higher temperature area will flow to lower temperature areas so the heat flow can be demonstrated in the following picture:

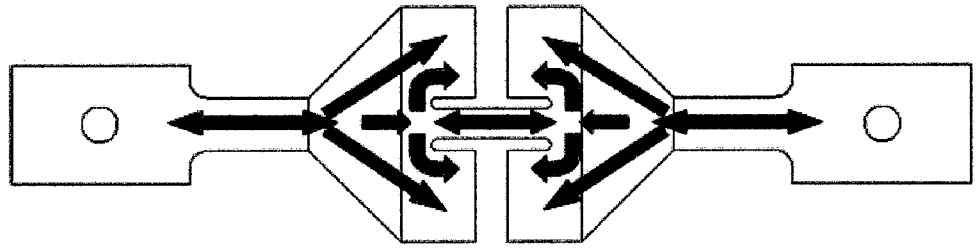

Figure 4.5 Conductive heat flow in Sample A when heated to a peak temperature of 980°C

Because of the high surface area/volume ratio, there is a large heat loss in all of the central area through surface radiation. Because the connecting bridges have large surface areas, the radiation loss through their surfaces is higher than the adjacent areas, so they act basically as a heat sink.

The result of this experiment suggests that the radiation emissivity for the CuNi alloy is higher than those from the reference book [46] and should be adjusted.

Also from this experiment, it was decided that the next effort should be focused on decreasing the surface area of the connectors while retaining their flexibility during tensile test.

2) The sample D

Table 4.2 Dimensions of the Sample D

Length of Extension (E section)	20mm
Total width of central zone (C section)	29mm
Length of central zone(C section)	30mm
Thickness of the bridge connectors	1.0mm

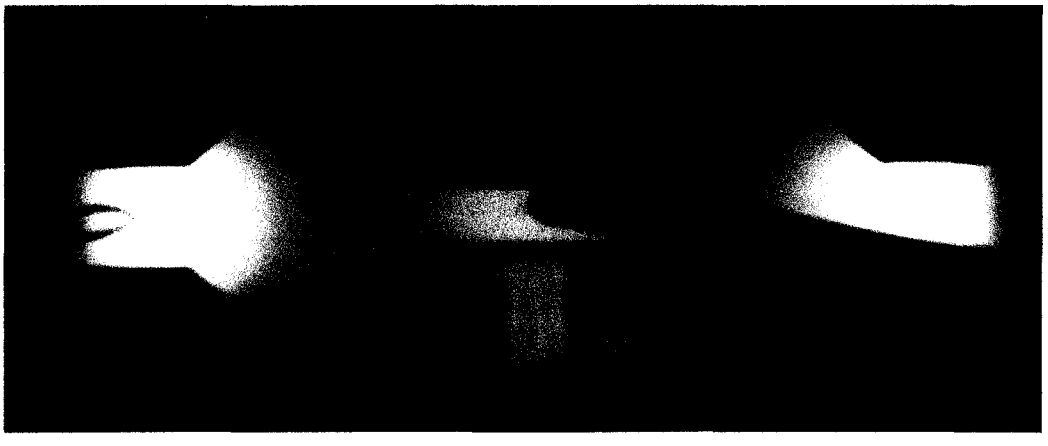

Figure 4.6 Temperature profile with time during the resistance heating and cooling for Sample D with the modified flank width of 10mm and bridge connectors thickness of 1mm.

This test specimen had been modified according to the previous testing results. The width of the wings of the sample was reduced to 10mm and the thickness of connecting bridges had been increased to 1mm in order to keep their electrical resistance relatively

unchanged. By this adjustment of the sample's dimensions, it is expected that the profile of the current flow through the sample will not change much while the radiation heat loss through radiation in the wings and connecting bridges will be lower due to the reduced surface area. Temperature variation with time and the temperature difference during the resistance heating and cooling for Sample D are shown in Figure 4.7 and Figure 4.8.

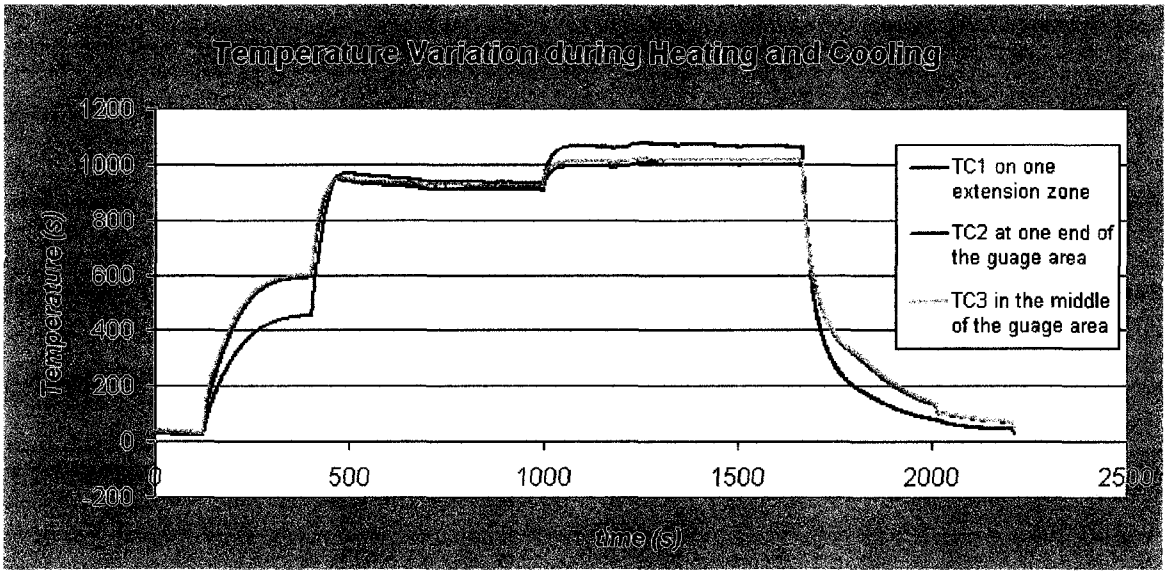

Figure 4.7 Temperature variation with time during the resistance heating and cooling for Sample D with the modified wing width of 10mm and connector thickness of 1mm.

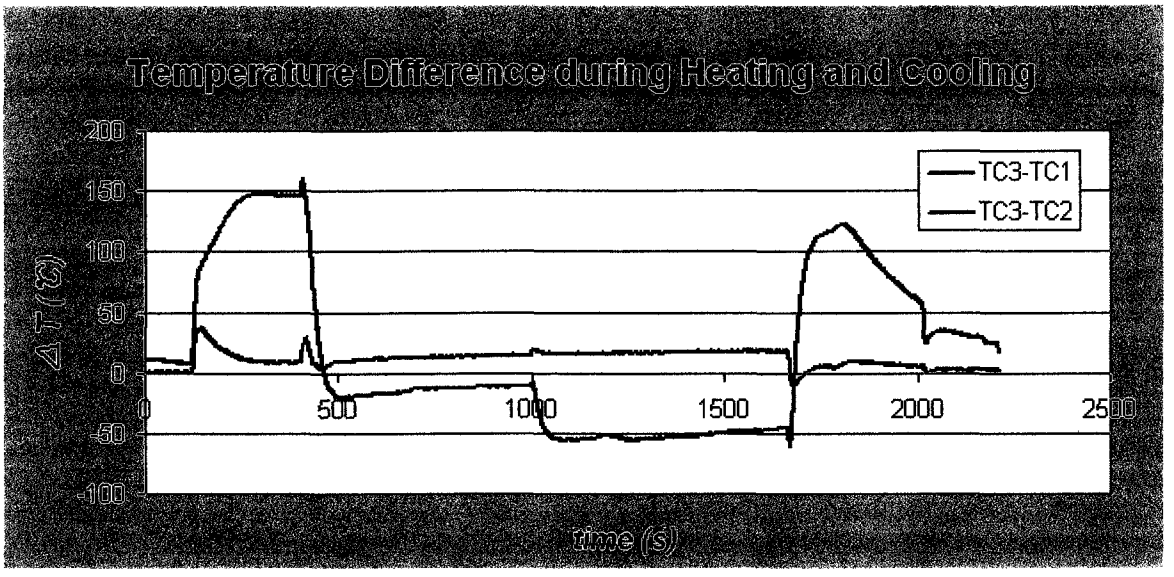

Figure 4.8 Temperature difference during the heating and cooling for Sample D

During the first stage of heating, the electrical current was first set to be 250A and the middle and one end of the gauge length quickly heated up to 600°C and 590°C respectively and then stabilized at those temperatures. Note that there was a temperature difference of only about 8.5°C between them. The temperature in the extension zone was around 453°C because a large part of resistance-generated heat was used to compensate for the conduction heating loss at the water-cooled ends. Note the extensions were only 20mm long on this sample.

After the stabilization of temperatures, the current was subsequently increased to 450A, and the temperature in the middle of the gauge length and at the end being measured increased to 960-955°C quickly before stabilizing at 929 and 914°C respectively. The temperature difference between them was about 15°C. At a constant variac setting, the current decreased slightly because of the increase of resistivity in the sample.

Subsequently, when the current was increased to 480A and the variac was adjusted to keep it at that level, the middle temperature reached 1017°C and was 17°C higher than that at the end of the gauge area. During the whole second stage of heating, the temperature in the extension zone was about 50°C higher than those in the middle of the gauge length. The heat generated in the extension zone was enough to compensate for the conduction heating loss to the water-cooled ends.

3) Sample E:

To further decrease the temperature difference along the gauge length, Sample E was prepared with all the dimensions kept the same as Sample D except that the transitional areas were trimmed (Figure 4.9). Because trimming the transitional area reduced the surface area, the overall heat radiated from the surface of the transitional areas will decrease, and so the heating there should be fortified. The temperature profile for Sample E is shown in Figure 4.9, and the heating and cooling temperature curve is shown in Figure 4.10.

Table 4.3 Dimensions of the Sample E

Length of extension (E section)	20mm
Total width of central zone (C section)	29mm
Length of central zone(C section)	30mm
Thickness of the connecting bridges	1.0mm

Figure 4.9 Temperature profile of Sample E with the trimmed transitional areas when heated to 1020°C in the central gauge area.

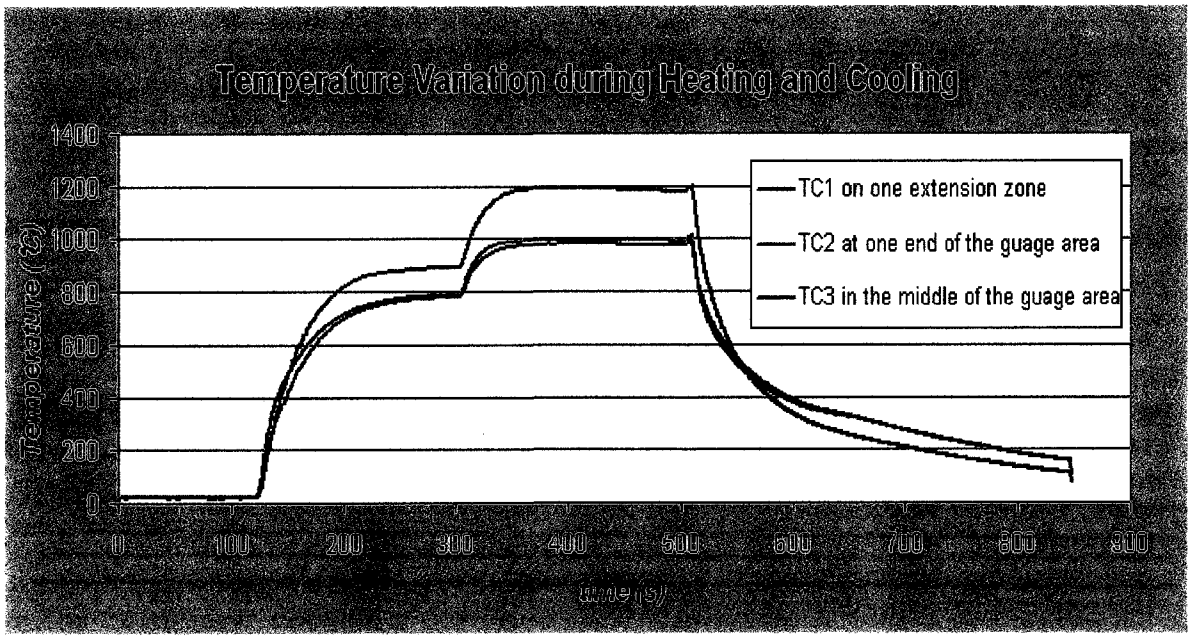

Figure 4.10 Temperature variation during heating and cooling for Sample E.

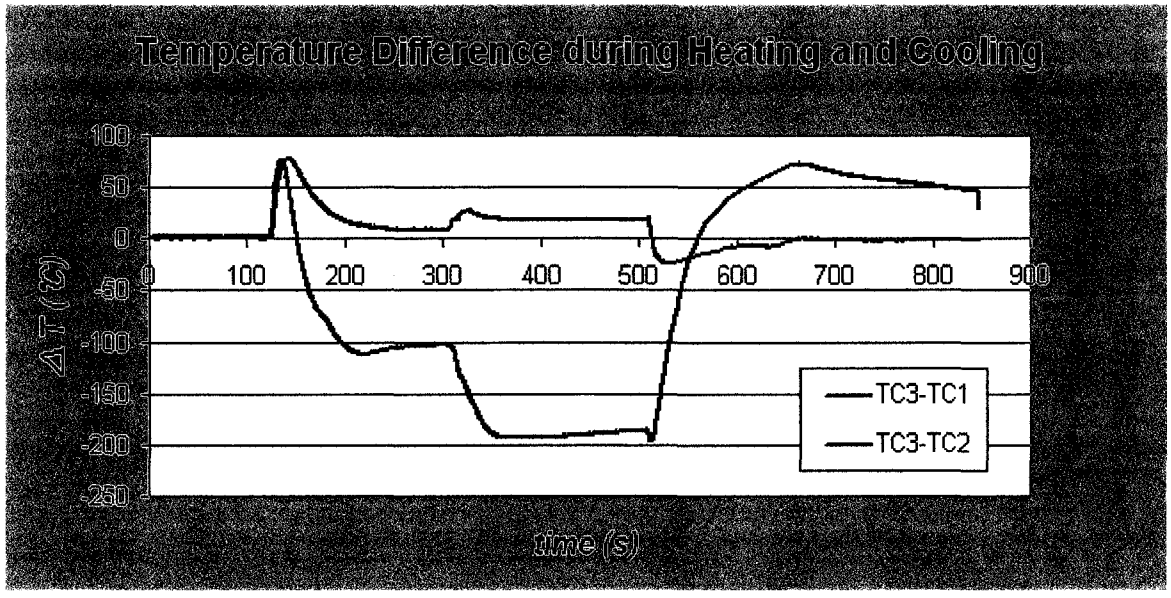

Figure 4.11 Temperature difference during heating and cooling for Sample E

For some reason, a temperature difference of about 20°C still existed when the sample was heated up to 1020°C in middle of the central gauge area. Later when the sample was further inspected, it was noticed that the thermocouple welded to the end of the gauge area was not welded properly. The TC wire connections at the end of the gauge area had formed on a small bead, which placed the temperature-measuring point a small distance above the surface. This may have caused the measured temperature to be a little lower than the surface temperature.

5) Sample F:

Sample F has an extension section length of 30mm, flank width of 12 mm and connecting bridges thickness of 0.8mm.

Table 4.4 Dimensions of the sample F

Length of extension (E section)	30mm
Total width of central zone (C section)	33mm
Length of central zone(C section)	30mm
Thickness of the connecting bridges	0.8mm

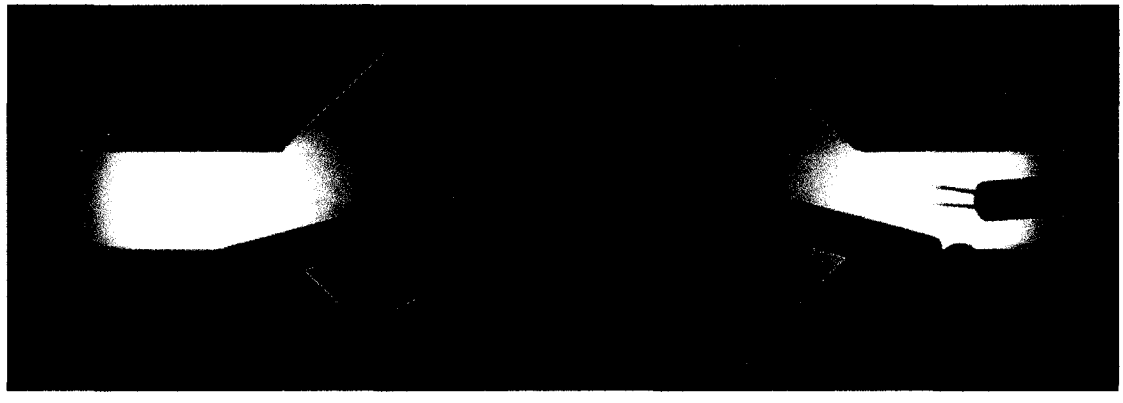

Figure 4.12 Temperature profile of Sample F with extension section length of 30mm each and the bridge connectors 12mm wide and 0.8mm thick when heating above 900°C.

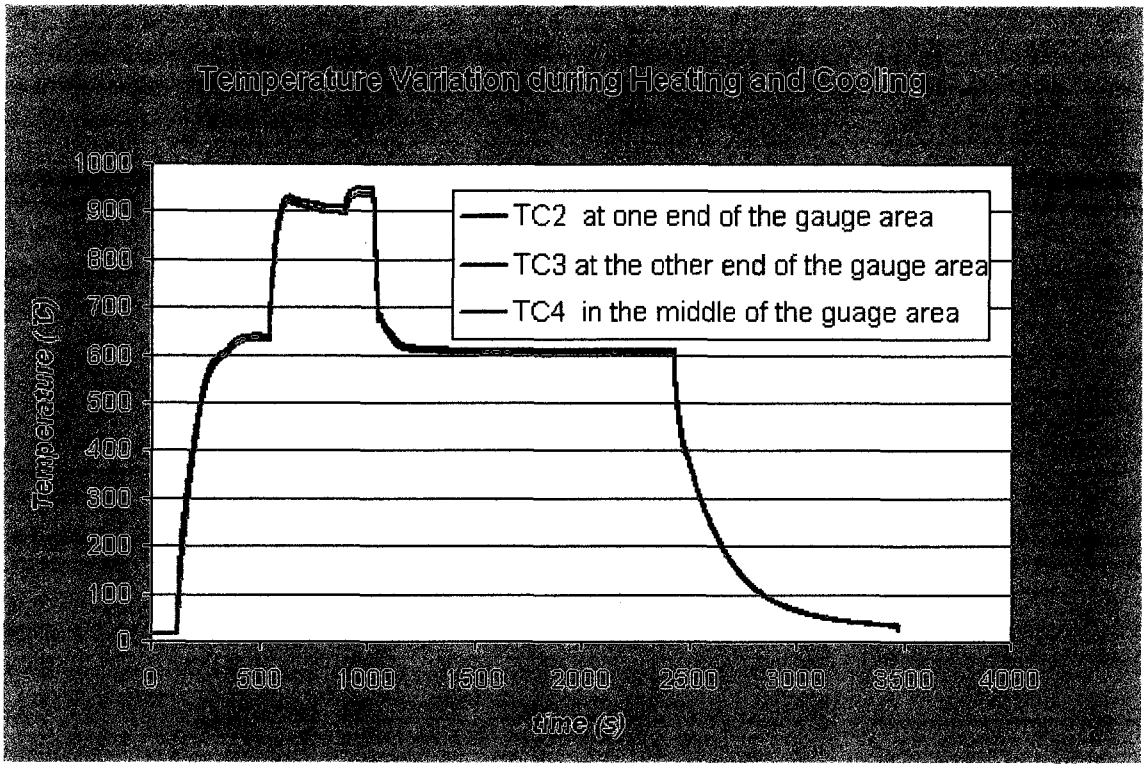

Figure 4.13 Temperature variation during heating and cooling for Sample F

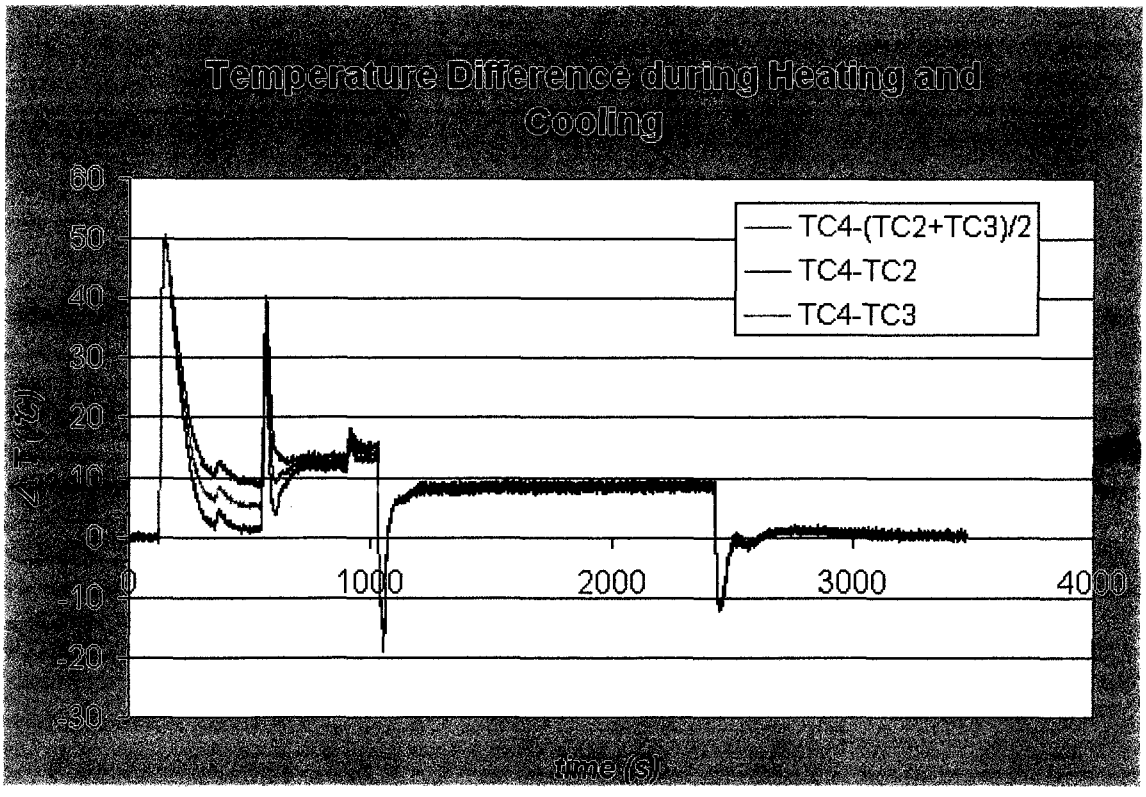

Figure 4.14 Temperature difference for Sample F

The difference between the temperature of the middle and the average temperature of the ends of the gauge area is shown in Figure 4.13 . During the quick heating period, there was a positive peak of temperature difference while during the cooling there was a negative peak of temperature difference, demonstrating the middle of the gauge area is always leading the ends of the gauge length whether heating or cooling when the current is increased or decreased. After the peak value, the difference will stabilize at some level. In this experiment, the biggest temperature difference was recorded as 50°C when the current to the second transformer was increased from zero to 25 amperes, and it stabilized at 5°C when the temperature in the middle of the gauge length was about 630°C. During the second stage heating when the current to the secondary transformer was increased further to 45A, the peak temperature difference was 35 °C (lower than the first peak value) and the temperature difference stabilized at 12°C when the temperature in the middle of the gauge length was around 950°C. During the cooling when the electrical current was deliberately cut off until the temperature in the middle of the gauge length reached 610°C before being raised back to 25 amperes. The middle of the gauge area was cooling faster, resulting in a negative peak temperature difference of about -17°C before stabilizing at a difference of around 9°C .

This complete temperature cycle represents a typical heating and quenching cycle that will be used to measure the properties of austenite-martensite mixtures. The temperature cycle can be controlled precisely as required in the physical simulation of quenching process and in-situ tensile test. This test proves that the design of the specimen will be a

viable one for measuring the properties of austenite and austenite-martensite mixtures for which experimental data is not available.

One temperature control system using the temperature from the central TC in the middle of the gauge length as a feedback will be implemented to replace the current manual control system to realize the electronic control of the heating and cooling cycle.

6) Sample H and Sample I:

Sample H and Sample I have all the same dimensions as shown in Table 4.5 except for the thickness of the bridge connectors which are 1.0mm and 0.8 mm for Sample H and Sample I respectively.

Table 4.5 Dimensions for Sample H and I :

Length of extension (E section)	30mm
Total width of central zone (C section)	33mm
Length of central zone(C section)	30mm
Thickness of the bridge connectors	1.0mm for Sample H 0.8mm for Sample I

Figure 4.15 Temperature profile of Sample H with extension section length of 30mm each and the connecting bridges 12mm wide and 1.0mm thick when heating up to about 950°C.

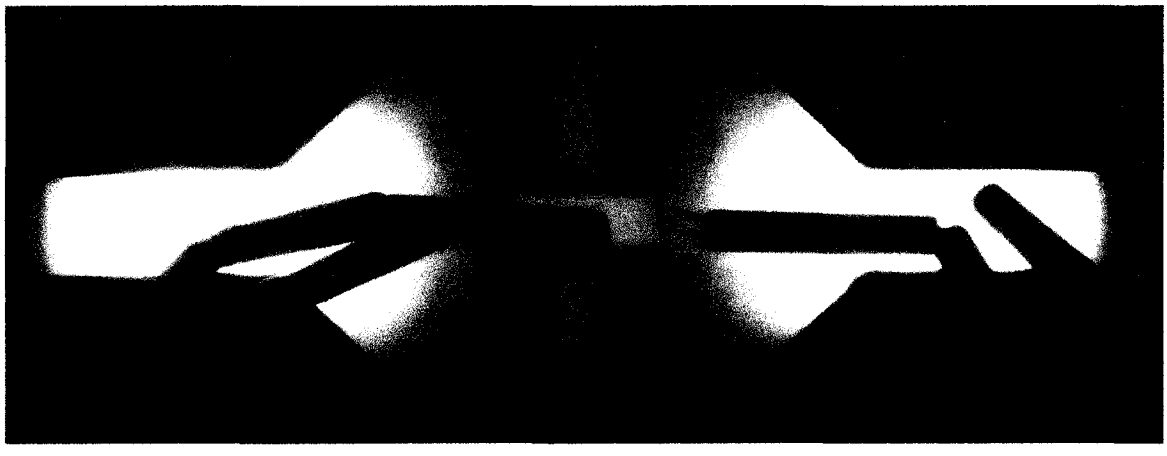

Figure 4.16 Temperature profile of Sample I with extension section length of 30mm each and the connecting bridges 12mm wide and 0.8mm thick when heating up to about 950C.

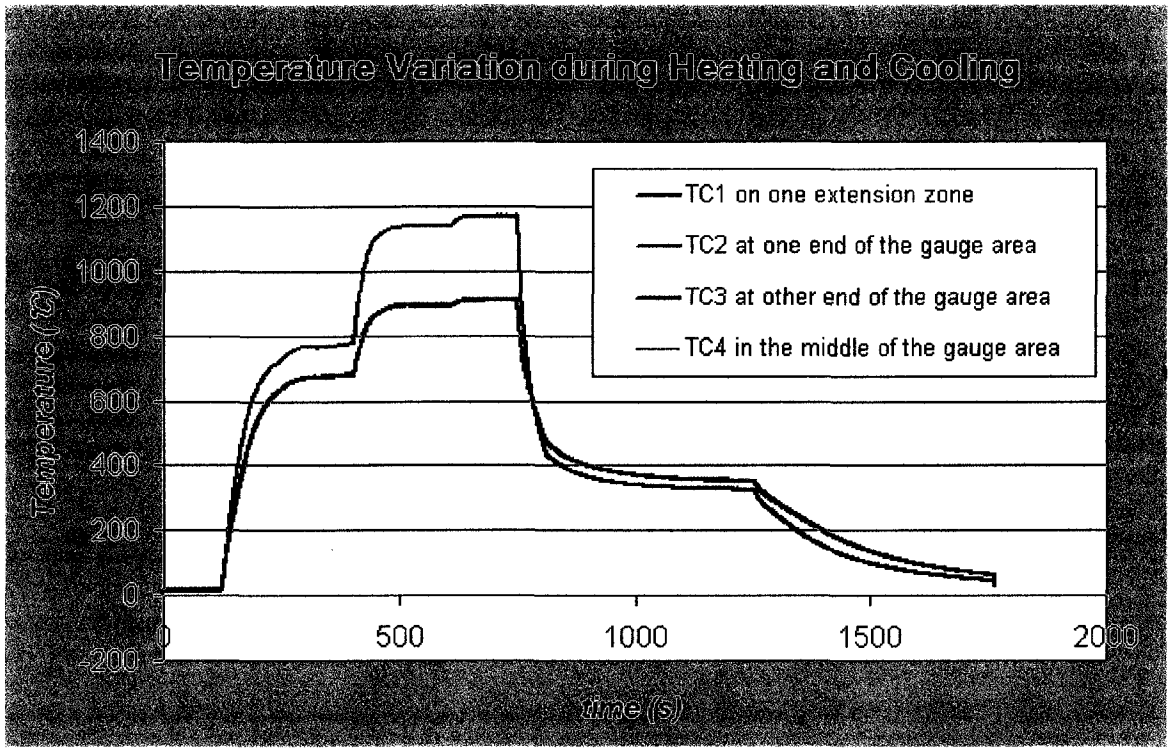

Figure 4.17 Temperature variation during heating and cooling for Sample H

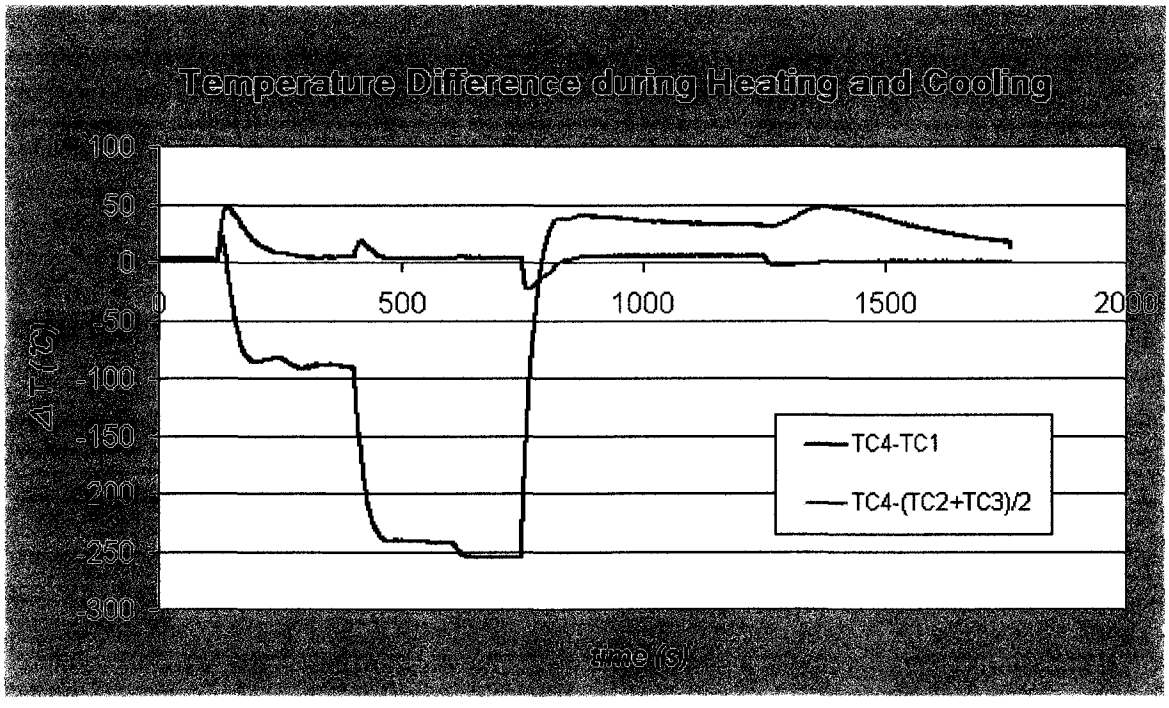

Figure 4.18 Temperature difference during heating and cooling for Sample H

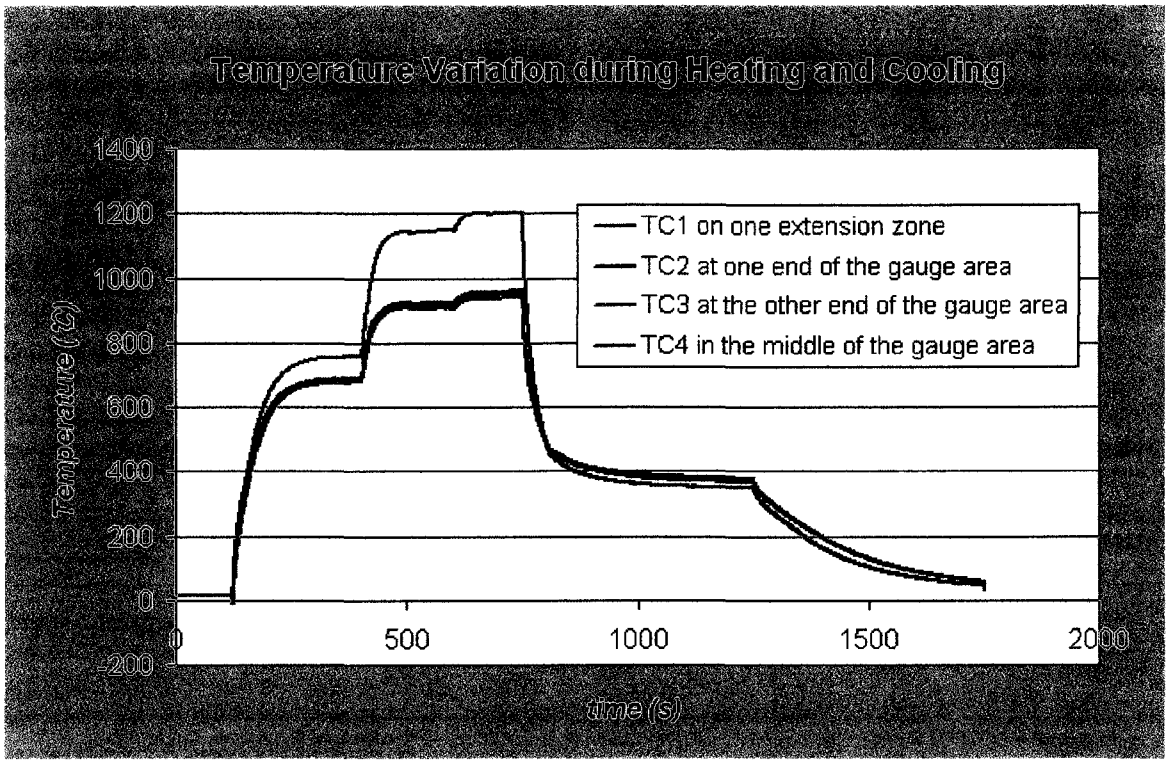

Figure 4.19 Temperature variation during heating and cooling for Sample I

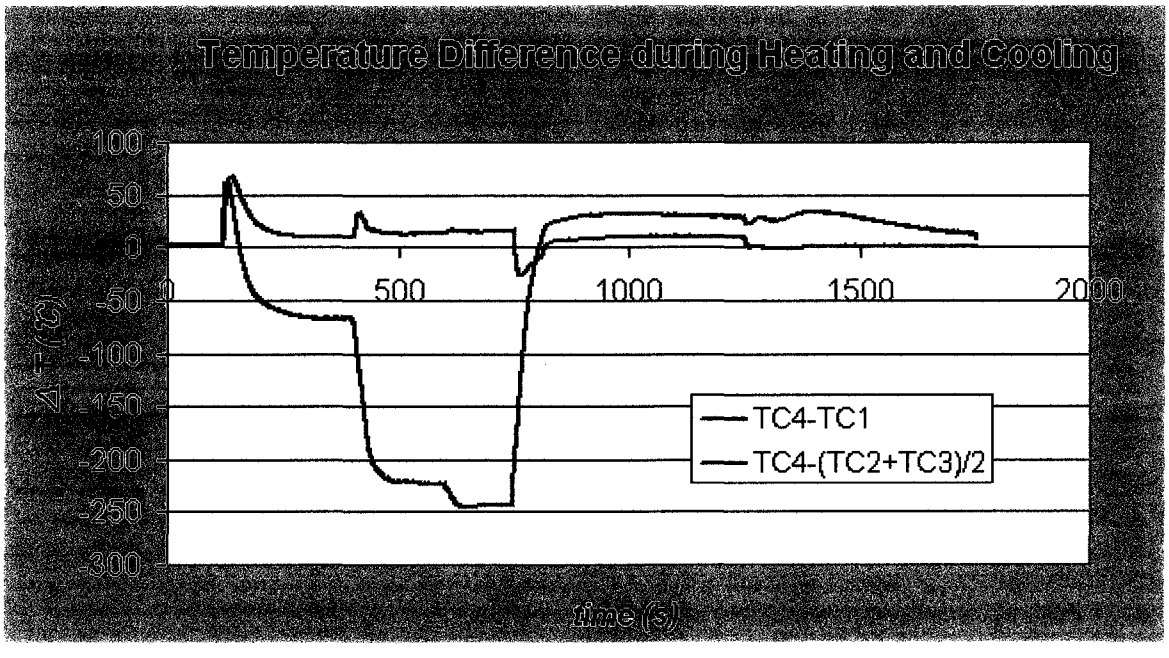

Figure 4.20 Temperature difference during heating and cooling for Sample I

The schedules for the electric current, as read on the panel ammeter, were kept the same for both specimens H and I through the heating and cooling process. For Sample H, when heated up to the temperature of 682°C, the temperature difference between the middle and ends of the gauge length was 4.4°C. And this difference changed to be about 3.3°C when reaching a temperature of 913°C for an electrical current of 436A. While for Sample I, the temperature difference when heated up to the temperature of 698°C was 9.5°C. This difference was close to 14.8°C when reaching a maximum temperature of 959°C for an electrical current of 436A.

The impact of changing the thickness of connecting bridges can be summarized as follows:

1) For the same magnitude of applied current, increasing the thickness of the connecting bridges will enhance the uniform temperature distribution along the gauge length of the sample.
2) Increasing the thickness of connecting bridges will lower the overall temperatures along the gauge length. Because the current through the central gauge area will be lower with the increase of the thickness of the connecting bridges.

7) Sample J:

The dimensions of Sample J are shown in Table 4.6. Sample J is different from Sample H only in the length of extension zones. Its length of extension zone was shortened to 20mm with the expectation that this change would decrease the temperature on the

extension zone to avoid overheating there, while maintaining the uniform temperature achieved in Sample H.

Table 4.6 Dimensions for Sample J

Length of extension (E section)	20mm
Total width of central zone (C section)	33mm
Length of central zone(C section)	30mm
Thickness of the bridge connectors	1.0mm

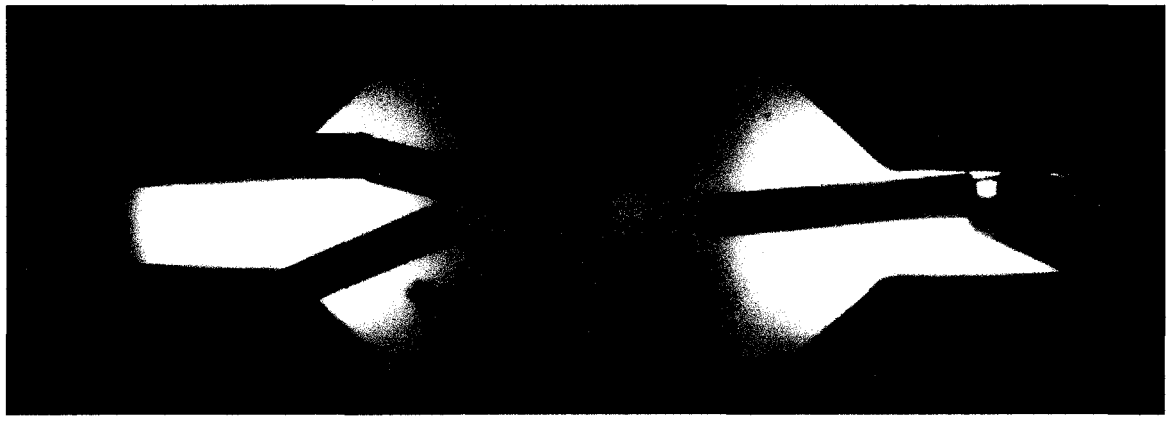

Figure 4.21 Temperature profile of Sample J with extension section length of 20mm each and the connecting bridges 12mm wide and 1.0mm thick when heated up to about 940°C.

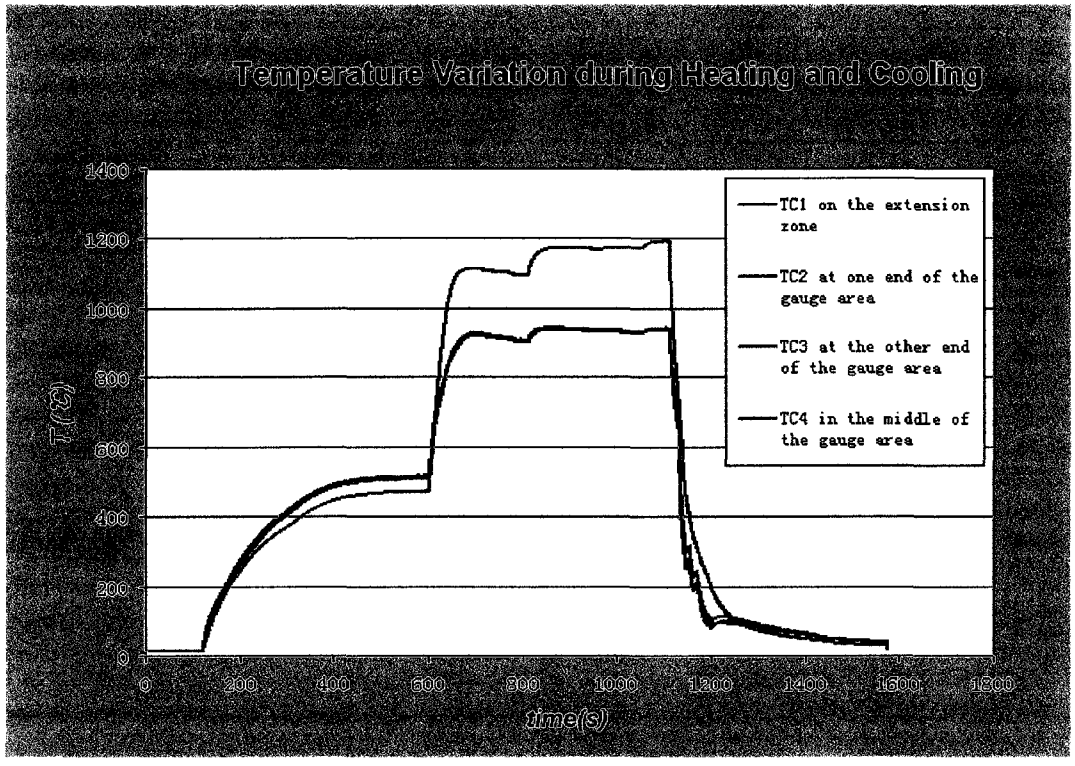

Figure 4.22 Temperature variation during heating and cooling for Sample J

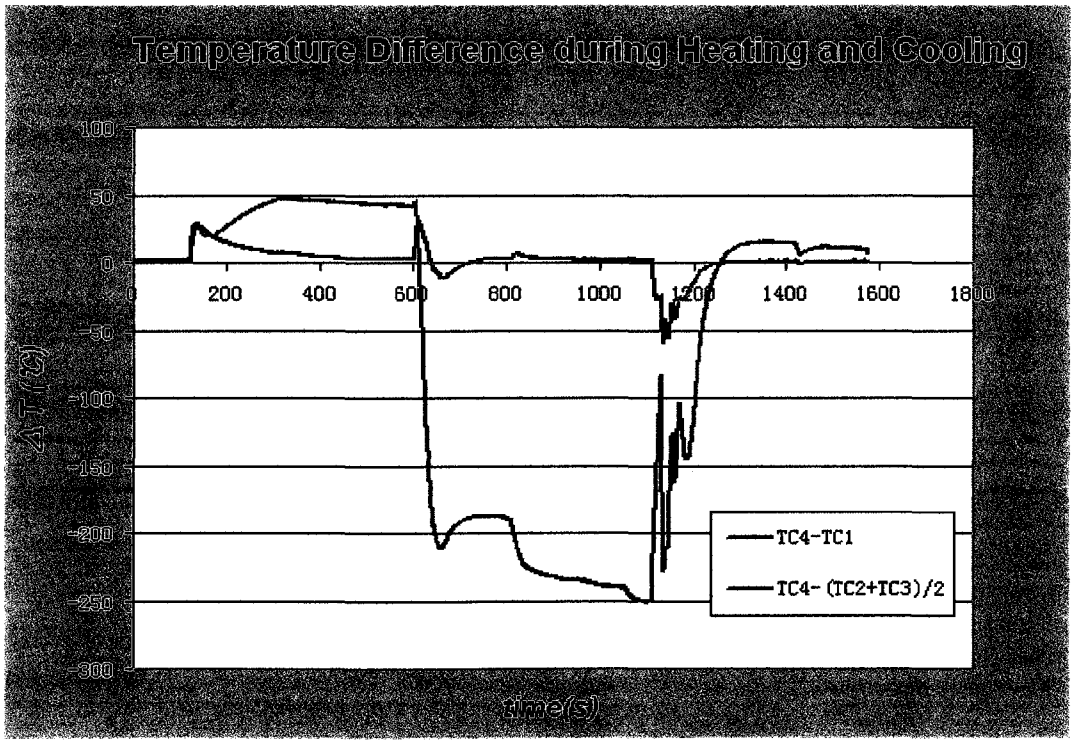

Figure 4.23 Temperature difference during heating and cooling for Sample J

Temperature variation and temperature difference during heating and cooling for Sample J are shown in Figure 4.21 and Figure 4.22 respectively. The temperature difference between the middle and ends of the gauge length when heated up to the temperature of 513°C was 2.7°C. And this difference was about 1.5°C when reaching a temperature of 940°C for a limited electrical current of 436A. The highest temperature difference between the extension zone and the middle of the gauge length was 251°C, a slight lower than the highest temperature difference of 256°C for Sample H.

Shortening the length of the extension zones from 30mm to 20mm can still let the extension zones generate enough heat to compensate the end heat loss and not sacrifice the uniform temperature distribution along the gauge length. Another advantage of shortening the length of the extension zones to the limitation of still keeping the uniform temperature distribution along the gauge length is to avoid overheating of the extension zones so that it will not become detriment to the subsequent tensile test.

4.3 Cooling Behaviour with or without Gas Cooling

The heating and cooling curves for Sample F with and without nitrogen gas cooling are shown in Figure 4.24 and Figure 4.26. And the temperature differences between TC at the middle of the gauge length and each of the other 3 TCs for the test with nitrogen gas cooling are shown in Figure 4.25 and Figure 4.27. The cooling behaviours for Sample F during cooling with or without nitrogen gas aid are compared in Figure 4.28.

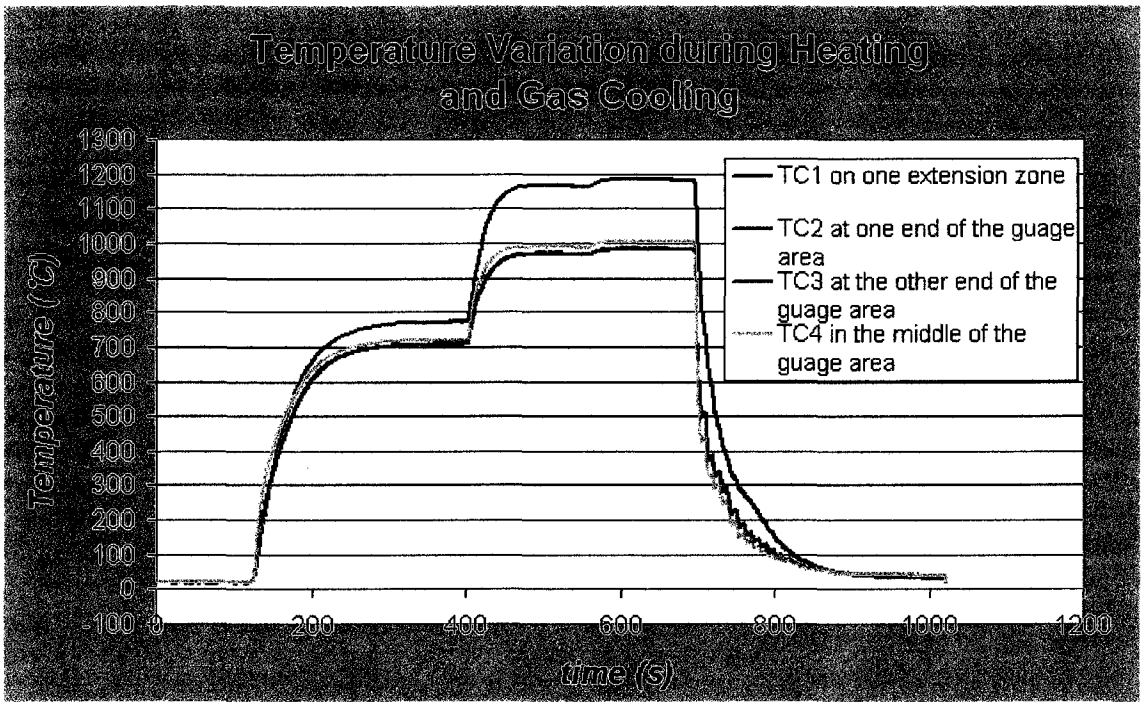

Figure 4.24 Temperature variation during heating and cooling (with gas cooling)

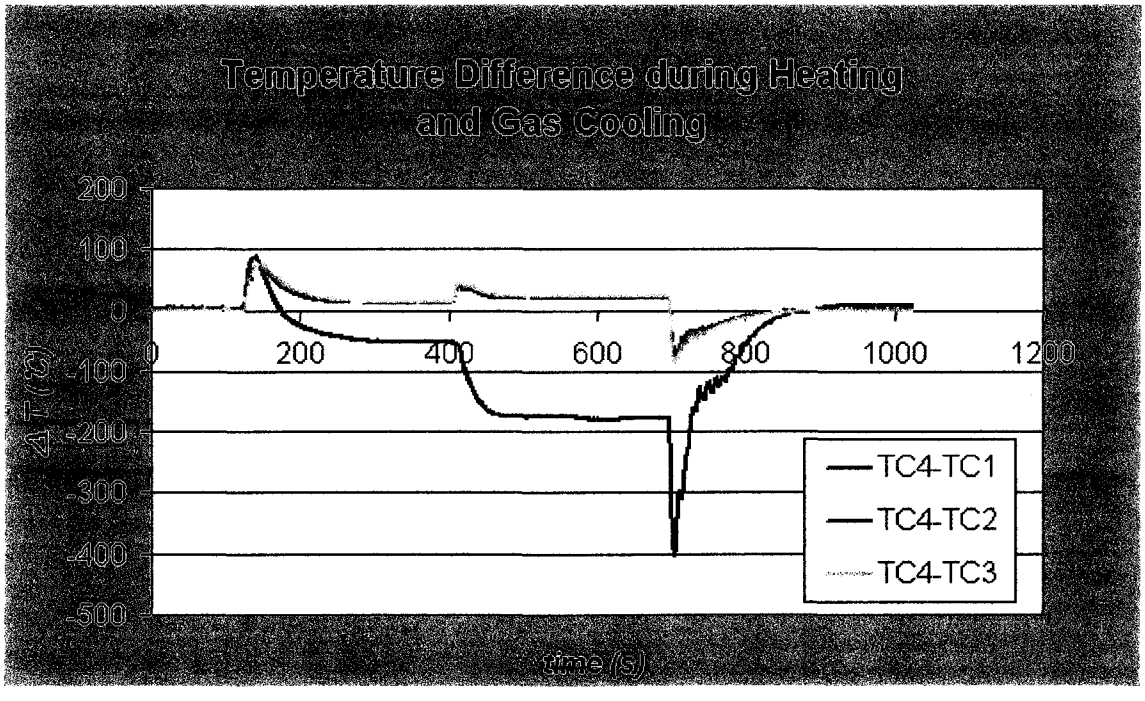

Figure 4.25 Temperature difference during the heating and cooling (with gas cooling)

For the case of with gas cooling, the cooling for the gauge area was much accelerated. The temperature in the middle of the gauge area was recorded to drop from 1003°C to 400 °C, 300°C, 200°C and 100°C in 17s, 34.5s, 48s and 103s respectively. The temperature drop from 1003°C to 300°C in 31s and the maximum cooling rate was (1003-400)/17=35.47°C/s. This meets the cooling rate requirement for quenching as specified in the CCT curves in Figure 2.6. With this cooling rate, all phases other than martensite will be suppressed.

For the case of without gas cooling, the cooling rate for the gauge area was much slower. The temperature in the middle of the gauge area dropped from 998°C to 400°C in 81s or at a cooling rate of (998-400)/81=7.38°C/s. From this test, it is learned that for the successful conduction of physical simulation of quenching process, it is not enough to depend on the end water cooling alone, gas cooling should be added to facilitate the cooling rate to make sure maximum cooling rate be achieved.

In the test without gas cooling, the current was turned back on in 120 seconds after being cut off to simulate the current cycle for a test at 380°C. This temperature is about 60°C above the Ms of the steel, and the bainite formation does not start until about 10000 seconds later at 380°C according to the CCT curves in Figure 2.6.

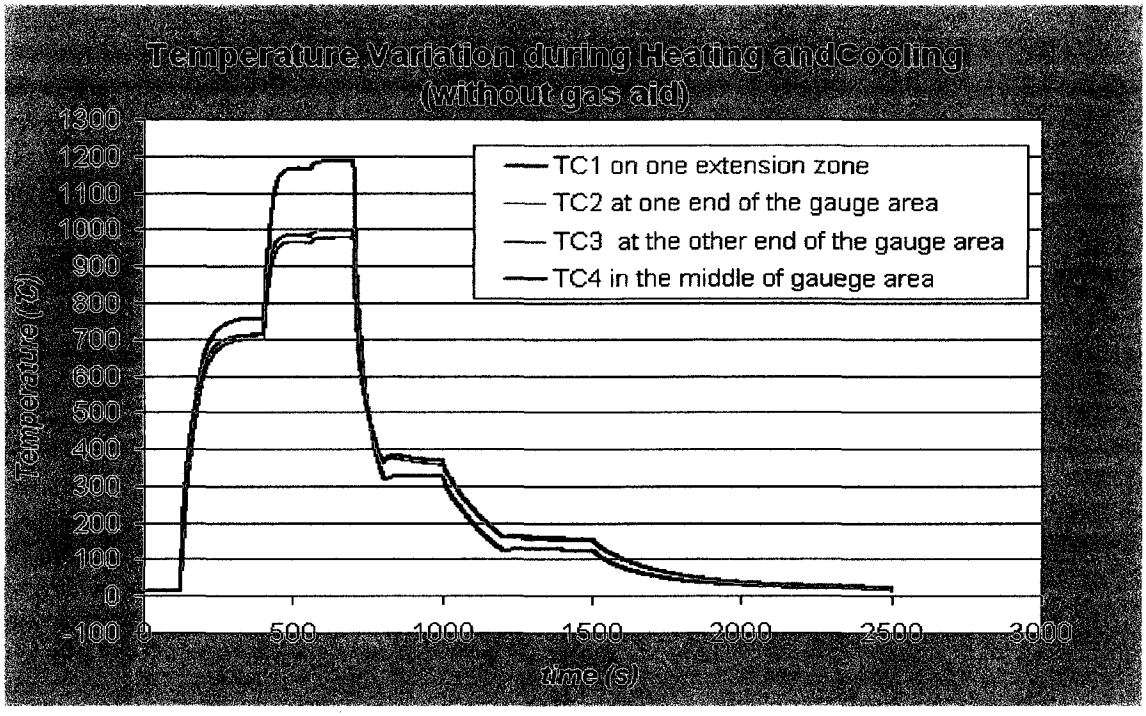

Figure 4.26 Temperature variation during heating and cooling for Sample F (without gas cooling)

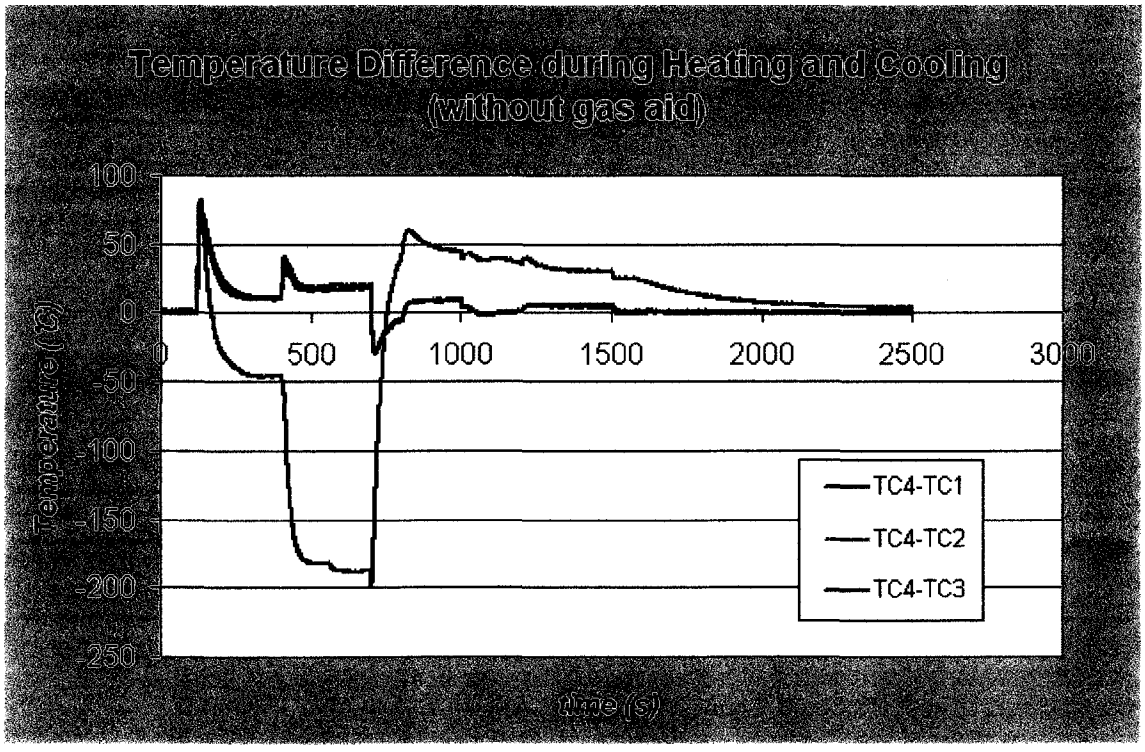

Figure 4.27 Temperature difference for Sample F without gas cooling

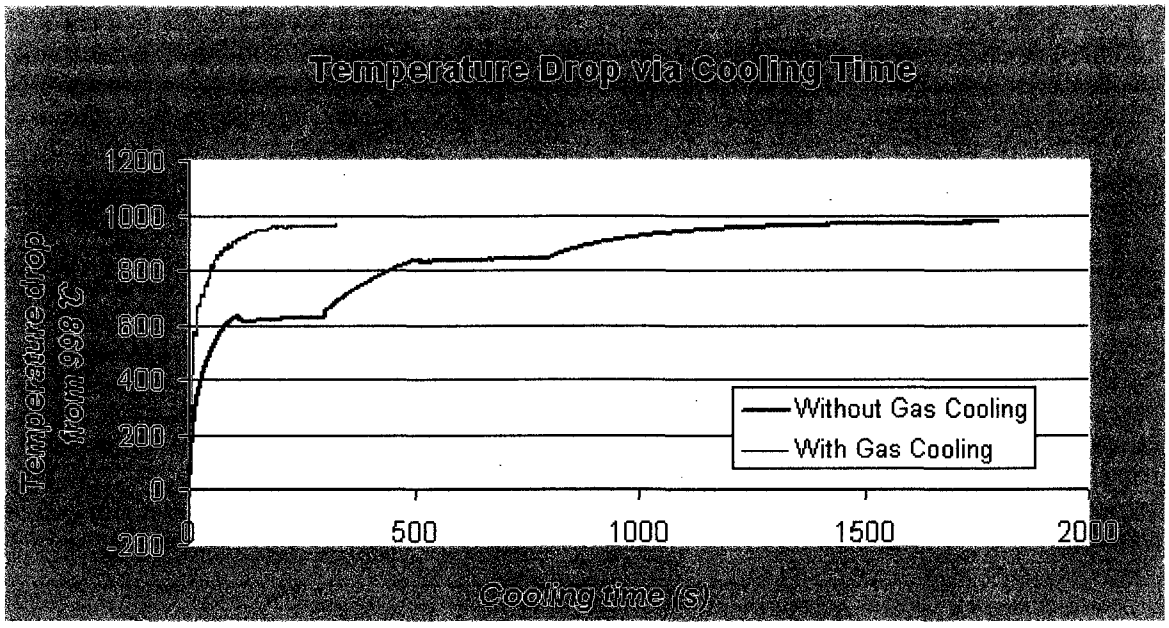

Figure 4.28 Temperature drop at the middle of gauge length during cooling for Sample F with or without gas cooling

4.4 Experiment to Study the Strength of the Connecting Bridges on the Tensile Test

Shown in Figure 4.29 are two samples which had been heated to 1000°C and then quenched to the room temperature. The gauge section of one sample was cut after quenching. The other sample was left as quenched. Tensile tests were done on the two samples to measure the relative strengths of the connecting bridges alone and an intact quenched H13 sample. Figure 4.30 shows the set-up of the tensile test.

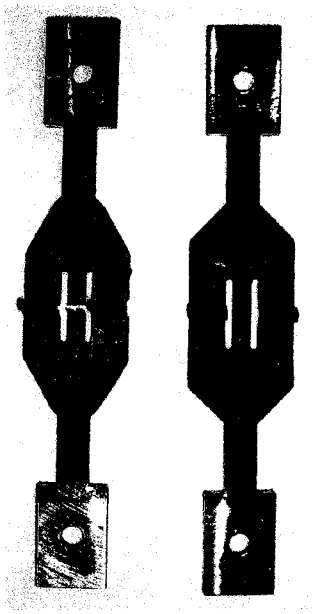

Figure 4.29 Left: Quenched sample with the central gauge area cut.

Right: Intact quenched sample without the central gauge area cut.

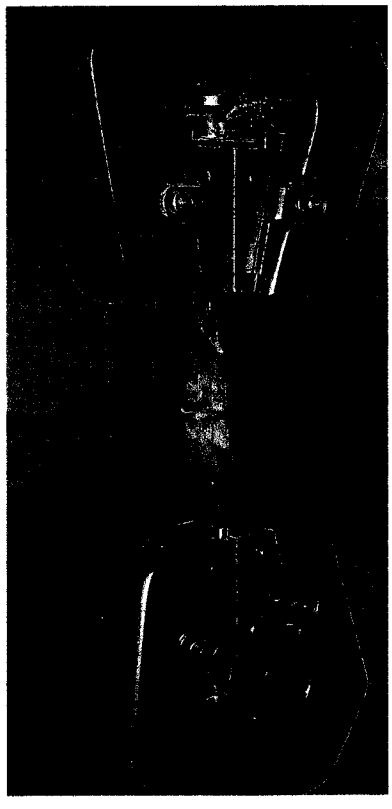

Figure 4.30 Tensile test set-up

The quenched intact sample had a linear force-displacement curve, and it broke at 6297 newtons(1416pounds). The bridge-only sample that had the severed gauge section loaded linearly up to 66 newtons (14.8 pounds force) for the same displacement required to fracture the gauge length of the intact sample, and it reached a force of 133 N at twice that displacement. Thus, the force resistance of the connecting bridges was about 1% of that of a quenched martensitic specimen.

The strength contribution of the connecting bridges to the total sample (without the central gauge area cut) is a ratio of 14.8 to 1415.6 or 1%. It is practicable to make a correction of about 1% in the tensile test result for the sample (without the central gauge area cut).

Two factors contribute to the low strength of the connecting bridges: the first factor is the special arch shape of the connecting bridges, which experience bending instead of stretching during the tensile test; the second factor is the annealed soft state of the connecting bridges after experiencing high temperatures during the heating and quenching process of the sample.

The temperature on the top point of one connecting bridge for Sample G (with the same dimensions as Sample F) was recorded during heating and cooling cycle and shown in Figure 4.31 . The temperature difference derived from Figure 4.31 is shown in Figure 4.32:

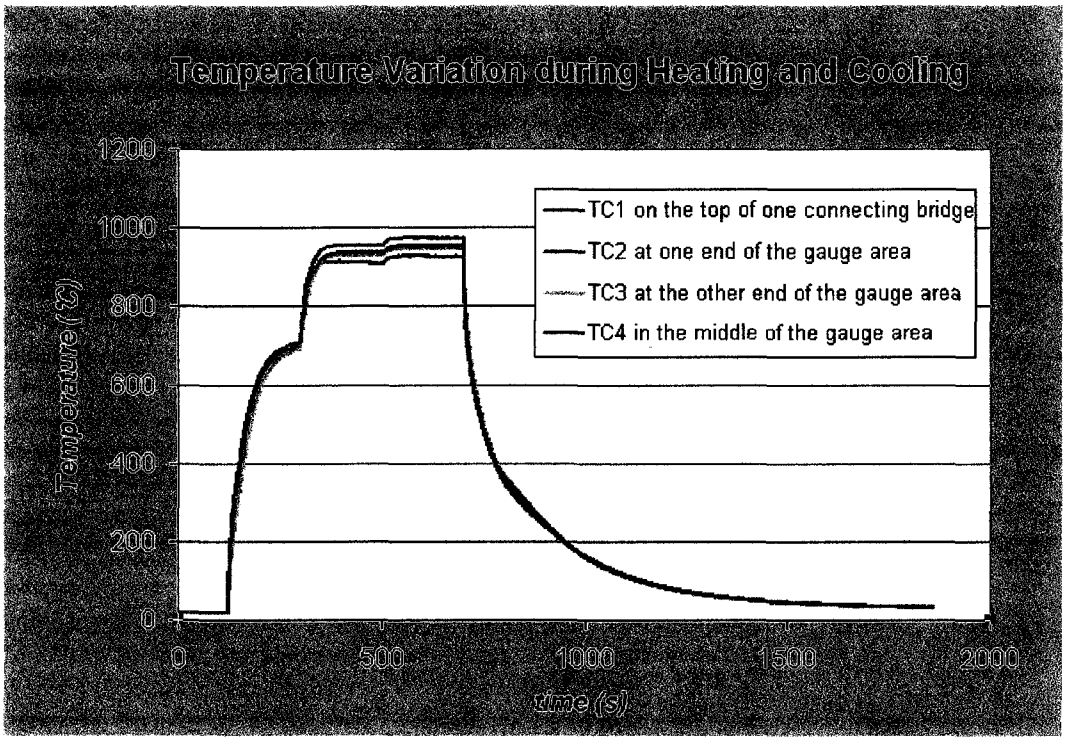

Figure 4.31 Temperature Variation during heating and cooling for Sample G

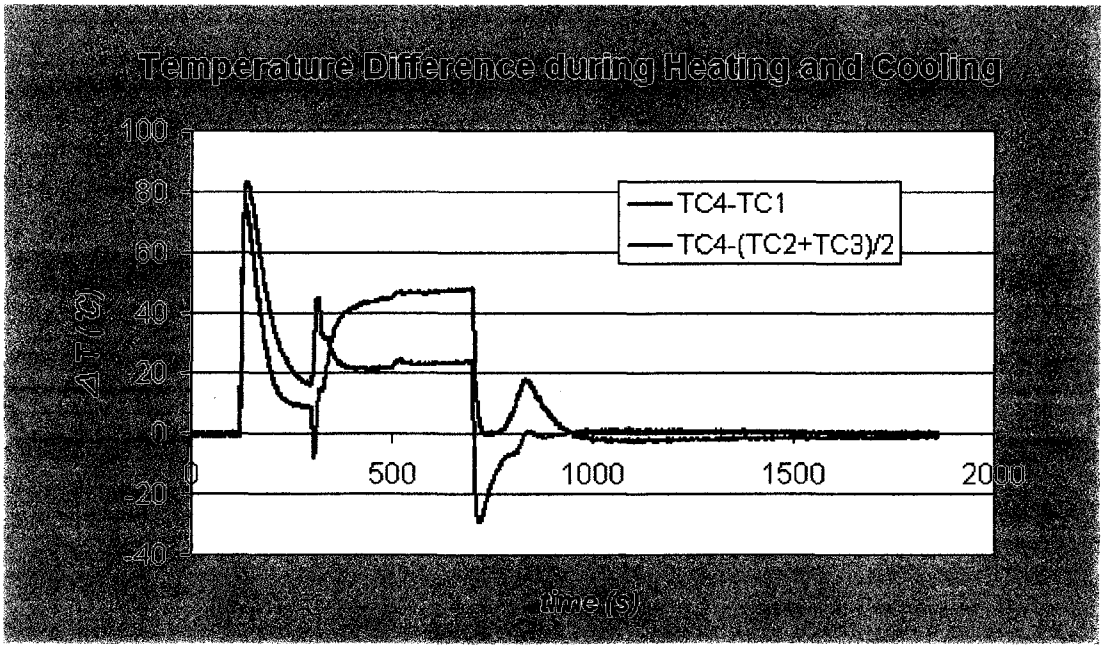

Figure 4.32 Temperature difference during heating and cooling

From Figure 4.31 and Figure 4.32, it is known that the temperature on the top of the connecting bridge reached as high as 900°C when the temperature in the middle of the gauge length was over 950°C and was only about 25°C lower than that in the middle of the gauge area. The temperature was well above the annealing temperature of 737.2°C or 1010.1K which is estimated as 70% of the absolute melting point 1443K for Cu70Ni30. At this temperature, the connecting bridges are fully annealed and become soft.

Even at a thickness of 1.0mm, the connecting bridges are soft and flexible, and will take only less than 1% of the total load from the central gauge area. It is practical to use this kind of sample in the physical simulation of quenching process and in-situ tensile test to measure the properties of the mixture of austenite and martensite during the process.

CHAPTER 5 DISCUSSION AND CONCLUSIONS

5.1 Discussion and Conclusions

In this study, a special kind of sample for tensile testing during the quenching process of steels has been conceived by taking into account the behaviour of steel during the quenching process as well as characteristics of resistance heating. This sample can best be described as an integrated parallel path specimen. It has parallel paths for both current flow and force resistance. The relative currents passing through the alternate paths compared to that flowing through the gauge section can be used to control heat transfer between the two paths. This allows the creation of a uniform temperature along the gauge section. The mechanical strengths of the alternate paths are negligible compared with that of the gague length. This allows the strength of the gauge section to be measured directly.

The initial dimensions of the sample were then parametrically studied through the simulation of electrical heating for different combination of the length of the extension zones and the thickness of connecting bridges. The results of those simulations suggest that:

a) When keeping the thickness of the connecting bridges constant, the temperature difference between the middle and the ends of the gauge length will decrease with the increase of the length of the extension zones. At a high temperature of about 1020°C, the profile of temperature distribution along the gauge length will change

from a ∩ shape to flat then to ∪ at a high temperature of around 1200°C with the increase of the length of the extension zones.

b) When keeping the length of the extension zones stable, increasing the thickness of the connecting bridges improves the profile of temperature distribution by changing the relative ratio of the currents through the connecting bridges to the current though the central gauge area.

The simulation results show that the most uniform temperature distribution along the gauge length can be achieved when the length of the extension zones is 30mm and the thickness of the connecting bridges is 0.6mm.

The sample with the optimized dimension (extension zones length of 30mm and connecting bridges thickness of 0.6mm) was manufactured and went through resistance heating and cooling experiment to measure the temperature distribution along the gauge length .

The experimental data on the optimized sample show that the connecting bridges behaves as a heat sink as expected but the heat loss through radiation is just too great due to the actual radiation effects being much larger than anticipated by the resistance heating simulation .

The subsequent work was an experimental program to improve the design of the sample by adjusting the dimensions of the real sample. Three measures have been taken to modify the dimensions of the sample:

a) In order to decrease the radiation from the central area, the surface area should be decreased. This can be done by decreasing the overall width of the central zone by trimming 2 mm off each outer edge of the wings.
b) In order to keep a close-to-uniform temperature distribution within the gauge length, the ratio of the current flow through the central gauge zone to the connecting bridges should be kept low. This can be done by increasing the thickness of the connecting bridges to the limitation that the connecting bridges will still be soft and flexible and not contribute significant resistance during the tensile test.
c) In order to keep the extension zones from overheating, the extension zone should be kept as short as possible but still be able to generate enough heat to compensate for the conduction heat loss through the water-cooled grips. There must also be a positive heat flow from the extension zones to the ends of the gauge length in order to keep a uniform temperature distribution within the gauge length.

A series of samples with dimensions adjusted according to the above-mentioned methods have been tested. The results can be summarized and listed in

Table 5.1 :

Table 5.1 Summery of experimental data

Sample label	Length of Extension section (mm)	Width of the central zone (mm)	Thickness Of the connecting bridges (mm)	Temperature On the extension zone (°C)	Temperature in the middle of the gauge area (°C)	Temperature difference along the gauge length. (°C)
A	30	40	0.6	1260	970	20
D	20	27	1.0	1068	1018	18
E	20	27	1.0	1191	999	18
F	30	33	0.8		950	14
H	30	33	1.0	1168	913	3.5
I	30	33	0.8	1200	958	14.8
G	30	33	1.0		973	23.6
J	20	33	1.0	1192	940	1.5

The comparison of the results from the resistance heating of the samples with different dimensions reveals that:

- Radiation from the central C zone (G+2W) has been significantly reduced by decreasing the width of the central zone and increasing the thickness of connecting bridges.
- Adjusting the thickness of connecting bridges has a great impact on the uniform of temperature distribution along the gauge length. Sample H and Sample J with the connecting bridges of 1.0mm in thickness have the lowest temperature differences of about 3.5-1.5°C. This easily conforms to the temperature uniformity requirement specified in the ASTM Designation: E21-05. The highest temperature in the extension zones can be still controlled to be well below its melting point on these samples.

6.2 Future Work

The future work for this project includes:

1. Realize electronic feedback control of the electrical current for resistance heating and the electronic gas valve so that heating and cooling can be controlled precisely.

2. Use infra-red sensors to map the temperature variations over the entire C section.

3. Set up an optimal dimension change detecting device so the gauge length variation can be recorded during tensile test. This will allow the stress-strain curve to be obtained, and the mechanical properties at elevated temperature can be determined.

4. Conduct a series of tensile tests on steel samples at elevated temperatures during the quenching process when the steel is in the state of a mixture of martensite and austenite.

CHAPTER 6 CONTRIBUTIONS AND FUTURE WORK

6.1 Contributions

The research in this thesis has addressed a critical problem on how to obtain high temperature mechanical properties of steels when they are going through a quenching process. The main contributions of this thesis are as follows:

1. A unique sample has been designed to meet the demand of achieving close-to-uniform temperature distribution along the gauge length in order to conduct the in-situ tensile test during the quenching process.
2. The design of the sample has been simulated using FEA software ABAQUS v6.5 and the results from the simulation have contributed constructively to the optimization of the final design.
3. A vacuum device for resistance heating and gas-aided cooling of steel has been designed with the function of conducting tensile tests during the quenching process at any expected temperature. The heating and cooling rate of the sample can be easily and rapidly modified and controlled by adjusting electrical current driven through the sample and using gas cooling.
4. The design of the sample has been verified and the best case dimensions of the sample have been finalized through experiments.

APPENDICES

APPENDIX A

PHYSICAL PROPERTIES FOR BOHLER W302 SUPERIOR (PREMIUM H13)

BOHLER W302 SUPERIOR®

Physical Properties

Density at	70°F (20°C)	.282 lbs/in³ (7.8 g/cm³)
	930°F (500°C)	.276 lbs/in³ (7.64 g/cm³)
	1100°F (600°C)	.275 lbs/in³ (7.60 g/cm³)
Specific heat at	70°F (20°C)	.110 Btu/lb°F 460 (J/kg K)
	930°F (500°C)	.131 Btu/lb°F 550 (J/kg K)
	1100°F (600°C)	.141 Btu/lb°F 590 (J/kg K)
Electric resistivity at	70°F (20°C)	0.020 Ohm x in²/in (0.52 Ohm mm²/m)
	930°F (500°C)	0.034 Ohm x in²/in (0.86 Ohm mm²/m)
	1100°F (600°C)	0.038 Ohm x in²/in (0.96 Ohm mm²/m)
Modulus of elasticity at	70°F (20°C)	31.2 x 10^6psi (215 x 10^3 N/mm²)
	930°F (500°C)	25.5 x 10^6psi (176 x 10^3 N/mm²)
	1100°F (600°C)	23.9 x 10^6psi (165 x 10^3 N/mm²)

Thermal expansion between 70°F and—

in/in °F x 10^{-6} from 70°F to: (m/m °C x 10^{-6} from 20°C to:)

200°F (100°C)	400°F (200°C)	570°F (300°C)	750°F (400°C)	930°F (500°C)	1100°F (600°C)	1300°F (700°C)
6.4 (11.5)	6.7 (12.0)	6.8 (12.2)	6.9 (12.5)	7.2 (12.9)	7.2 (13.0)	7.3 (13.2)

Thermal conductivity at 70°F and—

Btu/ft • h • °F from 70°F to : (W/m °C from 20°C to:)

70°F (20°C)	200°F (100°C)	400°F (200°C)	570°F (300°C)	750°F (400°C)	930°F (500°C)	1100°F (600°C)	1300°F (700°C)
Annealed Condition							
15.5 (26.8)	15.7 (27.2)	16.2 (28.1)	17.4 (30.1)	17.9 (31.0)	18.2 (31.5)	18.7 (32.3)	19.3 (33.4)
Hardened Condition							
14.4 (25.0)	14.7 (25.5)	15.6 (27.1)	15.9 (27.5)	16.0 (27.70)	16.3 (28.3)	16.9 (29.3)	17.5 (30.4)

APPENDIX B

A PARAMETER STUDY PROGRAM TO INVESTIGATE THE STEADY-STATE TEMPERATURE DISTRIBUTION UNDER DIFFERENT APPLIED CURRENT DENSITY

```
import string

#######################################################################
#
# This script runs to collect the temperatures of the central node in # the gauge
# area under a serious of distributed surface electrical current applied through the
# two ends of the sample and output the the central node temperature for each
# applied distributed surface electrical current density.
#
# Parameters used in study:
#
# distributed surface electrical current applied through the two ends:    # DSEC
#
# Output node:    middle node of the sample (set through nout)
#######################################################################
# SET PRESCRIBED OUTPUT NODE
nout =408

# DEFINE A FUNCTION TO OUTPUT DATA TO XYPLOT FILES

# CREATE THE STUDY
tp=ParStudy(par='DSEC', directory=OFF, verbose=ON)
```

```
# DEFINE THE PARAMETERS
tp.define('CONTINUOUS', par='DSEC',domain=(8000000,15000000))

# SAMPLE BY INTERVAL
tp.sample(INTERVAL, par='DSEC', interval=500000)

# COMBINE THE SAMPLES INTO DESIGNS
tp.combine('MESH', name='DSEC')

# GENERATE ANALYSIS JOB DATA
tp.generate(template='Job-4006PP')

# EXECUTE ALL JOBS SEQUENTIALLY
tp.execute(ALL)

# PARAMETRIC STUDY OUTPUT AT END OF STEP 1
tp.output(file=ODB,instance='SAMPLEHALF50-1',step=1, inc=LAST)

# GATHER RESULTS FOR OUTPUT NODE AND WRITE TO OUTPUT FILES
tp.gather(results='NodeTemp',instance='SAMPLEHALF50-1',variable=('NT11'),
node=nout)
fileName='4006'
fname_o = fileName + '_output.txt'
tp.report(FILE,par=('DSEC'),file=fname_o, results=('NodeTemp.1'))
fname_o_xyplot = fileName + '_output_XYPLOT'
tp.report(XYPLOT, par=('DSEC'), file=fname_o_xyplot, results=('NodeTemp.1'))
```

APPENDIX C

A POST-PROCESSING PROGRAM IN PYTHON TO ANALYZE THE TEMPERATURE DISTRIBUTION ALONG THE LENGTH OF THE SAMPLE

```
from odbAccess import *
from abaqusConstants import *
from odbMaterial import *
from odbSection import *

n='1'
input='Job-testParameter_VTemp_EPD_c'
output='output_c'

inputfilename=input+n+'.odb'
odb=openOdb(path=inputfilename)
assembly=odb.rootAssembly
centralNodes=assembly.nodeSets['SET-1']
center=centralNodes.nodes
lastFrame=odb.steps['ElectricalHeating'].frames[-1]

for m in lastFrame.fieldOutput.keys():
   print m
nodeTemp=lastFrame.fieldOutputs['NT11']
subnodeTemp=nodeTemp.getSubset(region=centralNodes)

nodeCoord=lastFrame.fieldOutputs['COORD']
subnodeCoord=nodeCoord.getSubset(region=centralNodes)
```

```
fieldValuesTemp=subnodeTemp.values
fieldValuesCoord=subnodeCoord.values

outputfilename=output+n
outputfile=open(outputfilename,"w")

for v in fieldValuesTemp:
 for n in center[0]:
  if v.nodeLabel==n.label:
    print  >outputfile,v.nodeLabel,n.coordinates[0],
          n.coordinates[1],n.coordinates[2],v.data

outputfile.close()
```

REFERENCE

1. SYSWELD ^{TM} , ESI GROUP, http://www.esi-group.com/SimulationSoftware/ Welding_ heat_treatment /heat_html on 12/12/2006.

2. DEFORM^{TM} -HT, Scientific Forming Technologies Corporation, http://www.deform.com on 12/12/2006.

3. DANTE ^{TM} - Software for Heat Treatment Simulation, Deformation Control Technology, Inc., http://www.deformationcontrol.com/dct_products.htm on 12/12/2006

4. Ferguson, B. L., " Heat Treatment Simulation Continues to Gain Users and Make Advances", http://www.industrialheating.com/CDA/Articles/Cover_Story/ 61ca29f15a9e8010VgnVCM100000f932a8c0 on 12/12/2006

5. Kenneth, G. and Budinski, "ENGINEERING MATERIALS: PROPERTIES AND SELECTION" ,5th edition ,1996 by Prentice Hall

6. Boitout, F., Dry, D., Morugue, P., Gooroochurn, Y. and Porzner, H., "SYSWELD FOR HEAT TREATMENT", http://www.esi-group.com/SimulationSoftware/ Welding_heat_treatment/Papers/ SYSWELDf-for-Heat-Treatment.pdf on 02/12/2006.

7. Koistinen, D. and Marburger, R., "A General Equation Prescribing the Extent of the Austenite-Martensite Transformation in Pure Iron-Carbon Alloys and Plain Carbon Steels", Acta Met., vol.7, pp. 50-60, 1959

8. Yu, H-J. , Wolfstieg,U. and Macherauch, E., Arch. Eisenhuettenwes vol.49, pp.499-504, 1978

9. Yu, H-J, Wolfstieg, U.and Macherauch, E., Arch. Eisenhuettenwes vol.50, pp.81-84,1979

10. Cheng, H., Jinag, F. and Wang, H. G., J. Mater. Proc. Technol. vol.63, pp.568-572, 1997

11. Walton, H. W., "Deflection Methods to Estimate Residual Stress", Handbook of Residual Stress and Deformation of Steel, Totten, G., Howes, M., Inoue, T., Ed., ASM International, 2002

12. Inoue, T., "Coupling of stress-strain, thermal, metallurgical behaviours", Handbook of Materials Behavior Models, Lemaitre, J., ed., vol.3, p884-895, 2001 by Academic Press,

13. Greenwood, G.W. and Johnson, R.H., " The deformation of metals under small stresses during phase transformations", Proc. Royal Soc. A, 283, pp.403-422,1965

14. Abrassart, F., These detat, Universite de Nancy I, 1972

15. Leblond, J.B., Devaux J., and Devaux, J. C., "Mathematical modelling of transformation plasticity in steels", Int. J. of Plasticity, vol.5, pp 551-591, 1989

16. Inoue, T., Ju, D. Y. and Arimoto, K., "Metallo-Thermo-Mechanical Simulation of Quenching Process – Theory and Implementation of the Computer Code HEARTS", 1st International Conference on Quenching and Distortion control, Totten, G. E. Ed., ASM International, pp.205-212, 1992

17. Denis, S., Archambault, P. and Gautier, E., "Models for stress phase transformation couplings in metallic alloys", Handbook of Materials Behaviour Models, Lemaitre, J., ed., vol.3, pp.896-904, 2001 by Academic Press

18. "SYSWELD – A predictive model for heat treat distortion",Southwest Research Institute and Framatome – Presentation at the National Center for manufacturing Science, Ann Arbor, Michigan, 1993

19. Homepage of SYSWELD software available from ESI-Group, htp:/www.esi-group.com/ SimulationSoftware/ Welding_heat_treatment/heat_html on 09/15/2006

20. Fischer, F. D., "Elastoplasticity coupled with phase changes, Handbook of Materials Behavior Models", Lemaitre, J., ed., vol. 3, p905-914, 2001 by Academic Press,

21. Leblond, J. B., "Mechanical behavior of steels during solid-solid phase transformations", Handbook of Materials Behavior Models, Lemaitre, J., ed., Vol. 3, pp.915-920, 2001 by Academic Press

22. Lusk, M.T., Krauss, G. and Jou, H., "A Balance Principle Approach for Modeling Phase Transformation Kinetics", Journal de Physique IV, 8, pp. 279-284, 1995,

23. Bammann, D. J., Prantil, V. C., Kumar, A. A., Lanthrop, J. F., Mosher, D. A., Lusk, M. T., Jou, H. J., Krauss, G. and Eliot W. H., "A Material Model for Low Carbon Steels Undergoing Phase Transformations", Proceedings of the 2nd International Conference on Quenching and the Control of Distortion , pp. 367-376, 1996,

24. Lusk, M. T. and Lee, Y. K., "A Global Material Model for Simulating the Transformation Kinetics of Low Alloy Steels", Proceedings of the 7th International Seminar of the International IFHT, pp. 273-282, 1999

25. Lusk, M. T., Lee, Y. K., Jou, H. J., Eliot , W. E. and Ludtka, G. M., "An Internal State Variable Model for the Low Temperature Tempering of Low Alloy Steels",

Journal of Shanghai Jiaotong University: Proceedings of the 1st International Conference on Thermal Process Modeling and Computer Simulation, 2000.

26. Bammann, D. J., Chiesa, M. L. and Johnson, G. C., "Modeling Large Deformation and Failure in manufacturing Processes", Proc. of the 19th International Congress of Theoretical and Applied Mechanics, Tatsumi et al. eds, Kyosto, Japan, pp. 359-376, 1996,

27. Bammann, D. J., Prantil, V. C. and Lanthrop, J. F., "A Plasticity Model for Materials Undergoing Phase Transformations", NUMIFORM'95: The 5th Int. Conf. on Numerical Methods in Industrial Forming Processes, Ithaca N.Y., pp. 219-223, 1995

28. Bammann, D. J. and Ortega, A. R., "The Influence of the Bauschinger Effect and Yield Definition on the Modeling of Welding Processes", Welding and Advanced Solidification Processes-VI, Piwonka, Voler and Katgerman, eds., The Minerals, Metals & Materials Society, Warendale, PA, pp. 543-551, 1993

29. "BOHLER W302 SUPERIOR", http://www.bucorp.com/files/BOHLER_W302_ Superior_Rev_Aug_2_2006.pdf on 02/10/2005

30. Bowen, R. M., "Theory of Mixture", Continuum Physics, Eringen, A. C. Ed., vol.3, pp.2-129, 1976 by Academic Press

31. Leblond, J. B., "A theoretical and numerical approach to the plastic behaviour of steels during phase transformations - II. Study of classical plasticity for ideal-plastic phases", J. Mech. Phys. Solids, Vol.34, pp. 411-432, 1986

32. Mehta, M. and Oakwood, T., "FINAL REPORT of Development of a Standard Methodology for the Quantitative Measurement of Steel Phase Transformation Kinetics and Dilation Strains using Dilatometric Methods (QMST)", April 28, 2004,

http://www.osti.gov/bridge/servlets/purl/840936-a1t1uq/native/840936.PDF on 05/20/2005

33. ASTM Designation: A1033-04, "Standard Practice for Quantitative Measurement and Reporting of Hypo-eutectoid Carbon and Low-Alloy Steel Phase Transformations", 2006

34. ASTM Designation: E21-05, "Standard Methods for Elevated temperature tension Tests of Metallic Materials", 2005

35. Shackelford, J. F., "Introduction to MATERIALS SCIENCE FOR ENGINEERS", 6th edition, pp.187, 2005 by Pearson Education, Inc.

36. Personal communication with Murray Lett at CANMET laboratory, Ottawa and Dr. S. David at Oak RNL .

37. Dynamic Systems Inc., http://www.gleeble.com on 05/10/2005

38. Norris, S. D. and Wilson, I., "Application of 3D numerical modeling for thermal profile optimization on the Gleeble thermomechanical simulator", Modeling Simul. Mater. Sci. Eng., vol. 7, pp.297-309, 1999

39. Liu, C. C., Yao, K. F., and Liu, Z., "Quantitative research on effects of stresses and strains on bainitic transformation kinetics and transformation plasticity", Materials Science and Technology, vol.16, pp. 643-647 ,2000

40. Ferguson, H. S., "Apparatus for providing enhanced self-resistive specimen heating in dynamic material testing systems and an accompanying method for use therein", http://www.freshpatents.com on 03/05/2006.

41. "Hot Torsion Testing on A Gleeble System", Dynamic Systems Inc., http://www.gleeble.com/AppNotes/application_note_20.htm on 01/15/2007.

42. Nagayama, K., Terasaki, T., Tanaka,K., Fischer, F. D., Antretter, T., Cailletaud, G. and Azzouz, F., "Mechanical properties of a Cr-Ni-Mo-Al-Ti maraging steel in the process of martensitic transformation", Materials Science and Engineering A308, pp.25-37, 2001

43. Pierer, R., Bernhard, C., Chimani, C., "Experimental and analytical analysis of the high-temperature mechanical properties of steel under continuous casting conditions", Computational Methods and Experimental Measurements XII ,Transaction: Modeling and Simulation, vol. 41, pp.944, 2005

44. Reiter, J. and Pierer, R., "Thermal-mechanical simulation of a laboratory test to determine mechanical properties of steel near the solidus temperature", http://library.mcc-cdl.at/8231.pdf on 04/20/2007

45. Yu, C. H. and Ahn, H. K., "Evaluation of mechanical properties under a temperature gradient field", Meas. Sci. Technol., vol.12, pp.1881-1885, 2001

46. "Smithells Metals Reference Book", 8th Edition, 2004 by Elsevier Butterworth Heinemann

47. "Properties of Wrought Coppers and Copper Alloys", Properties and Selection: Nonferrous Alloys and Special-Purpose Materials, ASM HANDBOOK, vol.2, pp.265-345 ,1995 ASM International,

VITA AUCTORIS

Chao Zheng got his B. S and M. S. in Materials Science and Engineering from Zhejiang University and Shanghai Jiao Tong University, in 1985 and 1988 respectively.

After his graduation, he spent several years as project manager, responsible for the set-up and administration of science and technology projects. Later he became the deputy manager for the export of various industrial products, solving engineering-related issues and assuring quality control from suppliers.

Long before immigrating to Canada in 2003, he became a software developer and system engineer, using advanced technology of programming, networking and database to develop MIS systems for telecommunication industry,

While pursuing all his interests, he still keeps his primary interest in Materials Science and Engineering, which led to the development and the successful conclusion of this thesis research in 2007.